STEREOSPECIFIC LONG-RANGE NUCLEAR SPIN-SPIN COUPLING CONSTANTS BETWEEN THE SIDE-CHAIN ^{13}C NUCLEUS AND ^{1}H, ^{13}C AND ^{19}F NUCLEI IN THE RING OF SOME BENZENE DERIVATIVES. CONFORMATIONAL APPLICATIONS.

by

Glenn H. Penner

A thesis submitted to
the Faculty of Graduate Studies
of the University of Manitoba in
partial fulfillment of the degree

Doctor of Philosophy

Winnipeg, Manitoba,
May, 1987 

ISBN 0-315-37208-7

STEREOSPECIFIC LONG-RANGE NUCLEAR SPIN-SPIN COUPLING CONSTANTS BETWEEN THE SIDE-CHAIN ^{13}C NUCLEUS AND ^{1}H, ^{13}C AND ^{19}F NUCLEI IN THE RING OF SOME BENZENE DERIVATIVES. CONFORMATIONAL APPLICATIONS

BY

GLENN H. PENNER

A thesis submitted to the Faculty of Graduate Studies of the University of Manitoba in partial fulfillment of the requirements of the degree of

DOCTOR OF PHILOSOPHY

ABSTRACT

Proton, carbon-13 and fluorine-19 nuclear magnetic resonance spectroscopies have been used to investigate the stereospecificity of long-range nuclear spin-spin coupling constants between the sidechain carbon-13 nucleus and the ring protons, carbon-13 or fluorine-19 nuclei in some benzene derivatives.

For symmetrically substituted benzene derivatives the angular dependence of the long-range coupling between the sidechain carbon-13 nucleus and the ring nuclei can be described by

$$J = J_{90} \langle \sin^2\theta \rangle + [0.5J_{180} + J_0],$$

where θ is the angle between the benzene ring and C_1-X-C_α planes. J_{90}, J_{180} and J_0 are the σ-π, σ and π contributions to the nuclear spin-spin coupling, respectively; $\langle \sin^2\theta \rangle$ is the value of $\sin^2\theta$ averaged over the hindered rotor states. With the assumption of a twofold barrier to internal rotation, $V(\theta) = V_2 \sin^2\theta$, $\langle \sin^2\theta \rangle$ is related to V_2, the barrier height, by a hindered rotor model.

Conformational preferences and internal rotational barrier heights are presented for ^{13}C enriched derivatives of thioanisole, anisole, selenoanisole, telluroanisole, N-methylaniline and benzyl cyanide.

ACKNOWLEDGEMENTS

I wish to thank Dr. Ted Schaefer for his encouragement, guidance and thoughtful criticism during the course of this work. His patience with me during my many tangents into other projects (and into some of Winnipeg's less reputable public houses) is greatly appreciated.

I thank Mr. Rudy Sebastian for his invaluable help with the many computer programs used during the course of this thesis work.

I also thank Mr. Kirk Marat for his help with the Bruker AM300 spectrometer. His high standards in maintaining the AM300 have enabled me to obtain some excellent high resolution spectra.

I am grateful for many helpful and engaging conversations with Rudy Sebastian, Mike Sowa and Craig Takeuchi. I would like to thank the staff of the Montcalm motor hotel, in which many of these conversations took place. A special thanks goes to the many ecdysiasts who entertained us during these often extended colloquies.

I am grateful to Donna Harris for her skillful typing of these pages.

The financial support of the Natural Sciences and Engineering Research Council of Canada and of the University of Manitoba is much appreciated.

TABLE OF CONTENTS

LIST OF FIGURES

LIST OF TABLES

A. INTRODUCTION

1. Stereospecific Coupling Between Sidechain Nuclei and Nuclei on the Benzene Ring

The long-range spin-spin coupling between sidechain nuclei and benzene ring nuclei can be discussed in terms of several mechanisms; the σ mechanism, the σ-π mechanism and the through-space mechanism.

In the σ mechanism, the coupling is transmitted by the σ bond framework. Karplus[1] predicted the dependence of the vicinal proton-proton coupling in ethane on the dihedral angle, θ, between the two proton carbon bonds. Wasylishen and Schaefer[2] proposed that the angular dependence of the σ electron contribution to $^5J(CH_3,H_3)$ in toluene is

$$^5J(CH_3,H_3) = B\sin^2(\theta/2) \qquad (1)$$

where B is $^5J^{\sigma}_{180}$, the maximum value of the coupling when θ is 180°. θ is the angle by which the C-H bond of the methyl group twists out of the benzene plane.

The σ-π mechanism involves a hyperconjugative transmission of spin information between the sidechain σ orbitals and the π orbital of the benzene ring followed by a σ-π interaction of the aromatic π orbitals with the σ orbitals of the ring carbon nucleus or the C-X bonds of the ring. By analogy to the McConnell-Heller equation[3] in electron spin resonance, the angular dependence of the σ-π coupling can be written as

$$J = J^{\sigma-\pi}_{90}\sin^2\theta \qquad (2)$$

where $J^{\sigma-\pi}_{90}$ is the value of the coupling when $\theta = 90°$.

The third mechanism involves a through-space coupling between spacially proximate nuclei. This coupling is likely transmitted via overlap of the electron orbitals associated with these nuclei and does not involve spin coupling through formal bonds. Because the through-space coupling has a very strong dependence on the average internuclear distance it is a valuable tool for conformational analysis. Two empirical relationships relating the through-space coupling to molecular geometry have been proposed[4,5].

If all three mechanisms contribute, the spin-spin coupling between sidechain nuclei and the benzene ring nuclei can be written as

$$J = J_{90}^{\sigma-\pi} \sin^2\theta + J_{180}^{\sigma} \sin^2\theta/2 + J_{TS} \qquad (3)$$

a) Stereospecific coupling between sidechain protons and nuclei on the benzene ring.

The conformational dependence of spin couplings between the sidechain protons and ring protons in toluene derivatives have been thoroughly studied. INDO MO FPT computations and experimental measurements of $^4J(CH,H_2)$ in aromatic systems[6] yield

$$^4J(CH,H_2) = 6.90\ \pi\sin^2\theta - 0.32\ \cos^2\theta \qquad (4)$$

where π is the mutual atom-atom polarizability associated with the 2p atomic orbitals in the C_1-C_2 bond. For toluene π is -0.157 and (4) becomes

$$^4J(CH,H_2) = -1.08\langle\sin^2\theta\rangle - 0.32\langle\cos^2\theta\rangle \quad (5a)$$

or

$$^4J(CH,H_2) = -0.76\langle\sin^2\theta\rangle - 0.32 \quad (5b)$$

where $\langle\sin^2\theta\rangle$ is the average or expectation value of $\sin^2\theta$ (expectation values will be discussed in more detail in part 2 of this introduction). The $\langle\sin^2\theta\rangle$ and $\langle\cos^2\theta\rangle$ terms in equation (5a) are attributed[6] to the σ-π and σ mechanisms respectively.

INDO MO FPT computations of $^4J(CH,H_2)$ are fitted by

$$^4J(CH,H_2) = -0.342(5) - 1.005(6)\ \sin^2\theta - 0.230(5)\ \sin^2(\theta/2) \quad (6)$$

The numbers in parentheses are standard deviations in the last decimal place.

The orthobenzylic couplings measured by Barfield and coworkers[6] for molecules in which θ was fixed (21 values) can be fitted by

$$^4J(CH,H_2) = -0.28(4) - 0.92(3)\ \langle\sin^2\theta\rangle \quad (7)$$

Including a $\sin^2(\theta/2)$ term does not improve the fit. Both equations 5 and 7 reproduce the observed coupling[8] in toluene.

Early INDO MO FPT computations by Wasylishen and Schaefer[2] imply that $^5J(CH,H_3)$ may take the form

$$^5J(CH,H_3) = {}^5J^{\pi}_{90}\ \sin^2\theta + {}^5J^{\sigma}_{180}\ \sin^2(\theta/2) \quad (8)$$

Using ortho difluoro derivatives of toluene, ethylbenzene and isopropyl benzene, for which $\langle \sin^2\theta \rangle$ has a sufficient range and $\langle \sin^2\theta/2 \rangle$ is 0.5, Schaefer and Laatikainen[7] proposed equation (8), which becomes

$$^5J(CH,H_3) = 0.336\langle \sin^2\theta \rangle + 0.540\langle \sin^2(\theta/2) \rangle \quad (9)$$

The observed ring substituent dependence of $^5J^{\sigma}_{180}$ is relatively large and in the absence of any ring substituents $^5J^{\sigma}_{180}$ becomes 0.322 Hz[8].

Experimentally and theoretically, it appears that $^6J(CH,H_4)$ is dependent on $\sin^2\theta$ [9]. In toluene, where $\langle \sin^2\theta \rangle$ is 0.5, $^6J(CH_3,H_4)$ is -0.602(2) Hz[8] and one can write

$$^6J(CH,H_4) = -1.20\langle \sin^2\theta \rangle \quad (10)$$

$^6J(CH,H_4)$ is rather insensitive to ring substitution although the electronic nature (electronegativity) of an atom attached to the methyl carbon will have some effect on $^6J^{\pi}_{90}$ [10,11].

The conformational dependence of the couplings between the sidechain proton and the ring protons has also been investigated in thiophenols[12,13,14,15] and is described by equations (11), (12) and (13).

$$^4J(SH,H_2) = -1.10 \langle \sin^2\theta \rangle \quad (11)$$

$$^5J(SH,H_3) = 0.196\langle \sin^2\theta \rangle + 0.360\langle \sin^2(\theta/2) \rangle \quad (12)$$

$$^{6}J(SH,H_4) = -0.97\langle\sin^2\theta\rangle \quad (13)$$

These relationships have proven quite useful for investigating the effect of ring substituents on the conformation of the SH moiety.

In a manner analogous to the work on toluene derivatives Parr and Schaefer assume that $^{6}J(SiH,H_4)$ obeys a $\sin^2\theta$ law in phenyl silanes[16]. Taking $\langle\sin^2\theta\rangle$ as 0.5 in phenyl silane gave equation (14), which could be used to estimate two-fold barriers to internal rotation in some phenyl silanes.

$$^{6}J(SiH,H_4) = -0.686\langle\sin^2\theta\rangle \quad (14)$$

Investigations of the conformational dependences of the long-range couplings in phenols, benzaldehydes, anilines and styrenes have proven to be more difficult. It has been impossible to obtain experimental J_{90} values. The rather high barriers to sidechain rotation in many phenol and benzaldehyde derivatives allows the five bond coupling to be discussed in terms of a simple cis-trans equilibrium[17-25].

Based on INDO MO FPT calculations, a value for $^{6}J^{\pi}_{90}$ has been estimated from styrene[26,27] to yield equation (15).

$$^{6}J(CH,H_4) = -1.0\langle\sin^2\theta\rangle \quad (15)$$

The possibility of a non-zero constant term has also been suggested[28]. The rotational barrier about the C_1-C_α bond in styrene is not high enough[29,30] to allow discussion in terms of a simple cis-trans equilibrium. The conformational dependence of $^{4}J(CH,H_2)$ and $^{5}J(CH,H_3)$

conformational dependence of $^{4}J(CH,H_2)$ and $^{5}J(CH,H_3)$ have not yet been deduced.

Coupling between the sidechain protons and benzene ring fluorine nuclei have not received as much attention as the corresponding proton-proton couplings.

An investigation of 4-fluorotoluene derivatives[31] showed that the six-bond coupling, $^{6}J(CH,F_4)$ has a slight solvent dependence and is also dependent on ring substituents. For 4-fluorotoluene in CS_2 solution

$$^{6}J(CH,F_4) = 2.24\langle\sin^2\theta\rangle \qquad (16)$$

The nature of the substituent perturbation of $^{6}J(CH,F_4)$ is presently being investigated in this laboratory.

$^{4}J(CH,F_2)$ shows substantial substituent perturbations[32]. An empirical curve has been proposed for the angular dependence of $^{4}J(CH,F_2)$[32]. $^{5}J(CH,F_3)$ displays a small substituent effect[33,34]. An attempt is presently being made in this laboratory, to deduce a relationship like that of equation (8) for $^{5}J(CH,F_3)$.

An investigation of the conformational preference of long-range couplings between the sulfydryl proton and ring fluorine nuclei in thiophenols is presently being conducted.

When $\langle\sin^2\theta\rangle$ is know to be non-zero, the sign of the six-bond proton-fluorine coupling is always positive. For example, $^{6}J(CH_3,F_4)$ is +1.12 Hz in 4-fluorotoluene[31] and $^{6}J(SH,F_4)$ is +1.000 Hz in 4-fluorothiophenol[14]. In certain derivatives of 4-fluorophenol and 4-fluorobenzaldehyde, where $\langle\sin^2\theta\rangle$ is near zero, $^{6}J(H,F)$ is small and negative[17,23]. It has been suggested[35] that in 4-fluorobenzaldehyde

derivatives a pure π coupling mechanism may exist which takes the form $^6J_0^{\pi}\langle\cos^2\theta\rangle$ to give

$$^6J(CHO,F_4) = {}^6J_{90}^{\sigma-\pi}\langle\sin^2\theta\rangle + {}^6J_0^{\pi}\langle\cos^2\theta\rangle \qquad (17)$$

An equation analogous to (17) may be necessary to describe $^6J(OH,F_4)$ in 4-fluorophenol derivatives.

The conformational dependence of the coupling between sidechain protons and the <u>para</u> carbon nucleus has been examined in derivatives of toluene[36] and may be written as

$$^5J\ (CH,C_4) = 1.77\ \langle\sin^2\theta\rangle \qquad (18)$$

The coupling mechanism is only significantly perturbed by substituents at the <u>alpha</u> or <u>para</u> positions. An investigation of the dependence of this coupling on the nature of the <u>para</u> substituent has not yet been undertaken.

b) Coupling between sidechain carbon-13 nuclei and ring nuclei.

At present only the conformational dependence of the coupling between the sidechain carbon nucleus and the <u>para</u> ring proton or fluorine nucleus has been investigated in derivatives of anisole[37], thioanisole[38] and 4-fluorophenyl derivatives of methane, ethene and cyclohexane[39].

For anisole derivatives[37] one may write

$$^6J\ (O\ ^{13}C,\ H_4) = -0.63\langle\sin^2\theta\rangle \qquad (19)$$

and

$$^{6}J\ (O\ ^{13}C,\ F_4) \quad = \quad 1.48\langle \sin^2\theta \rangle \qquad (20)$$

These couplings were used to deduce the barriers to internal rotation about the C_1-O bond in some fluorinated anisoles[37].

Equation (21) has been proposed for $^{6}J(CC_\beta, F_4)$ in some derivatives of 4-fluoroethane 1[39].

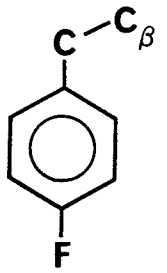

$\theta = 0°$

1

$$^{6}J\ (C_\beta,\ F_4) \quad = \quad 1.29\langle \sin^2\theta \rangle \qquad (21)$$

INDO MO FPT computations suggest that the coupling mechanism is dependent on the nature of the atom directly bonded to C_β. For example, in 4-fluorobenzyl ketones $^{6}J_{90}\ (C_\beta,\ F_4)$ is taken as 1.42 Hz.

Recently Schaefer and Baleja[38] have used coupling between the methyl carbon nucleus and the para fluorine nucleus or proton to deduce the two-fold barriers to internal rotation about the C_1-S bond in some symmetrically substituted thioanisoles. The $\langle \sin^2\theta \rangle$ values were based on equations (22) and (23).

$$^{6}J\ (S\ ^{13}C,\ H_4) \quad = \quad -0.56\langle \sin^2\theta \rangle \qquad (22)$$

$$^{6}J\ (S\ ^{13}C,\ F_4) \quad = \quad 1.54\langle \sin^2\theta \rangle \qquad (23)$$

Very few couplings between the sidechain β-carbon nucleus and ring carbon nuclei have been reported[40,41]. In this thesis the conformational dependence of these long-range $^{13}C,^{13}C$ coupling constants will be investigated in several benzene derivatives. An attempt will be made to relate these coupling constants to $\langle \sin^2\theta \rangle$ values. Values of $\langle \sin^2\theta \rangle$ may in turn be used to deduce the barrier to internal rotation about the C_1-X bond. The next section will describe how barriers to internal rotation may be derived from $\langle \sin^2\theta \rangle$ values.

2. Internal Rotation in Benzene Derivatives

Internal rotation in a molecule involves the rotation of one part of the molecule relative to another part about the bond that joins the two parts. The smaller part is called the top and is assumed to rotate relative to the larger stationary part, designated the frame. In small benzene derivatives the sidechain is usually considered the top and the benzene ring the frame.

Now consider the internal rotation about the C_1-S bond in thioanisole where the resonance stabilized minimum energy conformation

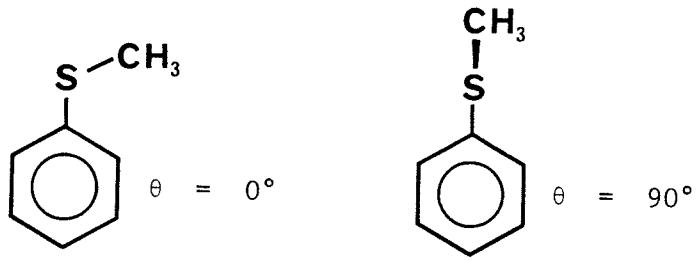

2 3

is 2 and the maximum energy conformation is 3. The dihedral angle between the C_1-S-Cα plane and the plane of the benzene ring, θ, is 0° and 90° in 2 and 3, respectively.

Figure 1 shows the potential energy function for rotation about the C_1-S bond in thioanisole. The function repeats itself twice over one full rotation of 360° and hence is referred to as two-fold rotation. Thus there can be 1-, 2-, 3- or n-fold rotation. For example, the rotation about the carbon-carbon bond in ethane is considered a 3-fold rotation and the rotation about the C_1-Cα bond in toluene is a 6-fold rotation. A 1-fold potential is usually described as asymmetric.

Figure 1

The potential energy curve for internal rotation of thioanisole about the C_1-S bond. The squares are energies calculated at the STO-3G level of ab initio molecular orbital theory. The solid line is a least squares fit of the points to yield the equation

$$V(\theta) = 4.48(9) \sin^2\theta + 0.52(9) \sin^2 2\theta.$$

The numbers in parentheses are the standard deviations in the last decimal place.

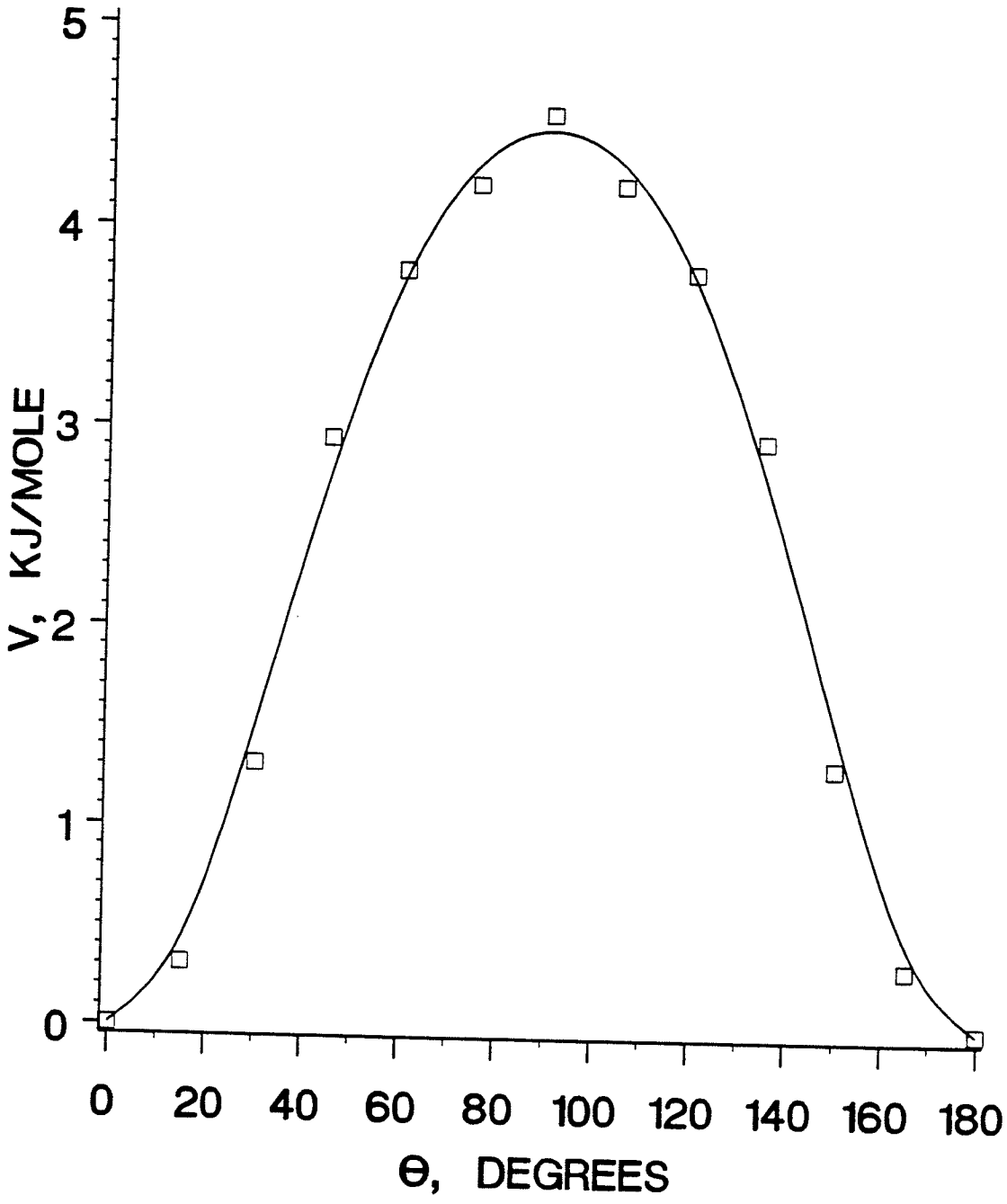
5
4
3
2
1
0
V, KJ/MOLE
0
20
40
60
80
100
120
140
160
180
Θ, DEGREES

Since the above rotations are periodic functions of θ, they can be described by a Fourier series

$$V(\theta) = \frac{b_o}{2} + \sum_{n=1}^{\infty} b_n \cos n\theta + a_n \sin n\theta \qquad (24)$$

The potentials are even functions of θ and so may be represented by the cosine Fourier series,

$$V(\theta) = \sum_{n=1}^{\infty} V_n \cos n\theta \qquad (25)$$

Equation (25) may be manipulated in order to have the potential energy equal to zero when θ is zero.

$$V(\theta) = \sum_{n=1}^{\infty} \frac{V_n}{2} [1-\cos n\theta] \qquad (26)$$

For an n-fold potential only the coefficients, V_n, which have multiples of n may contribute to the potential. Thus the rotational potential function for thioanisole would take the form

$$V(\theta) = \sum_{n=1}^{\infty} \frac{V_{2n}}{2} [1-\cos 2n\theta]. \qquad (27)$$

This equation may be rewritten in the form

$$V(\theta) = \sum_{n=1}^{\infty} V_{2n} \sin^2 n\theta . \qquad (28)$$

The internal rotations discussed in the remainder of this thesis may be described by equations (27) and (28).

Experimental and theoretical values for the coefficients, V_{2n}, show that the series is rapidly convergent and that more than two terms need seldom be considered. In many cases it is sufficient to describe the potential function with a single term

$$V(\theta) = \frac{V_2}{2}[1 - \cos 2\theta] = V_2 \sin^2\theta \ . \qquad (29)$$

If the potential can be described by two terms, i.e. $V(\theta) = V_2 \sin^2\theta + V_4 \sin^2 2\theta$, one can think of V_2 as the barrier height* and V_4 as affecting the shape of the potential function. Potential curves for different ratios of V_4/V_2 are shown in figure 2.

The dependence of the long-range spin couplings on $\langle \sin^2\theta \rangle$ has already been mentioned. It is of interest now to relate $\langle \sin^2\theta \rangle$ to the 2-fold barrier to internal rotation, V_2, following the procedure of Ayschough et al.[42]

In the quantum mechanical picture $\langle \sin^2\theta \rangle$ is the quantum statistical average of $\sin^2\theta$ over the hindered rotor states m.

$$\langle \sin^2\theta \rangle = \frac{\sum_{m=1} \exp\left(\frac{-E_m}{RT}\right) \langle \psi_m | \sin^2\theta | \psi_m \rangle}{\sum_{m=1} \exp\left(\frac{-E_m}{RT}\right)} \qquad (30)$$

The states ψ_m and their energies, E_m, are found by solving the Schrödinger equation for the hindered rotor.

$$\hat{H}\psi_m = E_m\psi_m \qquad (31)$$

*The barrier height is V(90) - V(0) and may take both negative and positive values.

Figure 2

Potential energy curves for functions of the form

$$V(\theta) = V_2 \sin^2\theta + V_4 \sin^2 2\theta$$

The labeled curves correspond to the following combinations of V_2 and V_4, given in kJ/mole.

a	$V_2 = 10$	$V_4 = 0.0$	$V_4/V_2 = 0$
b	10	2.5	0.25
c	10	5.0	0.5
d	10	7.5	0.75
e	10	10.5	1.0
f	10	0	0
g	10	-2.5	-0.25
h	10	-5.0	-0.50
i	10	-7.5	-0.75
j	10	-10.0	-1.00

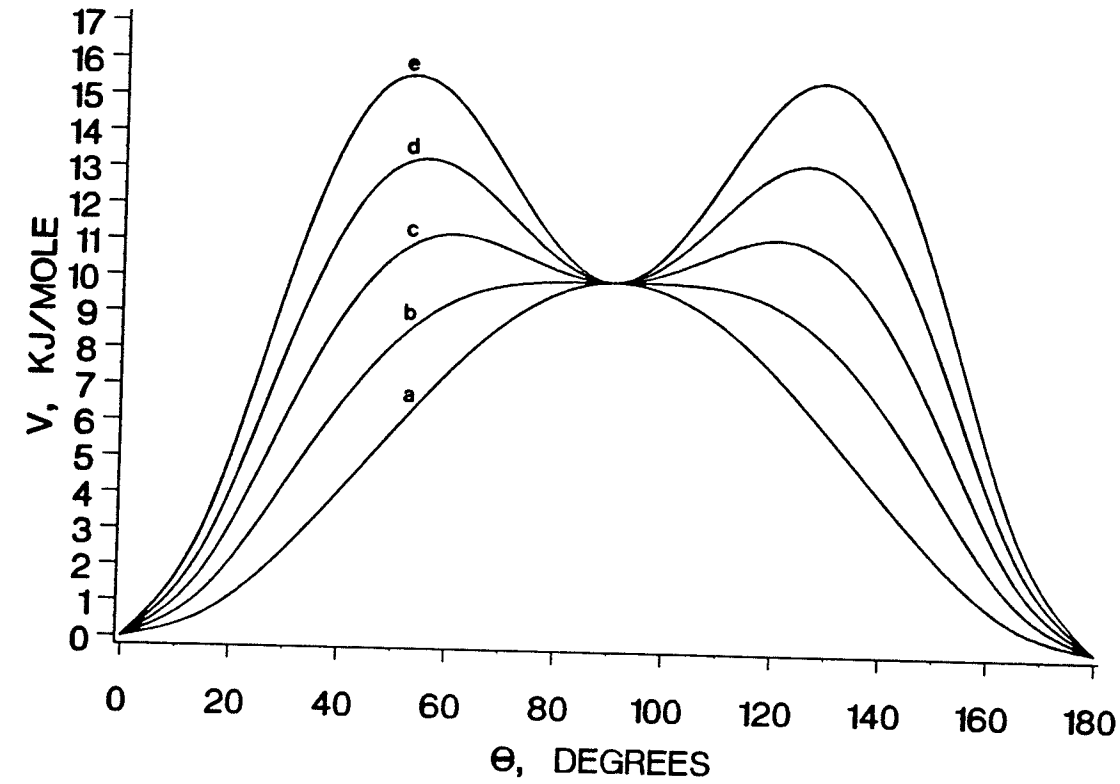
V, KJ/MOLE
17
16
15
14
13
12
11
10
9
8
7
6
5
4
3
2
1
0
e
d
c
b
a
0
20
40
60
80
100
120
140
160
180
Θ, DEGREES

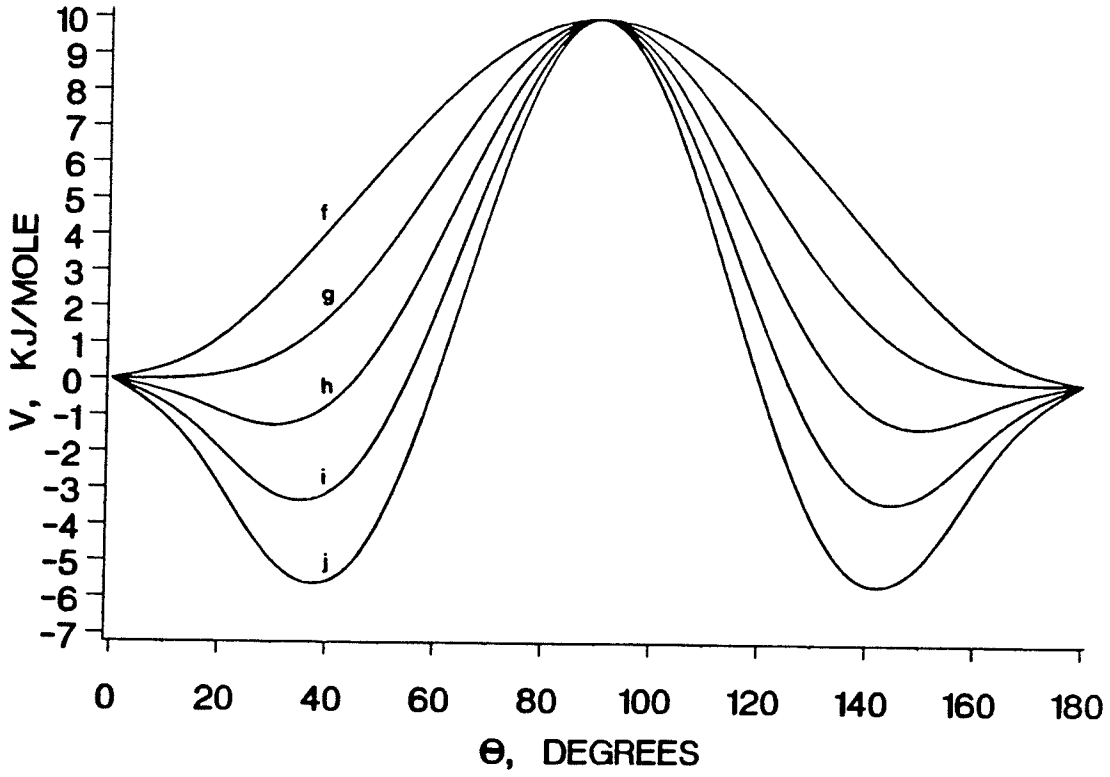
V, KJ/MOLE
10
9
8
7
6
5
4
3
2
1
0
-1
-2
-3
-4
-5
-6
-7
f
g
h
i
j
0
20
40
60
80
100
120
140
160
180
Θ, DEGREES

The Hamiltonian operator, $\hat{H}$, may be separated into kinetic and potential energy operators, $\hat{T}$ and $\hat{V}$, respectively. The kinetic energy operator is simply that for the "particle on a ring",

$$\hat{T} = \frac{-\hbar^2}{2I_r} \frac{d^2}{d\theta^2} \tag{32}$$

where I_r is the reduced moment of inertia of the molecule. The potential energy operator is the 2-fold potential function,

$$\hat{V} = \frac{V_2}{2} [1 - \cos(2\theta)]. \tag{33}$$

The Schrödinger equation now becomes

$$\left\{ \frac{-\hbar^2}{2I_r} \frac{d^2}{d\theta^2} + \frac{V_2}{2} [1-\cos(2\theta)] \right\} \psi_m = E_m \psi_m . \tag{34}$$

This equation is related to Mathieu's differential equation and the solutions, ψ_m, can be expressed as Fourier series.

$$\psi_m^{odd} = \sum_{\lambda} a_{m\lambda} \pi^{-1/2} \sin 2\lambda\theta \tag{35a}$$

$$\psi_m^{even} = b_{mo}(2\pi)^{-1/2} + \sum_{\lambda} b_{m\lambda} \pi^{-1/2} \cos 2\lambda\theta \tag{35b}$$

Diagonalization of the even (e) and odd (o) hamiltonian matrices will yield the energies, E_m, and the expansion coefficients $a_{m\lambda}$ and $b_{m\lambda}$ for each state m.

The matrix elements are

$$\langle \psi_o^e | \hat{H} | \psi_o^e \rangle = \frac{V_2}{2} \tag{36}$$

$$\langle \psi_o^e | \hat{H} | \psi_1^e \rangle = \langle \psi_1^e | \hat{H} | \psi_o^e \rangle = \frac{-V_2}{2\sqrt{2}} \tag{37}$$

$$\langle \psi_m^e | \hat{H} | \psi_m^e \rangle = \langle \psi_m^o | \hat{H} | \psi_m^o \rangle = \frac{\hbar^2 m^2}{2I_r} + \frac{V_2}{2} \tag{38}$$

$$\langle \psi_m^e | \hat{H} | \psi_{m\pm1}^e \rangle = \langle \psi_m^o | \hat{H} | \psi_{m\pm1}^o \rangle = -\frac{V_2}{4} \tag{39}$$

$m = 1, 2, \ldots, n$

All other matrix elements are zero.

Application of the kinetic energy operator is straightforward,

$$\hat{T}\, \psi_m^o = \frac{-\hbar^2}{2I_r} \sum_\lambda a_{m\lambda}\, \pi^{-1/2} \frac{d^2}{d\theta^2} (\sin 2\lambda\theta) \tag{40}$$

$$= \frac{2\hbar^2}{I_r} \sum_\lambda \lambda^2\, a_{m\lambda}\, \pi^{-1/2} \sin 2\lambda\theta \tag{41}$$

Therefore the expectation value of the kinetic energy operator becomes

$$\langle \psi_m^o | \hat{T} | \psi_m^o \rangle = \frac{2\hbar^2}{I_r} \sum_\lambda \lambda^2 |a_{m\lambda}|^2 \tag{42}$$

for the odd terms, and

$$\langle \psi_m^e | \hat{T} | \psi_m^e \rangle = \frac{2\hbar^2}{I_r} \sum_\lambda \lambda^2 |b_{m\lambda}|^2 \tag{43}$$

for the even terms.

If the Hamiltonian matrix is divided into its kinetic and potential energy parts, the matrix elements may be written as

$$\langle\psi_m^o|\hat{H}|\psi_m^o\rangle = \langle\psi_m^o|\hat{T}|\psi_m^o\rangle + \langle\psi_m^o|\hat{V}|\psi_m^o\rangle \tag{44}$$

$$\langle\psi_m^e|\hat{H}|\psi_m^e\rangle = \langle\psi_m^e|\hat{T}|\psi_m^e\rangle + \langle\psi_m^e|\hat{V}|\psi_m^e\rangle \tag{45}$$

Recognizing that the left hand sides of equation (44) and (45) are simply E_m^o and E_m^e respectively, substitution into equations (42) and (43) for the kinetic energy parts yields, after rearrangement,

$$\langle\psi_m^o|\hat{V}|\psi_m^o\rangle = E_m^o - \frac{2\hbar^2}{I_r}\sum_\lambda \lambda^2|a_{m\lambda}|^2 \tag{46}$$

$$\langle\psi_m^e|\hat{V}|\psi_m^e\rangle = E_m^e - \frac{2\hbar^2}{I_r}\sum_\lambda \lambda^2|b_{m\lambda}|^2 \tag{47}$$

Substitution of the potential energy operator and division by V_2 gives

$$\langle\psi_m^o|\sin^2\theta|\psi_m^o\rangle = \frac{E_m^o}{V_2} - \frac{2\hbar^2}{V_2 I_r}\sum_\lambda \lambda^2|a_{m\lambda}|^2 \tag{48}$$

$$\langle\psi_m^e|\sin^2\theta|\psi_m^e\rangle = \frac{E_m^e}{V_2} - \frac{2\hbar^2}{V_2 I_r}\sum_\lambda \lambda^2|b_{m\lambda}|^2 \tag{49}$$

Again, the energies and expansion coefficients are found by diagonalizing the Hamiltonian matrix. Substitution of the matrix elements from equations (48) and (49) into equation (30) will yield the quantum statistical average value of $\sin^2\theta$.

A simplifying feature of the above calculation is that the potential energy operator is also the function whose expectation value is being calculated, namely $\sin^2\theta$.

If the expectation value of another function, $f(\theta)$, is required, equation (30) becomes

$$\langle f(\theta)\rangle = \frac{\sum_m \exp\left[\frac{-E_m}{RT}\right] \langle\psi_m|f(\theta)|\psi_m\rangle}{\sum_m \exp\left[\frac{-E_m}{RT}\right]} \tag{50}$$

Evaluation of $\langle\psi_m^o|f(\theta)|\psi_m^o\rangle$ and $\langle\psi_m^e|f(\theta)|\psi_m^o\rangle$ involves solution of integrals of the form

$$C_{km}^o\, C_{lm}^o \int_0^{\pi/2} f(\theta)\, \sin 2k\theta\, \sin 2l\theta\, d\theta \tag{51a}$$

and

$$C_{km}^e\, C_{lm}^e \int_0^{\pi/2} f(\theta)\, \cos 2k\theta\, \cos 2l\theta\, d\theta \tag{51b}$$

respectively, where k and l are integers. In some cases the analytic solutions of these integrals are simple functions of k and l.

If one wished to calculate an expectation value of a function of θ for rotation under a potential of the form $\sum V_i \sin^{2i}\frac{\theta}{2}$, the matrix elements of the potential part of the Hamiltonian matrix, $\langle\psi_m|\hat{V}|\psi_m\rangle$, would differ from those of equations (36)-(39). General expressions for

these matrix elements under an n-fold hindering potential are given by Lister, Macdonald and Omen[43].

The calculation of an expectation value of a function under the influence of certain n-fold barriers may involve the solution of rather complicated trigonometric integrals. Alternatively, the classical expectation value may be evaluated.

$$\langle f(\theta) \rangle = \frac{\int_0^{\pi} f(\theta) \exp\left[\frac{-V(\theta)}{RT}\right] d\theta}{\int_0^{\pi} \exp\left[\frac{-V(\theta)}{RT}\right] d\theta} \qquad (52)$$

A simple computer program has been written* in which the function, $f(\theta)$, the temperature, and the coefficients V_n in the expansion of the function $V(\theta)$ are given as input and numerical integration is performed. Table 1 compares quantum mechanical and classical expectation values of θ and $\sin^2\theta$ for various 2-fold barriers.

*Program Classical.XPT written by Rudy Sebastian, 1985.

Table 1

Classical and quantum mechanical[a] values of $\langle\theta\rangle$ and $\langle\sin^2\theta\rangle$ for various two-fold barriers under the hindered rotor model[b].

V_2(kJ/mole)	$\langle\theta\rangle$ (deg)		$\langle \sin^2\theta\rangle$	
	classical	quantum mechanical	classical	quantum mechanical
0	45	45	0.500	0.500
2	38	38	0.402	0.410
4	31	32	0.314	0.329
10	19	20	0.151	0.173
20	12	13	0.068	0.089
∞	0	0	0.000	0.000

[a]Using 30 hindered rotor basis functions, $I_r = 1 \times 10^{-47}$ kg m^2, T = 305K.

[b]with θ_{min} as 0°

3. Methods for Conformational Analysis and the Determination of Barriers to Internal Rotation

Throughout this thesis information about molecular conformations and barriers to internal rotation obtained from long-range coupling constants will be compared to that derived from other physical methods and from theoretical calculations. What follows is a brief description of the methods to be mentioned and how the observable properties are related to the conformation or rotational barriers in the molecules studied.

a) Dynamic nuclear magnetic resonance

In the DNMR method, the resonance signal of an exchanging nucleus is measured as a function of the temperature. In the slow-exchange region the resonances of the nucleus in its possible low energy environments (conformations) are well resolved. As the temperature is increased the exchange becomes faster, the linewidth of the resonances increases and the signals eventually coalesce to the weighted average of the slow-exchange spectrum. The exchange is described by a rate constant for the transfer of magnetization between the different sites, and exact computer simulation of the experimental lineshapes yields this rate constant. The temperature dependence of the rate constant is used to determine the thermodynamic activation parameters, $\Delta G^{\ddagger}$, $\Delta H^{\ddagger}$ and $\Delta S^{\ddagger}$, the free energy, enthalpy and entropy of activation respectively. $\Delta G^{\ddagger}$ values ranging from about 20 kJ/mol to 150 kJ/mol have been determined by this method.

Figure 3

Temperature dependence of the 25.16 MHz ^{13}C spectrum of N-methylaniline in $(CH_3)_2O$. Taken from reference 44. Rate constants were obtained from spectra taken between -113°C (160K) and -126°C (147 K). The temperature dependence of the rate constant yielded $\Delta G^{\ddagger}$ = 30.3 kJ/mol, $\Delta H^{\ddagger}$ = 31.8 ± 0.8 kJ mol and $\Delta S^{\ddagger}$ = 8.4 ± 6.3 J/mol K for rotation of the methylamino group.

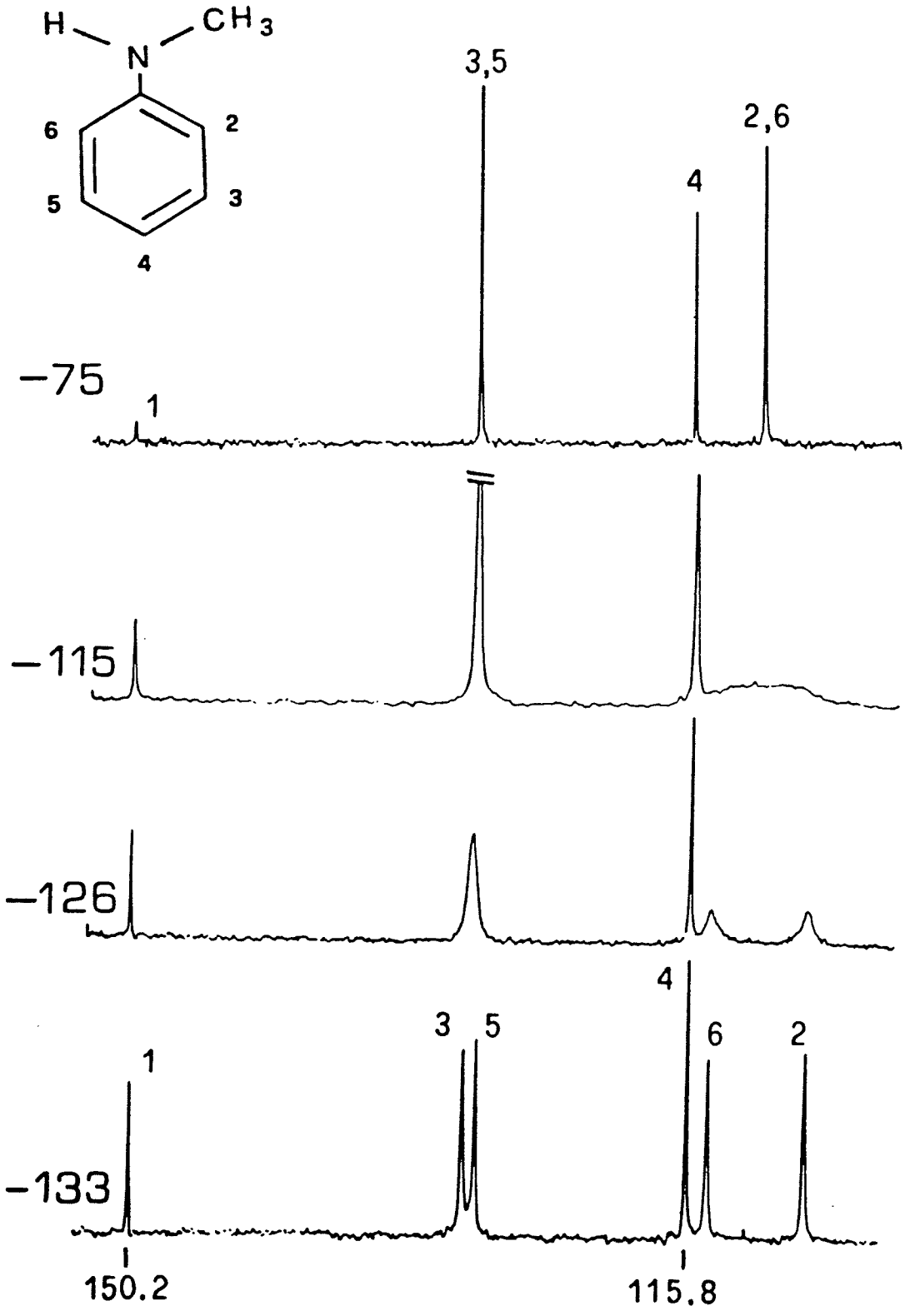
H
N
CH3
6
2
5
3
4
3,5
2,6
4
−75
1
−115
−126
4
3
5
6
2
1
−133
150.2
115.8

In symmetrically substituted benzene derivatives the resonance of the ortho and meta magnetic nuclei are normally observed. For example, in N-methylaniline[44], the ortho resonance broadens and eventually splits into two peaks as the temperature is lowered (see figure 3). N-methylaniline is a nearly planar molecule and the two peaks correspond to the ortho carbons cis and trans to the methyl group. A smaller separation of the meta carbons is also observable. The activation parameters for rotation about the C_1-N bond have been determined by computer simulation of the carbon spectrum at different temperatures.

The DNMR of organic molecules has recently been reviewed by Oki[45]. A description of the theory and experimental methods of DNMR are given in a book by Sandström[46].

b) Dipole moments and Kerr effects

Both the dipole moment, μ, and the molar Kerr constant, mK, of a molecule are dependent on its conformation. For a given molecule, the measured dipole moment or molar Kerr constant may be compared to those calculated for different conformations of the molecule. In most simple benzene derivatives one need only consider rotation about the C_1-X bond, where X is the sidechain whose conformation is being studied. Dipole moments may be calculated using molecular orbital theory or by vector additivity of group dipoles. The latter method has the disadvantage that the group dipole contributions may not be strictly additive. Dipole moments calculated by molecular orbital theory are very dependent on the level of calculation and it is often difficult to choose the appropriate basis set.

Calculation of mK requires the components of the permanent dipole moment vector, μ_i, and the elements of the polarizability tensor, b_{ij}. These are both obtained by additivity of group dipole moments and polarizabilities. Substitution of the dipole moment vector components and the elements of the diagonalized polarizability tensor into the Langevin-Born equation yields the calculated molar Kerr constant.

For a non-rigid molecule, μ and mK are averages over all possible molecular conformations. For example the molar Kerr constant can be expressed as

$$\langle mK \rangle = \frac{\int mK(\theta) \exp\left\{\frac{-V(\theta)}{RT}\right\} d\theta}{\int \exp\left\{\frac{-V(\theta)}{RT}\right\} d\theta} \qquad (53)$$

Experimental measurements actually yield the square of the dipole moment, hence $\langle \mu^2 \rangle$ must be calculated. Using equation (53) requires knowledge of the form of $mK(\theta)$ and $V(\theta)$. $V(\theta)$ can be expressed as the truncated series of equation (28). $mK(\theta)$ may take on a simple form, as for phenylalkyl ketones[47] 4 or benzyl halides[48] 5 where

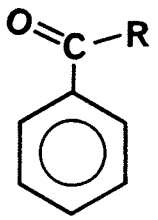

4

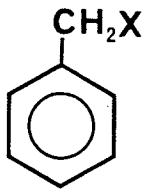

5

the functional form is given by equation (54).

$$mK(\theta) = a + b\cos^2\theta = A + B\sin^2\theta \qquad (54)$$

Therefore, in some cases, measurement of mK is equivalent to determination of $\langle \sin^2\theta \rangle$.

Where no simple functional form is calculated a weighted average over a number of conformations will yield the average value.

$$\overline{mK} = \frac{\sum_i mK(\theta_i)\exp[\frac{-V(\theta_i)}{RT}]}{\sum_i \exp[\frac{-V(\theta_i)}{RT}]} \qquad (55)$$

An iterative APL program has been written in this laboratory, by which V_2 for an assumed 2-fold barrier is varied until mK is equal to the observed mK*.

A simple description of the Kerr effect in conformational analysis has been given by Aroney[49].

c) Nematic phase nmr.

In nematic phase nmr, the solute is dissolved in a substance called a liquid crystal. The solute molecule dissolved in the nematic phase will assume a preferred orientation within the liquid crystal, which itself is ordered in the external magnetic field. Although the degree of ordering is relatively low, the environment of the solute molecules is anisotropic and dipole-dipole couplings are observed in addition to scalar spin-spin couplings. Because the diffusion of the solute in the liquid crystal is rapid enough, only intramolecular dipole-dipole interactions are observed.

The dipolar coupling D_{ij} is related to the inverse of the cube of the internuclear distance, r_{ij}, and the angle, ϕ_{ij}, between the vector

*R. Sebastian, program KERR (1984).

r_{ij} and the direction of the magnetic field, B_o, by the expression

$$D_{ij} = \frac{-h\gamma_i\gamma_j}{4\pi^2} \quad \frac{1}{2}[3\cos^2\phi_{ij} - 1]\, r_{ij}^{-3} \qquad (56)$$

In simple benzene derivatives the dipolar coupling between nuclei within the benzene ring or sidechain can be directly related to the internuclear distance. Dipolar coupling between sidechain and ring nuclei are average values,

$$D_{ij} = \frac{h\gamma_i\gamma_j}{8\pi^2} \left\langle \frac{3\cos^2\phi_{ij} - 1}{r_{ij}^3} \right\rangle \qquad (57)$$

which must be properly weighted with respect to the barrier to rotation about the C_1-X bond. Unfortunately $\langle(3\cos^2\phi_{ij})r_{ij}^{-3}\rangle$ is a complicated function of the dihedral angle θ between the sidechain and the ring, so expressions similar to equations (50) and (52) are difficult to use[50,51]. In most cases the molecule is assumed to be rigid and the dipolar coupling will yield the internuclear distances between the sidechain and ring nuclei, which can be related to the angle θ.

d) Electron diffraction

In the gas-phase electron diffraction (ed) experiment, a beam of electrons is scattered by a jet of sample vapor. The intensity of the scattered beam is a function of the scattering angle. After subtracting the background curve, which contains no molecular information, the molecular intensity curve, $I_m(s)$, is obtained (s is a parameter related to the scattering angle)

$$I_m(s) = k \sum_{i \neq j} \sum g_{ij}(s) \int P_{ij}(r) \frac{\sin(rs)}{rs}\, dr$$

where $g_{ij} = [Z - f(s)]_i[Z - f(s)]_j \cos \Delta\eta_{ij}(s)$, Z is the atomic number, f(s) is the scattering amplitude and $\Delta\eta_{ij}$ is the phase difference between waves scattered coherently by atoms i and j. $P_{ij}(r)$ is the probability density function for distance r_{ij} and is usually approximated by a Gaussian function. This curve contains information on the interatomic distances and the mean square amplitudes of atomic vibrations.

Fourier transformation of a slightly modified form of $I_m(s)$ yields the radial distribution function

$$\frac{\sigma(r)}{r} = \int_{S_{min}}^{S_{max}} I'_m(s) \exp(-ks^2) \sin(rs)\, ds \qquad (59)$$

An exponential damping factor is included to reduce the envelope effect and spurious ripples in the radial distribution curve. These are due to the restricted limits of integration imposed by the experimental data available.

The radial distribution (RD) curve is a function of distance (r) and consists of a number of peaks with maxima at distances corresponding to interatomic distances within the molecule. The intensity of each peak is a function of the atomic numbers of the atoms, the interatomic distance and the number of times that distance occurs in the molecule. Hence the strongest peaks are those for directly bonded heavy atoms.

As the size of the molecule increases, difficulty in the analysis of the RD curve arises due to overlapping peaks. Deconvoluation of overlapping peaks into Gaussian components is usually performed. The

half height peak width is related to the mean amplitudes of the vibration of the atoms.

If the molecule is assumed to be rigid or undergoing only small amplitude vibration, then the structure of the molecule may be obtained by simply simulating the $I_m(s)$ curve and the RD curve for different interatomic distances until there is best agreement.

Internal rotation may be taken into account by a Boltzmann weighting of the $I_m(s)$ and RD curves over the rotational potential. This may be done quantum mechanically or classically using equations (50) or (52) respectively. The potential function may be varied until best agreement between calculated and experimental curves is achieved. The dependence of the $I_m(s)$ and RD curves on the torsional angle, θ, is rather complex and is discussed elsewhere in more detail[52,53,54].

e) Microwave spectroscopy

There are several methods by which barriers to internal rotation may be extracted from microwave spectra. The simplest of these methods is the intensity method. In this method, the ratios of intensities, at a particular temperature, of the same rotational transition in two different torsional states of a molecule, provide a value for the energy difference between the torsional states. The intensity method assumes that the intensities, after correcting for factors such as dipole moments and statistical weight effects, are proportional to the relative populations of the two torsional states. These populations are taken to follow a Boltzman distribution so the ratios of intensities for torsional states 0 and i are given by

$$\frac{I_i}{I_o} = \frac{N_i}{N_o} = \frac{g_i}{g_o} \exp\left[\frac{-\Delta E_{o\leftarrow i}}{kT}\right] = \frac{g_i}{g_o} \exp\left[\frac{-h\nu_{o\leftarrow i}}{kT}\right] \quad (60)$$

where I are the intensities, N are the populations, g represents the degeneracy of the vibrational (torsional) state and $\nu_{0\leftarrow i}$ is the torsional frequency of the transition from state 0 to i.

For high barriers (>15 kJ/mol), internal rotation may be approximated by large amplitude motion about the potential minimum. Under this approximation sin $\theta \simeq \theta$ and the potential function can be written as

$$V(\theta) = V_n \sin^2\left(\frac{n\theta}{2}\right) \simeq V_n\left(\frac{n\theta}{2}\right)^2 \quad (61)$$

The associated Schroedinger equation is that for the harmonic oscillator and the torsional frequency may be related to the barrier height by equation (62).

$$V_n = \frac{8\pi^2 I_r}{n^2} \nu^2 \quad (62)$$

For slightly lower barriers this approximation cannot be applied and the Schroedinger equation (34) is solved for different values of V_2 until the energy difference between the two torsional levels matches that derived from experiment.

At room temperature several states may be appreciably populated and energy differences between these states may be determined. If relative energies of a number of torsional states can be determined it is possible to "map out" the shape of the potential energy curve. The part of the curve that is defined by these relative energies may be fit to a Fourier series (equation 28). Alternatively, the Schroedinger equation

may be solved for different coefficients, V_n, to obtain a least squares fit between the observed and calculated energy differences.

The intensity method suffers from experimental difficulties such as variation of spectrometer response with frequency. Experimental errors of 10-20% in the determination of energy differences are common.

Another method, called the splitting method, is used extensively for obtaining barriers to rotation for symmetric top groups.

Internal rotation and overall rotation of the molecule are coupled. This coupling yields line splittings, due to splitting of the rotational energy levels, which are a sensitive function of the potential barriers to internal rotation. Many 3-fold barriers for the rotation of methyl groups have been studied by this method, as well as several 6-fold barriers. Rotational potentials for some CF_3 and SiH_3 groups have also been studied. The details of the calculation of barriers by the splitting method are given in several monographs[43,55,56].

The splitting method has an advantage over the intensity method in that all measurements are of frequencies which can be measured to much greater accuracy than the intensity in a microwave spectrum. The two methods also differ in that they provide information about different parts of the potential energy curve. This difference is illustrated in figure 4.

For rigid planar molecules the largest principle moment of inertia is equal to the sum of the other two

$$I_C = I_A + I_B \tag{63}$$

and the inertial defect

Figure 4

Showing those parts of a potential function best determined by the splitting method (shaded area) and torsional frequency method (curvature of minimum). Taken from reference 43.

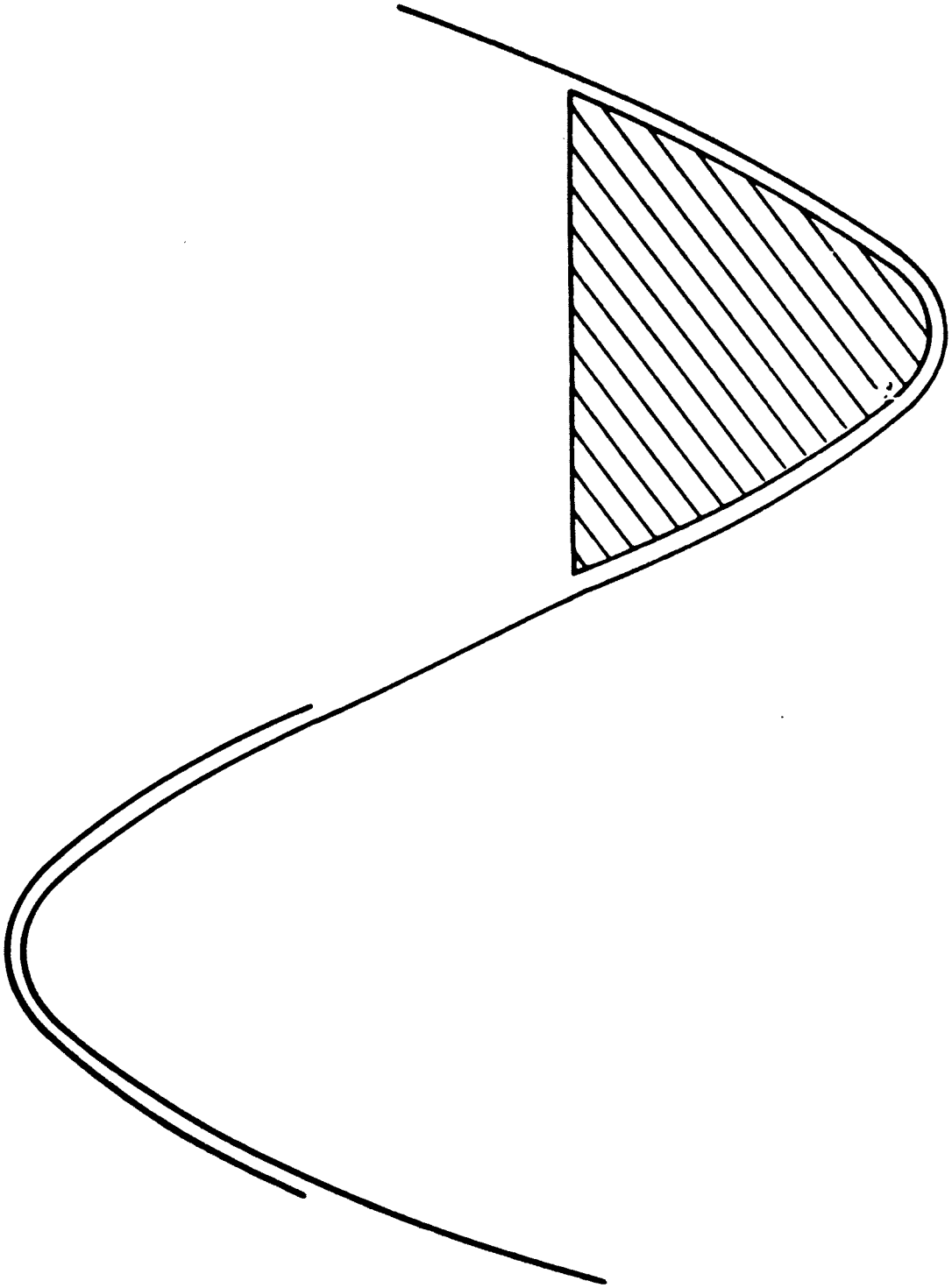

$$\Delta = I_C - I_A - I_B \qquad (64)$$

is near zero. In a molecule such as nitrobenzene the inertial defect will become non-zero with large amplitude motion (rotation) of the nitro group. If the large amplitude vibration is harmonic, the inertial defect is a linear function of the torsional quantum number, ν_t.

The difference in the inertial defect in the first excited torsional and ground states is related to the torsional frequency[57,58] by the approximate equation

$$\Delta(\nu_t = 1) - \Delta(\nu_t = 0) = -\frac{h}{2\pi^2}\nu_t \,. \qquad (65)$$

For high barriers, the torsional frequency may be substituted into equation (65). Rotational barriers in nitrobenzene[57] and phenyl difluoroborane[58] have been deduced in this way.

f) Infrared and Raman spectroscopy

Direct observation of the torsional frequency associated with high barriers to internal rotation may be observed in the far-infrared region below 200 cm^{-1}. Equation (62) can be used to obtain the potential barrier height. Occasionally transitions involving higher torsional states are observed. These transitions may be used to further improve the description of the shape of the potential function. For example the 1←0, 2←1, 3←2 and 4←3 transitions have been assigned in the far-infrared spectrum of benzaldehyde[59]. The absorptions associated with torsional vibration are weak; this makes the assignment of the torsional band

rather difficult. Raman spectroscopy is sometimes used to aid in the assignment of a weak band.

g) Molecular orbital calculations

With neglect of relativistic effects and within the Born-Oppenheimer approximation of fixed nuclei the exact wave-function, Ψ, and the energy, E, for a molecule are the solutions of the Schroedinger equation

$$\hat{H}\Psi = E\Psi \qquad (66)$$

The Hamiltonian, $\hat{H}$, is

$$\hat{H} = \sum_i (-1/2\ \nabla_i^2 - \sum_N \frac{Z_N}{r_{N_i}}) + \sum_{i<j} \frac{1}{r_{ij}} + \sum_{M<N} \frac{Z_M Z_N}{r_{MN}}$$

where i and j are summed over the electrons and M and N are summed over the nuclei. The equation cannot be solved exactly for systems of more the one electron. The wave-function is approximated by a product of one-electron molecular orbitals (MO's)

$$\Psi(1, 2, \ldots n) = \chi_1(1)\ \chi_2(2) \ldots \chi_n(n)$$

$$= \prod_i^n \chi_i(i)$$

This is known as the Hartree product. The molecular orbitals are functions of space (x, y, z) and spin (α,β) variables. Since the Hamiltonian is spin independent the MO's are written as products of spin and space functions, eg. $\chi_1(1) = \psi_1(1)\alpha(1)$. The Hartree product does

not satisfy the antisymmetry requirement with respect to exchange of two electrons (Pauli principle). The wave function may be antisymmetrized by representing it as a Slater determinant

$$\Psi = \frac{1}{\sqrt{n!}} \begin{vmatrix} \psi_1(1)\alpha(1) & \psi_1(1)\beta(1)\psi_2(1)\alpha(1)\ldots. \; \psi_{n/2}(1)\beta(1) \\ \psi_1(2)\alpha(2) & \psi_1(2)\beta(2)\psi_2(2)\alpha(2)\ldots. \\ \cdot & \\ \cdot & \\ \cdot & \\ \psi_1(n)\alpha(n) & \psi_n(n)\beta(n)\psi_2(n)\alpha(n)\ldots.\psi_{n/2}(n)\beta(n) \end{vmatrix}$$

$$= \frac{1}{\sqrt{n!}} \; |\chi_1\chi_2\cdots\chi_n| \qquad (69)$$

For a closed-shell system of 2n electrons with paired spins, the best orbitals are the solutions of the Hartree-Fock (HF) or Self-Consistent-Field (SCF) equations,

$$\hat{F}\psi_i = \varepsilon_i\psi_i \qquad (70)$$

The Hartree-Fock equations are a set of n non-linear integro-differential equations which can be solved directly only for atoms. The molecular orbitals may be expanded in terms of atomic orbitals. The individual orbitals ψ_i can be written

$$\psi_i = \sum_{\mu=1}^{N} C_{\mu i}\,\phi_\mu \qquad (71)$$

where $C_{\mu i}$ are the molecular orbital expansion coefficients and ϕ_μ are the atomic orbitals. This is the LCAO (Linear Combination of Atomic Orbitals) - MO method. The corresponding LCAO-MO-SCF equations are the Roothaan equations

$$\underline{\underline{F}}\,\underline{\underline{C}} = \varepsilon \underline{\underline{S}}\,\underline{\underline{C}} \tag{72}$$

where $\underline{\underline{F}}$ is the Fock matrix, $\underline{\underline{C}}$ is the matrix of expansion coefficients and $\underline{\underline{S}}$ is the overlap matrix. For the molecular orbital, ψ_i with one-electron energy ε_i, the elements of the N x N overlap matrix, $\underline{\underline{S}}$, are

$$S_{\mu\nu} = \int \phi_\mu^*(1)\ \phi_\nu(1)\ dx_1\ dy_1\ dz_1 \tag{73}$$

The elements of the Fock operator, $\underline{\underline{F}}$, are

$$F_{\mu\nu} = H_{\mu\nu}^{core} + \sum_\lambda \sum_\sigma P_{\lambda\sigma}[(\mu\nu|\lambda\sigma) - 1/2(\mu\lambda|\nu\sigma)] \tag{74}$$

where

$$H_{\mu\nu}^{core} = \int \phi_\mu^*(1)\ \hat{H}^{core}(1)\ \phi_\nu(1)\ dx_1\ dy_1\ dz_1 \tag{75}$$

and

$$\hat{H}_{(1)}^{core} = -1/2\ \nabla_1^2 - \sum_{A=1}^{M} \frac{Z_A}{r_{1A}} \tag{76}$$

The quantity $(\mu\nu|\lambda\sigma)$ is the two electron repulsion integral

$$(\mu\nu|\lambda\sigma) = \iint \phi_\mu^*(1)\ \phi_\nu(1)\ \frac{1}{r_{12}}\ \phi_\lambda^*(2)\ \phi_\sigma(2)\ dx_1 dy_1 dz_1 dx_2 dy_2 dz_2 \tag{77}$$

$P_{\lambda\sigma}$ are elements of the density matrix

$$P_{\lambda\sigma} = 2 \sum_{i=1} c_{\lambda i}^* c_{\sigma i} \tag{78}$$

The electronic energy is given by

$$E^e = \frac{1}{2} \sum_\mu \sum_\nu P_{\mu\nu}(F_{\mu\nu} + H_{\mu\nu}^{core}) \tag{79}$$

Adding the nuclear repulsion energy,

$$E^n = \sum_{A<B}^{M} \sum \frac{Z_A Z_B}{R_{AB}}\ , \tag{80}$$

which is summed over all combinations of atoms A and B, yields the total energy.

The Roothaan equations do not form a system of linear equations. An iterative method must be used to solve these equations. A flow chart for the solution of the Roothaan equations is given in figure 5.

The atomic orbitals, ϕ, are usually represented by Slater-type atomic orbitals (STO's). Unfortunately the integrals involving STO's are difficult to evaluate both analytically and numerically; the two-electron four-centered integrals are particularly difficult to evaluate. An alternative is the gaussian-type atomic function. These functions have the advantage that all integrals may be analytically evaluated with relative ease. The gaussian orbitals provide a less satisfactory description of the atomic orbitals, but this may be partially overcome by taking linear combinations of gaussian type orbitals

$$\phi_\mu = \sum_{k=1}^{K} d_{k\mu}\, g_x(\alpha_k, r) \tag{81}$$

$$g_x(\alpha, r) = N \times \exp(-\alpha r^2) \tag{82}$$

where N is the normalization constant and x specifies the type of gaussian function (S, P_x, P_y, P_z, d_x2 etc.). The disadvantage of having to evaluate a larger number of integrals (K times as many) is greatly offset by the ease of integral calculation. Note that in equation (81), $d_{k\mu}$ and α_k are not varied in the SCF calculation; they have been preset to values that will best describe the corresponding Slater-type orbital. It is the coefficient, $C_{\mu i}$, in equation (71) that is varied. At the Hartree-Fock level there are three groups of basis sets commonly

Figure 5

Sequence of program steps required for the SCF solution of the Roothaan equations for a closed-shell system. Taken from reference 60.

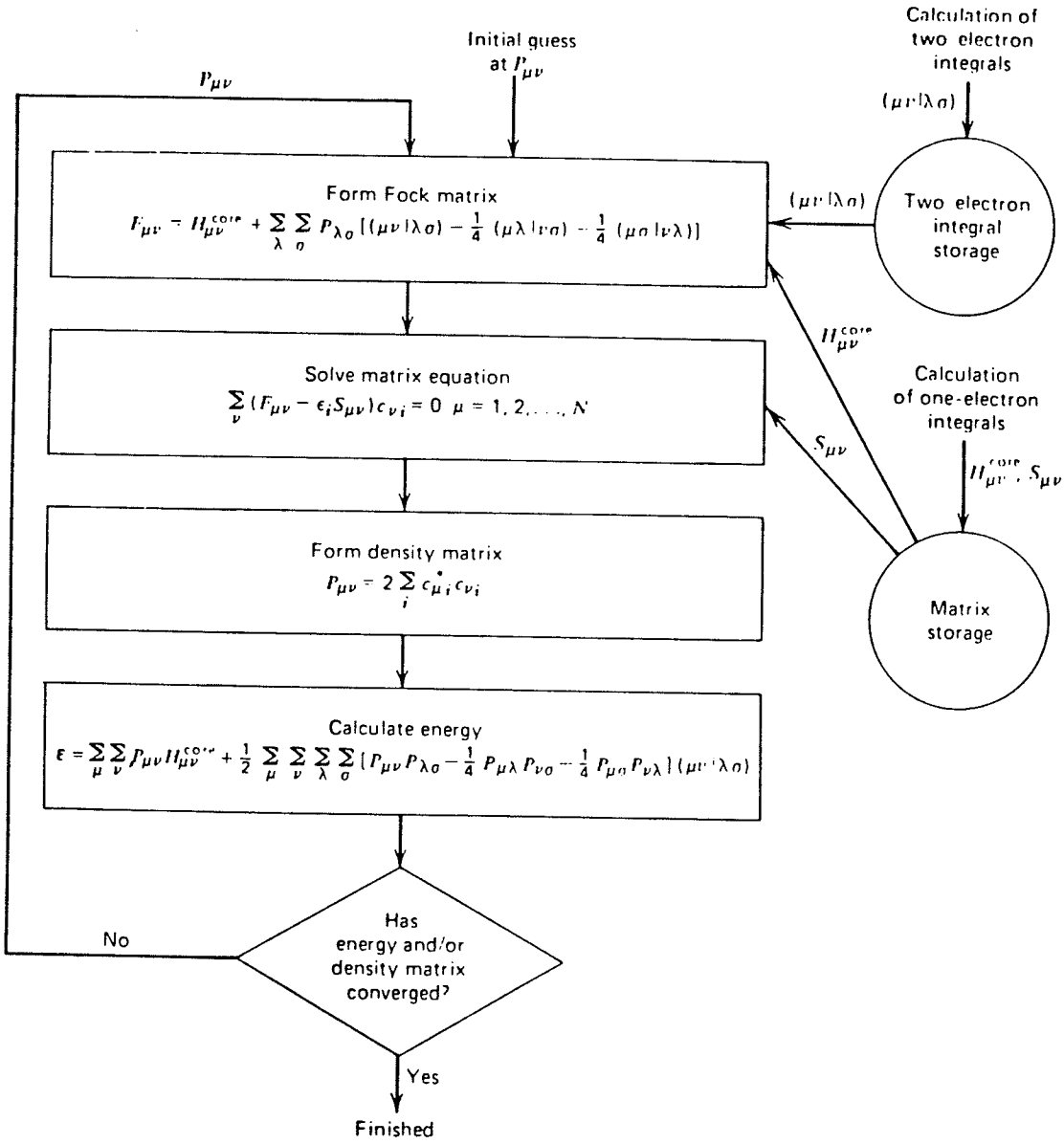
Initial guess at $P_{\mu\nu}$
$P_{\mu\nu}$
Calculation of two electron integrals
$(\mu\nu|\lambda\sigma)$
Form Fock matrix
$F_{\mu\nu} = H_{\mu\nu}^{core} + \sum_{\lambda}\sum_{\sigma} P_{\lambda\sigma}[(\mu\nu|\lambda\sigma) - \frac{1}{4}(\mu\lambda|\nu\sigma) - \frac{1}{4}(\mu\sigma|\nu\lambda)]$
$(\mu\nu|\lambda\sigma)$
Two electron integral storage
$H_{\mu\nu}^{core}$
Solve matrix equation
$\sum_{\nu}(F_{\mu\nu} - \epsilon_i S_{\mu\nu})c_{\nu i} = 0 \quad \mu = 1, 2, \ldots, N$
$S_{\mu\nu}$
Calculation of one-electron integrals
$H_{\mu\nu}^{core}, S_{\mu\nu}$
Form density matrix
$P_{\mu\nu} = 2\sum_{i} c_{\mu i}^{*} c_{\nu i}$
Matrix storage
Calculate energy
$\epsilon = \sum_{\mu}\sum_{\nu} P_{\mu\nu} H_{\mu\nu}^{core} + \frac{1}{2}\sum_{\mu}\sum_{\nu}\sum_{\lambda}\sum_{\sigma}[P_{\mu\nu}P_{\lambda\sigma} - \frac{1}{4}P_{\mu\lambda}P_{\nu\sigma} - \frac{1}{4}P_{\mu\sigma}P_{\nu\lambda}](\mu\nu|\lambda\sigma)$
Has energy and/or density matrix converged?
No
Yes
Finished

in use; minimal basis sets, split valence basis sets and polarization basis sets.

Minimal basis sets, designated STO-KG, simply have every Slater-type atomic orbital expanded as K gaussian-type orbitals. In the split valence basis set, designated K-LMNG, the inner shell orbitals are described by K gaussians and the valence shell orbitals are described by L + M + N gaussians split into a set of L, M and N gaussians where each set has a different exponential, α, which determines how diffuse the function is. Not splitting the inner shell functions has some effect on the total energy, but little effect on most chemical properties. An example of a split valence basis is the 6-31G basis set, where each inner shell orbital is described by six gaussians and each outer (valence) shell orbital is described by 4 gaussians split into a group of three with exponential factor α' and one with exponential factor α''. Some commonly used split valence basis sets are 3-21G, 4-31G, 6-31G and 6-311G.

Polarization basis sets have d-type functions added to heavy atoms (Li-F) and/or p-type functions added to hydrogen or helium. The commonly used polarization functions are 3-21G*, 6-31G* and 6-31G**. The symbol * denotes that a 3d orbital is added to a heavy atom (Li-F) and the symbol ** denotes that 3d orbitals have been added to Li-F and 2p orbitals have been added to hydrogen atoms.

At the Hartree-Fock level, ab initio molecular orbital theory does not take correlation between the motions of electrons with opposite spin into account. Correlation between electrons of the same spin is only partially accounted for. Therefore the correlation energy is the

difference between the exact (nonrelativistic) and Hartree-Fock energies,

$$E_{(exact)} = E_{(Hartree-Fock)} + E_{(correlation)} \qquad (83)$$

Computations involving electron correlation are demanding, particularly of computer disk space. Hence, electron correlation has only been taken into account in the calculation of barrier to internal rotation for small molecules. These calculations show that inclusion of electron correlation usually has little effect on the barrier height[60,61].

Geometry optimization of a molecule requires the evaluation of the energy gradient, i.e. the negative forces on each nucleus. This is done by analytical differentiation of the corresponding energy expressions. Differentiation of the total energy obtained from the solution of the Roothaan equations, with respect to any nuclear coordinate, R, yields equation (84).

$$\frac{\partial E}{\partial R} = \sum_{\mu}\sum_{\nu} P_{\mu\nu} \frac{\partial H^{core}_{\mu\nu}}{\partial R} + \frac{1}{2}\sum_{\mu}\sum_{\nu}\sum_{\lambda}\sum_{\sigma} P_{\mu\nu}P_{\lambda\sigma}\left[\frac{\partial}{\partial R}(\mu\nu||\lambda\sigma)\right] + \frac{\partial E^{nr}}{\partial R} - \sum_{\mu}\sum_{\nu} w_{\mu\nu}\frac{\partial S_{\mu\nu}}{\partial R} \qquad (84)$$

where the two-electron interals $(\mu\nu||\lambda\sigma)$ are defined

$$(\mu\nu||\lambda\sigma) = \iint \phi^{*}_{\mu}(1)\,\phi^{*}_{\lambda}(2)\,\frac{1}{r_{12}}\,[\phi_{\nu}(1)\phi_{\sigma}(2) - \phi_{\sigma}(1)\phi_{\nu}(2)]\,dx_1 dx_2 dy_1 dy_2 dz_1 dz_2 \qquad (85)$$

and the energy-weighted density matrix, w, is given as

$$w_{\mu\nu} = \sum_{i}^{occ} \epsilon_i c^{*}_{\mu i} c_{\nu i} \cdot \qquad (86)$$

ϵ_i are the one-electron energies and the summation is over all occupied orbitals. The evaluation of energy gradients has been treated in greater detail in a review by Pulay[62]. Figure 6 shows the program steps involved in the optimization of a molecular geometry for a particular basis set.

One of the criteria for geometry optimization is that the energy gradient must be below a small threshold value, that is, the energy is a minimum with respect to the molecular geometry parameters. Of course, for a potential energy surface the gradient vanishes not only for a minimum but also for maxima and saddle points. The evaluation of second derivatives is necessary in order to distinguish between these extrema.

Now the calculation of a barrier to internal rotation becomes straightforward. Two parts of a molecule are rotated about a bond, the dihedral angle is held constant while the bond angles and bond lengths for the rest of the molecule are optimized. This is done for a number of dihedral angles. The energies may then be fit to a function of the dihedral angle, θ. A truncated Fourier series is usually used (see equation 26).

Figure 6

Sequence of execution of program modules resulting in the optimization of molecular geometry for a particular basis set. Taken from reference 60.

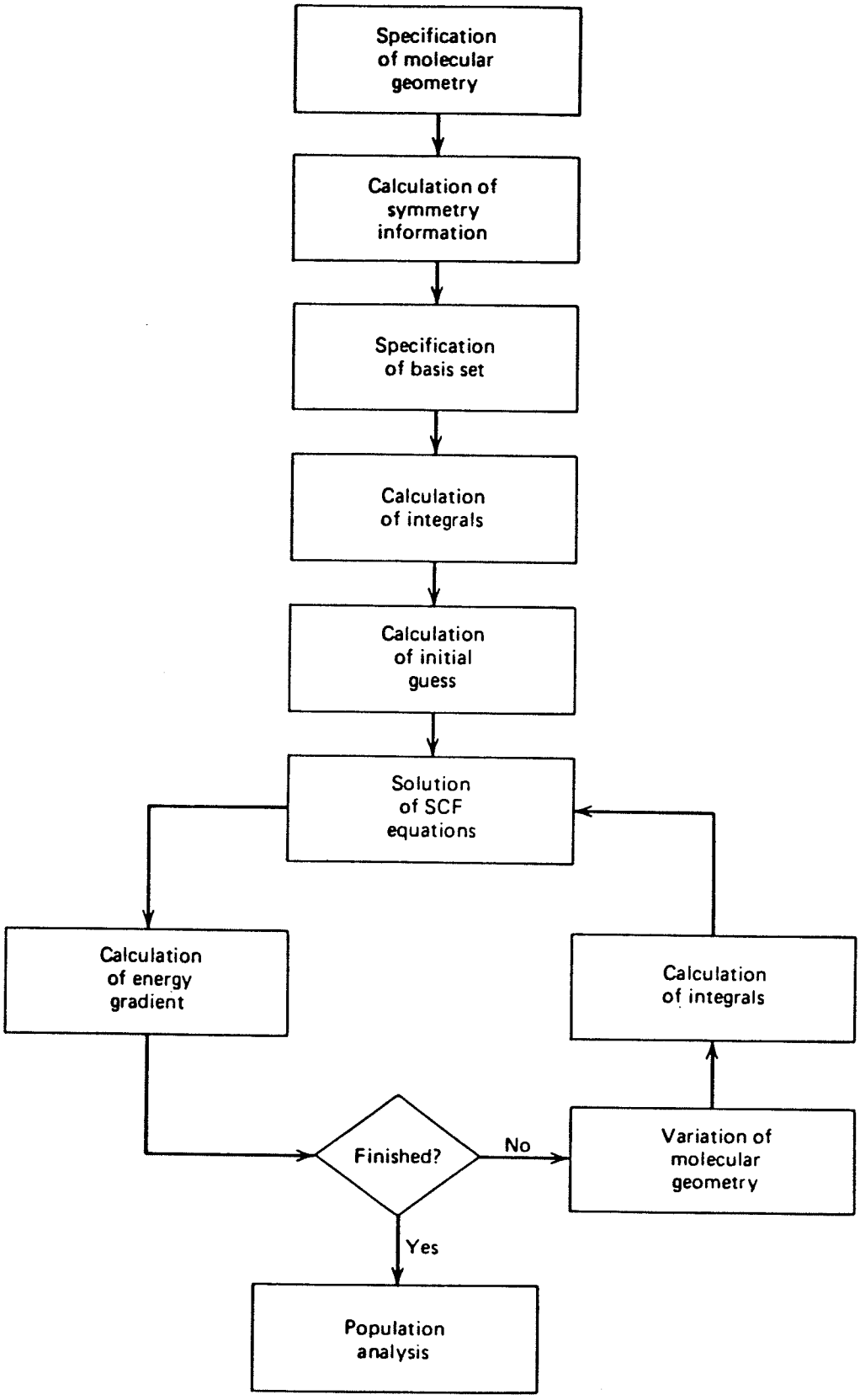
Specification of molecular geometry
Calculation of symmetry information
Specification of basis set
Calculation of integrals
Calculation of initial guess
Solution of SCF equations
Calculation of energy gradient
Calculation of integrals
Finished?
No
Variation of molecular geometry
Yes
Population analysis

4. Introduction to the Problem

Much work has been done on the mechanisms and conformational dependences of spin-spin coupling constants between the sidechain protons and ring protons or fluorine nuclei in benzene derivatives and on their use for the determination of molecular conformations and barriers to internal rotation.

It is the intent of the work described in this thesis to establish the conformational dependences of long-range spin-spin couplings between side-chain ^{13}C nuclei and ring nuclei in some benzene derivatives and to apply the stereospecificities of these couplings to the determination of molecular conformations and internal rotational barriers. Special emphasis will be placed on long range $^{13}C,^{13}C$ couplings.

B. EXPERIMENTAL METHODS

1. Preparation of Compounds

All ^{13}C enriched precursors were purchased from MSD isotopes and were of 95 atom % or higher isotopic purity. The following describes typical syntheses performed as part of this thesis work:

a) Synthesis of ^{13}C enriched thioanisoles.

About 0.1 g of sodium metal was added to 10 ml of absolute methanol. 2 mmoles of the thiophenol were added. Then 2.3 mmoles (0.33 g) of $^{13}CH_3I$ were added with stirring. The solution was stirred for 15 min and water was added to give a cloudy suspension. The mixture was extracted with ether and the ether layer was separated, dried over anhydrous $MgSO_4$, filtered and rotary evaporated. The synthesis of selenoanisoles from selenophenol (benzeneselenol) was identical to that above. Ethylations used 0.36 g (2.3 mmoles) of $CH_3{}^{13}CH_2I$.

b) Synthesis of ^{13}C enriched anisoles.

4.0 mmoles of the phenol were dissolved in 5 ml of dry acetone. 0.8 g of dried K_2CO_3 was added and the mixture was stirred. Then 0.5 g of $^{13}CH_3I$ in 5 ml of dry acetone was added and the mixture was stirred overnight. Water was added and the cloudy suspension was extracted with ether, the ether extract was dried over anhydrous $MgSO_4$, filtered and rotary evaporated.

c) Synthesis of ^{13}C enriched N-methylanilines.

0.010 moles of the aniline and 0.010 moles (1.46 g) of triethylamine were dissolved in 15 ml of CH_2Cl_2 in a 50 ml round bottom

flask. A solution of 0.011 moles (2.20 g) trifluoroacetic anhydride in 10 ml of CH_2Cl_2 was added to the flask with stirring and cooling in a water-ice bath. The yields of trifluoroacetanilides were about 75 to 80%.

2.0 mmoles of the trifluoroacetanilide and 4 mmoles (0.6 g) of $^{13}CH_3I$ were dissolved in 10 ml of acetone. The solution was heated almost to reflux. Then 0.1 g of dry powdered KOH was added and the mixture was refluxed for 10 min. The acetone was evaporated off under vacuum and 10 ml of water was added. This solution was refluxed for 15 min. The product was extracted with ether. The ether solution was dried over anhydrous $MgSO_4$, filtered and rotary evaporated.

d) Synthesis of ^{13}C enriched benzyl cyanides.

2.5 mmoles of the benzyl bromide or chloride were dissolved in 10 ml of acetone. 3.8 mmoles (0.25 g) of $K^{13}CN$ in 15 ml of water were added with stirring. This was refluxed for about 1 hour. About 50 ml of water were added and the product was extracted with ether. The ether solution was dried over $MgSO_4$, filtered and rotary evaporated.

e) Synthesis of ^{13}C enriched α-methyl benzyl alcohols and acetophenones.

A Grignard reagent was made with 0.2 g (7 mmoles) of Mg in 2 ml of ether and adding 1 g (7 mmoles) of $^{13}CH_3I$ in 1 ml of ether. The reaction started after a minute or two. After the reaction was complete, the Grignard reagent was transferred to a second flask. This flask was placed in an ice bath and a solution of 6 mmoles of the benzaldehyde in 5 ml of ether was added dropwise over a period of 10

min. A yellow precipitate formed and then redissolved. This mixture was refluxed for 1 hour. During the reflux a pale yellow precipitate of the magnesium salt formed. About 10 ml of 10% HCl was added and the salt dissolved with bubbling. More ether was added and the two layers were shaken and separated. The ether layer was washed with about 10 ml of saturated sodium bisulfite solution, dried over $MgSO_4$, filtered and rotary evaporated.

About 1 g of pyridinium chlorochromate was suspended in 5 ml of CH_2Cl_2 and the alcohol product in 5 ml of CH_2Cl_2 was added with stirring. This mixture was stirred for over two hours. The orange crystals of pyridinium chlorochromate soon turned to dark brown goo. The CH_2Cl_2 solution was decanted and the blackish tar was washed twice with ether. The combined extracts were dried over $MgSO_4$, filtered through some chromatography-silica and rotary evaporated to give a greenish-brown liquid. This liquid was distilled to give the acetophenone.

f) Synthesis of methyl phenyl telluride.

0.5 g of diphenyl ditelluride were dissolved in 5 ml methanol and 2 ml benzene (didn't quite dissolve). 0.5 of $NaBH_4$ in 5 ml 1N (5 wt%) NaOH were added dropwise. There was effervescence upon addition. The undissolved diphenyl ditelluride went into solution and the solution eventually turned colorless then slightly cloudy. The addition of $NaBH_4$ solution was stopped. 0.5 g of $^{13}CH_3I$ in about 1 ml methanol were added. The solution was stirred for ½ hour then poured over crushed ice and 10% HCl was added. A methylene chloride extract of this mixture was

dried over anhydrous $MgSO_4$, filtered and rotary evaporated to give a light brown liquid.

2. Sample Preparation

Solutions of the compound were prepared in a number of different solvents (concentrations and solvents for each solution are given in tables 2-20). Samples for ^{13}C experiments were transferred to 10 mm od tubes together with 10 drops of TMS. Samples for proton experiments were transferred to 5 mm od tubes together with one drop of TMS. A drop of C_6F_6 was also added if ^{19}F spectra were to be recorded. These samples were then degassed using the freeze-pump-thaw technique. At least three degassing cycles were performed before the nmr tubes were flame-sealed.

3. Spectroscopic Method

All nmr spectra were taken on an AM300 Bruker spectrometer at a probe temperature of 300K. For proton decoupled ^{13}C experiments, typically 128 to 256 FIDs were accumulated. For proton coupled ^{13}C experiments 400 to 2800 FIDs were accumulated. Acquisition times were 20s to 30s; for example, a spectral width of 100 Hz was assigned to a 4K data region, to give an acquisition time of 20.48 s.

Proton and ^{19}F spectra were usually the results of 8 to 32 accumulated FIDs with acquisition times of 25s to 40s.

Some FIDs were zero-filled to twice the original data region before Fourier transformation, using a small amount of gaussian multiplication. Line widths at half height were typically 0.05 to 0.25 Hz.

4. Computations

Spectral analysis and simulations were performed with the program NUMARIT[63] in the iterative and non-iterative modes; the program was coupled to a plotting routine.

Ab initio molecular orbital calculations utilized the computer programs MONSTERGAUSS[64], GAUSSIAN 80[45] and GAUSSIAN 82[66]. The gradient and Murtagh-Sargent methods were used for geometry optimization. Calculations were performed at the STO-3G, 4-21G, 4-31G and 6-31G levels.

INDO MO FPT[67] computations of coupling constants utilized the geometries optimized at the STO-3G level. All curves were statistically fit using the SAS nonlinear regression procedure, NLIN. SAS/GRAPH programs were written in order to plot curves and molecular structures on a XEROX laser printer.

All computations employed Amdahl 470/V8, 580/5850 or 5870 systems.

"There is an analogy between complex nuclei and complex molecules, but there is a fundamental difference too; for molecules the first principles with which we cannot calculate their properties are far better known."

Hendrik Casimir

C. EXPERIMENTAL RESULTS

In the following tables, all coupling constants (J) are given in Hz. Proton and fluorine-19 chemical shifts (ν) are also given in Hz, with respect to internal TMS and C_6F_6, respectively. All ^{13}C chemical shifts (δ) are in ppm with respect to internal TMS. In all cases, coupling constants between carbon-13 nuclei are set equal to the corresponding splittings observed in the ^{13}C nmr spectra.

Uncertainties in carbon-13 shifts and $^{13}C,^{13}C$ coupling constants are taken as less than 0.01 ppm and 0.01 Hz, respectively, unless otherwise stated. The uncertainties are based on the reproducibility of the spectra of several of the compounds studied and on comparisons between spectral parameters with those previously measured in this laboratory.

Signs of coupling constant were determined by double resonance experiments. Signs in parentheses are taken from closely related compounds. Uncertainty in the sign of a coupling constant is shown by the symbol ±. Proton, carbon-13 and fluorine-19 spectra were taken on a Bruker AM300 spectrometer at 300.135 MHz, 75.486 MHz and 282.363 MHz, respectively.

Table 2

^{13}C nmr chemical shifts and $^{13}C,^{13}C$ coupling constants for some symmetrically substituted thioanisoles.

Parameter	H[a]	2,6-diF[b]	2,6-diCl[c]	3,5-diCl[d]
$\delta(S^{13}CH_3)$	15.45	17.78	18.32	14.80
$\delta(C_1)$	139.57	113.59	135.16	114.14
$\delta(C_2)$	127.13	163.68	141.42	124.55
$\delta(C_3)$	129.68	112.59	129.71	135.59
$\delta(C_4)$	125.66	130.79	131.32	125.09
$^2J(^{13}C,C_1)$	(-)1.38	(-)1.76	(-)2.11	-1.39
$^3J(^{13}C,C_2)$	(+)2.95	(+)1.29	(+)1.33	+3.25
$^4J(^{13}C,C_3)$	(+)0.28	(-)0.55	-0.69	(+)0.42
$^5J(^{13}C,C_4)$	(+)0.20	(+)0.63	+0.77	+0.11

[a] 2.7 mol% in acetone-d_6.

[b] 2.8 mol% in acetone-d_6. The couplings to fluorine are $^1J(C_2,F_2)$ = −246.10, $^2J(C_1,F)$ = 21.98, $^2J(C_3,F) + {}^4J(C_5,F)$ = 22.70, $^3J(C_2,F_6)$ = 5.26, $^3J(C_4,F)$ = 10.36, $^4J(^{13}C,F)$ = 3.57.

[c] 2.6 mol% in acetone-d_6.

[d] 3.4 mol% in acetone-d_6.

Table 2...cont'd...

	4-OCH_3[e]	4-CH_3[f]	4-F[g]	4-Cl[h]
$\delta(S^{13}CH_3)$	17.65	16.06	16.56	15.58
$\delta(C_1)$	130.11	135.90	134.83	138.59
$\delta(C_2)$	130.64	127.73	129.74	128.52
$\delta(C_3)$	115.46	130.38	116.58	129.57
$\delta(C_4)$	159.20	135.51	161.01	130.92
$^2J(^{13}C,C_1)$	(-)1.46	(-)1.40	(-)1.42	(-)1.38
$^3J(^{13}C,C_2)$	(+)2.34	(+)2.74	(+)2.70	(+)2.95
$^4J(^{13}C,C_3)$	$\leq$0.10	(+)0.14	$\leq$0.10	(+)0.25
$^5J(^{13}C,C_4)$	(+)0.41	(+)0.31	(+)0.33	(+)0.26

[e] 3.5 mol% in acetone-d_6. $^7J(S\underline{C}H_3, O\underline{C}H_3) \leq 0.05$ Hz.

[f] 3.0 mol% in acetone-d_6. $^6J(S\underline{C}H_3, \underline{C}H_3) = 0.10$ Hz.

[g] 4.0 mol% in acetone-d_6. The couplings to fluorine are $^1J = 142.71$, $^2J = 22.11$, $^3J = 7.88$, $^4J = 3.17$, $^6J = 0.47$.

[h] 5.1 mol% in acetone-d_6.

Table 2...cont'd...

	4-t-Bu[i]	4-Br[j]	4-NO_2[k]	4-NH_2[l]
$\delta(S^{13}CH_3)$	15.83	15.43		19.18
$\delta(C_1)$	135.88	138.24		
$\delta(C_2)$	127.29	138.77	126.04	132.24
$\delta(C_3)$	126.53	132.50	124.54	115.80
$\delta(C_4)$	148.66	118.62		
$^2J(^{13}C,C_1)$	(-)1.40	(-)1.40		
$^3J(^{13}C,C_2)$	(+)2.78	(+)2.97	(+)3.35	(+)1.94
$^4J(^{13}C,C_3)$	(+)0.18	(+)0.27	(+)0.47	<0.10
$^5J(^{13}C,C_4)$	(+)0.28	(+)0.21		

[i] 5.3 mol% in acetone-d_6. [6] $^6J(S^{13}\underline{C}H_3, \underline{C}(CH_3)_3) = 0.070$ Hz.

[j] 4.5 mol% in acetone-d_6.

[k] ca 2 mol% in acetone-d_6.

[l] ca 2 mol% in acetone-d_6.

Table 2...cont'd...

	3,5-diCl-4-OCH_3[m]	3,5-diCl-4-OH[n]	H[o]
$\delta(S^{13}CH_3)$	15.78		15.88
$\delta(C_1)$			139.04
$\delta(C_2)$	127.13	128.29	126.75
$\delta(C_3)$	130.22		128.72
$\delta(C_4)$	150.38		124.87
$^2J(^{13}C,C_1)$			(-)1.42
$^3J(^{13}C,C_2)$	(+)3.01	(+)2.67	(+)2.93
$^4J(^{13}C,C_3)$	(+)0.23		(+)0.24
$^5J(^{13}C,C_4)$	(+)0.18		(+)0.22

[m] 3.5 mol% in acetone-d_6. $^7J(S\underline{C}H_3, O\underline{C}H_3)$ = 0.093 Hz.

[n] 2.0 mol% in acetone-d_6.

[o] 7.0 mol% in CS_2/C_6D_{12}.

Table 3

Long range coupling from ring fluorine nuclei and protons to the methyl carbon-13 nucleus in 2,6-difluorothioanisole

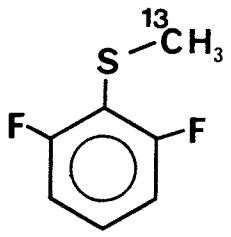

$^{4}J(^{13}C,F_2)$ = ±3.57(2)

$^{5}J(^{13}C,H_3)$ = (+)0.212(3)

$^{6}J(^{13}C,H_4)$ = (-)0.421(2)

Couplings are the averages over the four multiplets of the methyl quartet. Numbers in parentheses are the standard deviations in the last decimal place.

Table 4

^{13}C chemical shifts and $^{13}C,^{13}C$ coupling constants for some symmetrically substituted ethyl phenyl sulfides.

parameter	H[a]	4-CH_3[b]	4-OCH_3[c]
$\delta(^{13}CH_2)$	27.61	28.34	29.85
$\delta(CH_3)$	14.63	14.76	14.91
$\delta(C_1)$	137.71	133.84	127.32
$\delta(C_2)$	129.43	130.37	133.64
$\delta(C_3)$	129.72	130.39	115.36
$\delta(C_4)$	126.41	136.46	159.87
$^1J(^{13}\underline{C},\underline{C}H_3)$	35.05	35.40	35.46
$^2J(^{13}C,C_1)$	(-)1.40	(-)1.41	(-)1.46
$^3J(^{13}C,C_2)$	(+)2.20	(+)2.05	(+)1.68
$^4J(^{13}C,C_3)$	<0.05	(-)0.09	(-)0.23
$^5J(^{13}C,C_4)$	(+)0.34	(+)0.43	(+)0.54

[a] 2.4 mol% in acetone-d_6.

[b] 2.5 mol% in acetone-d_6. $\delta(4\text{-}CH_3)$ = 20.91 ppm. $^6J(\underline{C}H_2,\underline{C}H_3) = \pm 0.15$ Hz.

[c] 3.1 mol% in acetone-d_6. $\delta(O\underline{C}H_3)$ = 55.51 ppm. $^7J(\underline{C}H_2,O\underline{C}H_3) < 0.05$ Hz.

Table 5

^{13}C nmr chemical shifts and $^{13}C,^{13}C$ coupling constants for some ortho substituted thioanisoles.

parameter	2-OH[a]	2-OH[b]	2-NH_2[c]	2-F[d]
$\delta(S^{13}CH_3)$	19.70	16.11	17.56	14.85
$\delta(C_1)$	120.72	124.60	119.63	126.64
$\delta(C_2)$	156.93	155.92	147.30	160.71
$\delta(C_3)$	115.04	115.44	114.38	115.76
$\delta(C_4)$	130.76	128.00	128.96	127.53
$\delta(C_5)$	120.54	121.07	118.33	125.69
$\delta(C_6)$	134.94	129.99	136.16	128.77
$^2J(^{13}C,C_1)$	(-)1.75	(-)1.42	(-)1.72	(-)1.35
$^3J(^{13}C,C_2)$	(+)1.13		(+)1.10	(+)1.63
$^4J(^{13}C,C_3)$	(-)0.77	<0.5	(-)0.65	±0.09
$^5J(^{13}C,C_4)$	(+)0.91	(+)0.46	(+)0.76	(+)0.29
$^4J(^{13}C,C_5)$	(-)0.76	<0.1	(-)0.59	±0.23
$^3J(^{13}C,C_6)$	(+)1.26	(+)2.99	(+)1.68	

	2-OCH_3[e]	2-Br[f]	2-OH-α-CH_3[g]
$\delta(S^{13}CH_3)$	14.23	15.38	14.90
$\delta(C_1)$	128.17	140.82	118.72
$\delta(C_2)$	157.10	121.68	157.73
$\delta(C_3)$	109.66	133.30	115.00
$\delta(C_4)$	126.36	126.46	131.05

$\delta(C_5)$	121.90	128.91	120.39
$\delta(C_6)$	126.34	126.27	136.16
$^2J(^{13}C,C_1)$	(-)1.25	(-)1.11	(-)1.64
$^3J(^{13}C,C_2)$	(+)1.38	(+)2.21	(+)1.01
$^4J(^{13}C,C_3)$	<0.05	<0.1	(-)0.72
$^5J(^{13}C,C_4)$	(+)0.25	<0.05	(+)0.86
$^4J(^{13}C,C_5)$	±0.36	(+)0.60	(-)0.74
$^3J(^{13}C,C_6)$	(+)4.01	+4.19	(+)1.05

[a] 4.0 mol% in CCl_4/C_6D_{12}.

[b] 5.2 mol% in acetone-d_6. All observed lines were broad.

[c] 3.6 mol% in CCl_4/D_6D_{12}.

[d] 5.0 mol% in acetone-d_6. The couplings to ^{19}F are $^6J(^{13}C,F) = 2.328$, $^2J(C_1,F) = 17.08$. $^1J(C_2F) = -242.25$. $^2J(C_3F) = 21.59$, $^3J(C_4F) = 7.73$, $^4J(C_5F) = 3.53$. The splitting of C_6 due to $^4J(C_6F)$ and $^3J(^{13}C,C_6)$ were of similar magnitude and could not be distinguished.

[e] 4.2 mol% in acetone-d_6. $^5J(S\underline{C}H_3,O\underline{C}H_3) \leq 0.05$ Hz.

[f] 3.8 mol% in acetone-d_6.

[g] 5.0 mol% in CCl_4/C_6D_{12}. $^1J(\underline{C}H_2\underline{C}H_3) = 34.9$.

Table 6

^{1}H nmr spectral parameters for a 4.5 mol% solution of 2-hydroxy-thioanisole-^{13}C in CCl_4/C_6D_{12}.

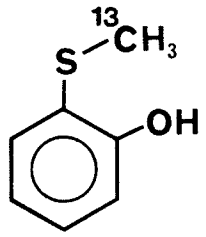

$\nu(^{13}C)$	5000.000[a]		
$\nu(H_3)$	2068.337(1)		
$\nu(CH_4)$	2148.495(1)		
$\nu(H_5)$	2032.271(1)	$^{5}J(H_3,H_6)$	0.387(1)
$\nu(H_6)$	2218.340(1)	$^{3}J(H_4,H_5)$	7.368(1)
$^{5}J(^{13}C,H_3)$	0.187(2)	$^{4}J(H_4,H_6)$	1.676(1)
$^{6}J(^{13}C,H_4)$	-0.563(2)	$^{3}J(H_5,H_6)$	7.712(1)
$^{5}J(^{13}C,H_5)$	0.186(2)	transitions calculated	128
$^{4}J(^{13}C,H_6)$	-0.532(2)	transitions assigned	118
$^{3}J(H_3,H_4)$	8.177(1)	largest difference	-0.017
$^{4}J(H_3,H_5)$	1.331(1)	rms error	0.005

[a]Arbitrary shift, held constant during iterations.

[b]Signs of $^{5}J(^{13}C,H_3)$ and $^{5}J(^{13}C,H_5)$ were determined by double resonance experiments; all other signs were assumed.

[c]Spectrum was taken under conditions of fast OH exchange; therefore no couplings to the hydroxyl proton were observed. No coupling to the thiomethyl protons was observed.

Table 7

^{1}H nmr spectral parameters for a 3.0 mol% solution of 2-amino-thioanisole-^{13}C in acetone-d_6.

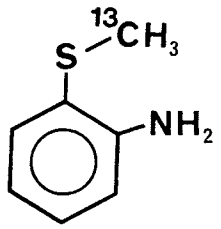

$\nu(^{13}C)^a$	5000.000		
$\nu(H_3)$	2032.252(1)		
$\nu(H_4)$	2109.156(1)		
$\nu(H_5)$	1981.451(1)	$^{5}J(H_3,H_6)$	0.380(2)
$\nu(H_6)$	2184.863(1)	$^{3}J(H_4,H_5)$	7.284(2)
$^{5}J(^{13}C,H_3)$	+0.183(2)	$^{4}J(H_4,H_6)$	1.552(2)
$^{6}J(^{13}C,H_4)$	-0.421(4)	$^{3}J(H_5,H_6)$	7.710(2)
$^{5}J(^{13}C,H_5)$	+0.117(2)	transitions calculated	160
$^{4}J(^{13}C,H_6)$	-0.371(2)	transitions assigned	159
$^{3}J(H_3,H_4)$	8.035(2)	largest difference	0.018
$^{4}J(CH_3,H_5)$	1.348(2)	rms error	0.006

[a]Shift held constant during iterations.

[b]Couplings from the methyl protons to ring protons were very small but broadened all the ring proton resonances slightly.

[c]Signs of all the couplings between the methylthio carbon and ring protons determined by double resonance experiments.

Table 8

^{13}C nmr chemical shifts and $^{13}C,^{13}C$ coupling constants at 75.486 MHz and 300 K for benzyl cyanide-8-^{13}C and its derivatives.

Parameter	Compound					
	2,6-diH			2,6-diCl		2,6-diF
δ(CN)	116.54[a]	117.86[b]	119.06[c]	114.99[d]	116.33[e]	115.76[f]
$\delta(CH_2)$	23.437	22.840	23.335	19.268	20.08	10.239
δC_1	130.578	130.802	132.261	127.532	128.73	107.464
δC_2	127.887	128.000	128.908	135.262	136.26	160.851
δC_3	129.103	129.082	129.831	128.145	129.67	111.478
δC_4	127.863	127.830	128.528	129.735	131.63	130.263
$^1J(C_\alpha,^{13}C)$	58.33	57.8	57.0	58.9	58.2	59.3
$^2J(C_1,^{13}C)$	(-)3.52	(-)3.53	(-)3.65	(-)4.82	(-)4.83	(-)4.41
$^3J(C_2,^{13}C)$	(+)3.51	(+)3.45	(+)3.31	(+)2.27	(+)2.28	(+)2.26
$^4J(C_3,^{13}C)$	(-)0.17	(-)0.19	(-)0.29	(-)1.02	-1.03[g]	(-)0.87
$^5J(C_4,^{13}C)$	(+)0.50	(+)0.51	(+)0.58	(+)1.08	+1.10[g]	(+)0.95

[a]For a 5 mol% solution in CS_2 solution containing ca 30 vol % of C_6D_{12}.

[b]For an 11 mol% solution in benzene-d_6.

[c]For a 3.0 mol% solution in acetone-d_6.

[d]3.0 mol% in benzene-d_6.

[e]7.1 mol% in acetone-d_6.

[f]5.0 mol% in benzene-d_6. The couplings in Hz to ^{19}F are $^1J(C,F)$ = -250.04, $^2J(C_1,F)$ = 19.29, $^3J(CH_2,F)$ = ±4.41, $^3J(C_2,F)$ = 6.90, $^2J(C_3,F)$ + $^4J(C_5,F)$ = 25.02, $^3J(C_4,F)$ = 10.12, $^4J(^{13}CN,F)$ = ±1.01 Hz.

[g]These signs are assumed also for those given in other columns and agree with theoretical calculations.

Table 9

^{1}H nmr spectral parameters for a 2.8 mol% solution of 2,6-dichlorobenzyl cyanide-8-^{13}C in benzene-d_6.

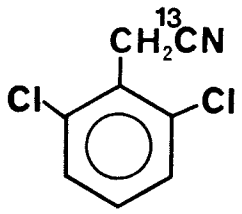

$\nu(CH_2)$	952.972(2)		
$\nu(H_3)$	2005.825(2)		
$\nu(H_4)$	1900.541(2)		
$^{2}J(CH_2,^{13}C)$	-11.114(3)	$^{3}J(H_3,H_4)$	9.135(2)
$^{5}J(^{13}C,H_3)$	+0.331(3)	calc. transitions(^{1}H)	96
$^{6}J(^{13}C,H_4)$	-0.718(5)	assigned transitions	77
$^{5}J(CH_2,H_3)$	+0.337(2)	largest difference	0.029
$^{6}J(CH_2,H_4)$	-0.334(3)	rms deviation	0.009

Table 10

^{1}H and ^{19}F spectral parameters for a 3.0 mol% solution in benzene-d_6 of 2,6-difluorobenzylcyanide-8-^{13}C.

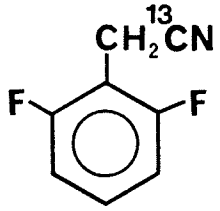

$\nu(CH_2)$	848.112(2)		
$\nu(F_2)$	13753.679(1)	$^{3}J(F_2,H_3)$	8.928(1)
$\nu(H_3)$	1898.320(1)	$^{4}J(F_2,H_4)$	6.519(1)
(H_4)	1953.362(1)	$^{5}J(F_2H_5)$	-1.362(2)
$^{2}J(CH_2,^{13}C)$	-11.027(4)	$^{3}J(H_3,H_4)$	8.475(1)
$^{4}J(F_2,^{13}C)$	±1.045(2)	$^{4}J(H_3,H_5)$	1.065(2)
$^{5}J(H_3,^{13}C)$	+0.329(2)	$^{4}J(F_2,F_6)$	4.373(2)
$^{6}J(H_4,^{13}C)$	-0.656(2)	calculated transitions (^{1}H and ^{19}F)	640
$^{4}J(F_2,CH_2)$	-1.045(2)	assigned transitions	383
$^{5}J(H_3,CH_2)$	+0.328(1)	rms deviation	0.012
$^{6}J(H_4,CH_2)$	-0.390(2)	largest difference	0.033

Table 11

^{1}H nmr parameters for a 7.0 mol% solution of benzyl cyanide-8-^{13}C in benzene-d_6.

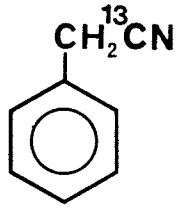

$\nu(CH_2)$	825.339(2)		
$\nu(H_2)$	2057.339(2)		
$\nu(H_3)$	2093.550(2)	$^{3}J(H_2,H_3)$	7.762(2)
$\nu(H_4)$	2088.929(3)	$^{3}J(H_3,H_4)$	7.499(3)
$^{2}J(CH_2,^{13}C)$	(-)10.580(4)	$^{4}J(H_2,H_6)$	2.042(3)
$^{4}J(H_2,^{13}C)$	(-)0.479(3)	$^{4}J(H_2,H_4)$	1.213(3)
$^{5}J(H_3,^{13}C)$	(+)0.230(4)	$^{4}J(H_3,H_5)$	1.449(3)
$^{6}J(H_4,^{13}C)$	(-)0.364(4)	$^{5}J(H_2,H_5)$	0.594(2)
$^{4}J(H_2,CH_2)$	(-)0.740(2)	calc. transitions(^{1}H)	620
$^{5}J(H_3,CH_2)$	(+)0.302(2)	assigned transitions	458
$^{6}J(H_4,CH_2)$	(-)0.585(3)	largest difference	0.049
		rms deviation	0.019

Table 12

^{13}C nmr chemical shifts and $^{13}C,^{13}C$ coupling constants for some symmetrically substituted anisoles.

	H[a]	β-CH_3[b]	4-OCH_3[c]	4-CH_3[d]	4-OCH[e]
$\delta(O^{13}CH_3)$	55.32	63.75	58.81	55.37	56.06
$\delta(C_1)$	160.69	160.01	154.77	158.62	165.53
$\delta(C_2)$	114.67	115.21	115.38	114.47	115.13
$\delta(C_3)$	130.22	130.18	115.38	130.58	132.47
$\delta(C_4)$	121.25	121.12	154.77	130.14	131.20
$^2J(^{13}C,C_1)$	(-)2.32	(-)2.19	(-)2.39	(-)2.38	(-)2.39
$^3J(^{13}C,C_2)$	(+)4.12	(+)3.90	(+)3.97	(+)4.05	(+)4.19
$^4J(^{13}C,C_3)$	(+)0.54	(+)0.49	(+)0.41	(+)0.49	(+)0.52
$^5J(^{13}C,C_4)$	<0.02	<0.05	(+)0.065	<0.03	<0.03

[a] 3 mol % in acetone-d_6.

[b] 1.8 mol% in acetone-d_6. $^1J(C\alpha,C\beta)$ = 39.0 Hz.

[c] 3.0 mol % in acetone-d_6. $^6J(O^{13}\underline{C},O\underline{C}) \leq 0.05$ Hz.

[d] 1.5 mol % in acetone-d_6. $^6J(O^{13}\underline{C},\underline{C}H_3) \leq 0.03$ Hz.

[e] 1.5 mol 5 in acetone-d_6. $^6J(O^{13}C,O\underline{C}H) \leq 0.05$ Hz.

Table 12...cont'd...

2,6-diF[f]	2,6-diBr[g]	2,6-diBr-4-F[h]	2,6-diBr-4-CH_3[i]	2,6-diBr-4-O-C-OC_2H_5[j]
62.17	60.72	61.04	60.80	61.17
137.44	154.81	152.16	152.72	158.82
156.92	118.6	118.68	118.11	118.83
113.17	133.59	120.72	134.07	134.63
124.09	127.46	159.08	138.03	129.55
(-)3.00	(-)3.60	(-)3.62	(-)3.63	(-)3.56
(+)1.70	(+)1.62	(+)1.60	(+)1.61	(+)1.61
(-)0.62	(-)0.87	(-)0.87	(-)0.89	(-)0.85
(+)0.69	(+)0.94	(+)1.02	(+)1.01	(+)0.92

[f]1.7 mol % in acetone-d_6. The couplings to fluorine are $^1J(C_2,F_2)$ = −246.74, $^2J(C_3,F_2) + {}^4J(C_3F_6)$ = 22.78, $^2J(C_1,F)$ = 14.11, $^3J(C_4,F)$ = 9.45, $^4J(^{13}C,F)$ = 3.23.

[g]10.0 mol% in acetone-d_6.

[h]2.3 mol % in acetone-d_6. The couplings to fluorine are $^1J(C_4F)$ = −249.25, $^2J(C_3F)$ = 25.67, $^3J(C_2F)$ = 10.96, $^4J(C_1,F)$ = 3.86 and $^6J(^{13}C,F)$ = 1.48.

[i]2.0 mol % in acetone-d_6. $^6J(O\underline{C}H_3,\underline{C}H_3)$ = (-)0.35.

[j]4.0 mol % in acetone-d_6. $^6J(O\underline{C}H_3,\underline{C}{=}O)$ = (+)0.42.

Table 12...cont'd...

2,6-diCl[k]	2,6-diCl-4-F[l]	2,3,5,6-tetraCl[m]	3,5-diCl[n]
60.90	61.11	61.24	56.36
153.21	150.21	155.50	162.02
129.96	130.49	128.09	114.04
130.14	117.16	132.63	135.97
126.12	158.62	127.22	121.20
(-)3.57	(-)3.60	(-)3.59	(-)2.36
(+)1.58	(+)1.53	(+)1.55	(+)4.26
(-)0.86	(-)0.86	(-)1.02	(+)0.62
(+)0.92	(+)1.00	(+)0.92	$\leq$ 0.03

[k] 2.0 mol % in acetone-d_6.

[l] 4.6 mol % in acetone-d_6. The couplings to fluorine are $^{1}J(C_4,F)$ = -247.16, $^{2}J(C_3,F)$ = 26.08, $^{3}J(C_2,F)$ = 12.19, $^{4}J(C_1,F)$ = 4.09, $^{6}J(^{13}C,F)$ = 1.46.

[m] 5.3 mol % in acetone-d_6.

[n] 3.5 mol % in acetone-d_6.

Table 12...cont'd...

4-F[o]
55.62
157.00
115.78
116.43
157.98
2.37
4.06
0.45
<0.05

[o]10 mol% in acetone-d_6 solution. The couplings to fluorine are $^{1}J(C_4,F)$ = 235.92, $^{2}J(C_3,F)$ = 23.21, $^{3}J(C_2,F)$ = 8.05, $^{4}J(C_1,F)$ = 1.97 and $^{6}J(^{13}C,F)$ = 0.108(1).

Table 13

^{13}C nmr chemical shifts and $^{13}C,^{13}C$ coupling constants for some ortho substituted anisoles.

	Br[a]	F[b]	OCH_3[c]
$\delta^{13}C$	56.38	56.34	
δC_1	156.83	148.70	150.44
δC_2	111.95	153.24	150.44
δC_3	133.88	116.57	112.94
δC_4	122.51	121.60	121.52
δC_5	129.58	125.40	121.52
δC_6	113.17	114.58	112.94
^2J	(-)2.05	(-)2.19	(-)2.33
^3J	(+)3.26	(+)2.76	(+)2.52
^4J	(+)0.28	(+)0.23	(+)0.17
^5J	< 0.05	$\simeq$0.08 ± 0.02	$(+)0.17_5$
^4J	(+)0.55	(+)0.42	(+)0.38
^3J	(+)4.94	(+)4.74	(+)4.77

[a] 6.4 mol% in acetonde-d_6.

[b] 3 mol% in acetone-d_6. The couplings to fluorine are $^1J(C_2,F) = 243.98$, $^2J(C_1,F) = 10.49$, $^2J(C_3,F) = 18.04$, $^3J(C_4,F) = 6.83$, $^3J(C_6,F) = 1.87$, $^4J(C_5,F) = 3.97$, $^4J(\underline{C}H_3,F) < 0.03$.

[c] mol% in acetone-d_6.

Table 14

^{13}C nmr chemical shifts and $^{13}C,^{13}C$ coupling constants for some ortho disubstituted N-methylanilines.

parameter	H[a]	H[b]	H[c]	F[d]
$\delta(N^{13}CH_3)$	30.43	30.37	30.45	33.29
$\delta(C_1)$	150.99	149.74	149.26	149.22
$\delta(C_2)$	112.73	112.66	153.87	112.36
$\delta(C_3)$	129.68	129.41	129.29	112.26
$\delta(C_4)$	116.86	117.36	117.17	117.35
$^2J(^{13}C,C_1)$	<1.0	(-)0.47	(-)0.9	<1.0
$^3J(^{13}C,C_2)$	(+)3.48	(+)3.40	(+)1.87	(+)3.37
$^4J(^{13}C,C_3)$	(+)0.48	(+)0.46	+0.20	(+)0.46
$^5J(^{13}C,C_4)$	<0.05	<0.03	(+)0.27	<0.05

[a] 3.0 mol% in acetone-d_6. C_1 resonance is broad due to coupling to quadrupolar ^{14}N nucleus.

[b] 5 mol% in C_6D_6. The couplings to ^{15}N are $^1J(\underline{C}H_3,^{15}N) = 9.97$, $^1J(C_1,^{15}N) = 13.25$, $^2J(C_2,^{15}N) = 2.54$, $^3J(C_3,^{15}N) = 1.36$, $^4J(C_4,^{15}N) = 0.33$.

[c] 7.0 mol% in CS_2/D_6D_{12}, C_1 resonance is broad.

[d] 5.0 mol% in acetone-d_6. C_1 resonance is broad. The couplings to fluorine are $^1J(C_2F_2) = -239.30$, $^2J(C_{3,F3}) + {}^4J(C_3,F_5) = 23.42$, $^2J(C_1,F) \simeq 13.6$, $^3J(C_2,F_6) = 8.38$, $^3J(C_4,F) = 9.46$, $^4J(N^{13}C,F) = 4.41$.

Table 15

^{13}C nmr chemical shifts and $^{13}C,^{13}C$ coupling constants for some phenyl selenides and phenyl tellurides.

parameter	$SeCH_3$[a]	$SeCH_2CH_3$[b]	$TeCH_3$[c]	$TeCH_2CH_3$[d]
$\delta(^{13}C)$	15.01	21.21	-17.14	0.1
$\delta(C_\beta)$		15.73		17.48
$\delta(C_1)$	132.82	131.17	112.95	112.16
$\delta(C_2)$	130.74	132.89	136.92	139.78
$\delta(C_3)$	129.85	129.34	129.26	129.30
$\delta(C_4)$	126.69	127.33	127.14	127.58
$^1J(^{13}C,C_\beta)$		35.79		36.0
$^2J(^{13}C,C_1)$	(-)1.51	(-)1.50	(-)1.10	(-)1.11
$^3J(^{13}C,C_2)$	(+)2.17	(+)1.62	(+)1.41	(+)1.06
$^4J(^{13}C,C_3)$	(+)0.080	(-)0.114	<0.05	<0.1
$^5J(^{13}C,C_4)$	(+)0.27	(+)0.38	(+)0.31	(+)0.37

[a] 3.5 mol% in acetone-d_6.

[b] 3.8 mol% in acetone-d_6.

[c] 13.0 mol% in C_6D_6.

[d] 5.0 mol% in C_6D_6. Shifts are relative to TMS from internal C_6D_6.

Table 16

^{1}H spectral parameters for a 5.2 mol% solution of acetophenone-α-^{13}C in acetone-d_6 at 300K.

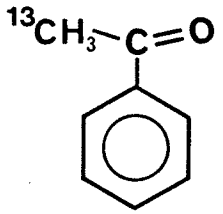

$\nu(CH_3)$	771.45[a]		
$\nu(H_2)$	2396.568(2)		
$\nu(H_3)$	2251.469(1)		
$\nu(H_4)$	2281.330(2)		
$^1J(^{13}C,H)$	127.358[a]	$^4J(H_3,H_5)$	1.332(3)
$^3J(H_2,H_3)$	7.858(2)	$^5J(H_2,H_5)$	0.617(1)
$^3J(H_3,H_4)$	7.449(2)	$^4J(^{13}C,H_2)$	<0.05[b]
$^4J(H_2,H_6)$	1.914(3)	$^5J(^{13}C,H_3)$	±0.220
$^4J(H_2,H_4)$	1.275(2)	$^6J(^{13}C,H_4)$	<0.03[b]

transitions calculated (ring proton)	132
transitions assigned	115
largest difference	0.023
rms error	0.009

[a]Not included in the iterative analysis.

[b]Estimated from linewidths.

Table 17

^{1}H nmr spectral parameters for a 5.0 mol% solution of 2,6-dichloroacetophenone-α-^{13}C at 300K.

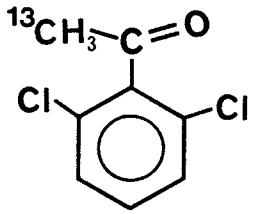

$\nu(CH_3)$	763.8[a]		
$\nu(H_3)$	2245.596(3)		
$\nu(H_4)$	2239.593(4)		
$^{1}J(^{13}C,H)$	128.8[a]		
$^{3}J(H_3,H_4)$	8.162(4)		
$^{5}J(^{13}C,H_3)$	0.131(5)[b]	$^{6}J(CH_3,H_3)$	±0.029(4)[c]
$^{6}J(^{13}C,H_4)$	-0.136(7)[b]	$^{7}J(CH_3,H_4)$	∓0.053(5)[c]

transitions calculated	96
transitions assigned	77
largest difference	0.043
rms error	0.014

[a]Not included in the iterative analysis.

[b]Sign determined from double resonance experiments.

[c]Relative signs of $^{6}J(CH_3,H_3)$ and $^{7}J(CH_3,H_4)$ determined from computer simulation of ring proton spectrum.

Table 18

^{13}C nmr chemical shifts and $^{13}C,^{13}C$ coupling constants for acetophenone-α-^{13}C and 2,6-dichloroacetophenone-α-^{13}C in acetone-d_6.

	H[a]	Cl[b]
$\delta(^{13}C)$	26.63	31.137
δ(C=O)	197.816	199.480
$\delta(C_1)$	138.175)	140.891
$\delta(C_2)$	128.941	130.435
$\delta(C_3)$	129.352	129.199
$\delta(C_4)$	133.669	131.946
$^1J(^{13}C,C{=}O)$	42.81	43.77
$^2J(^{13}C,C_1)$	13.92	12.93
$^3J(^{13}C,C_2)$	0.54	0.17
$^4J(^{13}C,C_3)$	<0.1	+0.21
$^5J(^{13}C,C_4)$	0.23	+0.13

[a] 7.7 mol% in acetone-d_6.

[b] 5.0 mol% in acetone-d_6.

Table 19

Long range coupling from the ring protons to the methoxy carbon-13 nucleus in 2,6-dimethylanisole.

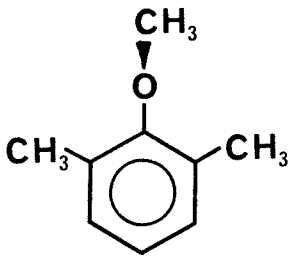

$^{5}J(O\underline{C}H_3,H_3) = 0.263(7)$

$^{6}J(O\underline{C}H_3,H_4) = 0.622(4)$

Methyl protons decoupled during spectrum acquisition.

Table 20

Long range coupling from the ring protons to the 2-methoxy ^{13}C nucleus in 1,2,3-trimethoxy benzene.

$^{5}J(C_a,H_3) = (+)0.239(4)$

$^{6}J(C_a,H_4) = (-)0.601$

$^{6}J(C_b,H_3) = {}^{4}J(C_b',H_5) \leq 0.05$

$^{5}J(C_b,H_4) = {}^{5}J(C_b',H_4) \leq 0.05$

$^{6}J(C_b,H_5) = {}^{6}J(C_b',H_3) \leq 0.05$

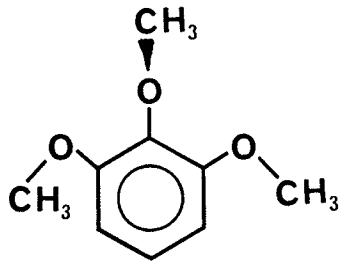

Figure 7

A Part of the proton coupled ^{13}C nmr spectrum for the ortho carbon in 3,5-dichlorothioanisole-^{13}C.

B While decoupling the methyl protons for the positive spin state of the methyl ^{13}C nucleus; ortho carbon peaks collapse for positive spin states of the methyl ^{13}C nucleus.

C While decoupling the methyl protons for the negative spin state of the methyl ^{13}C nucleus; ortho carbon peaks collapse for negative spin state of the methyl ^{13}C nucleus.

The observations are consistent with a positive $^{3}J(S^{13}C, C_2)$.

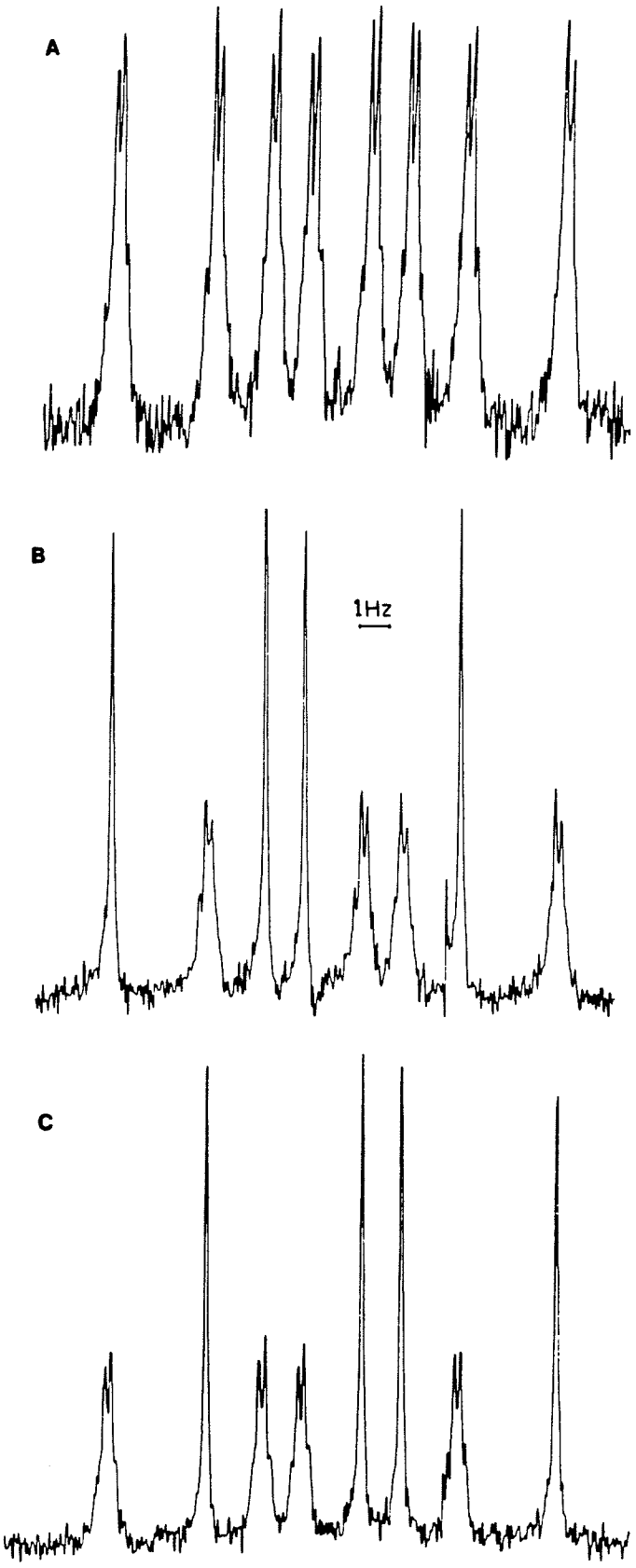
A
B
1Hz
C

Figure 8

A Part of the proton coupled ^{13}C nmr spectrum of the <u>meta</u> carbons in 2,6-dichlorothioanisole-^{13}C.

B While decoupling the high frequency half of the methyl proton doublet due to $^{1}J(S^{13}C,H)$; low frequency halves of <u>meta</u> carbon doublets, due to $^{4}J(S^{13}C,C_3)$, sharpen (collapse).

C While decoupling the low frequency half of the methyl proton doublet due to $^{1}J(S^{13}C,H)$; high frequency halves of the <u>meta</u> carbon doublets, due to $^{4}J(S^{13}C,C_3)$ sharpen (collapse).

The results are consistent with a negative $^{4}J(S^{13}C,C_3)$.

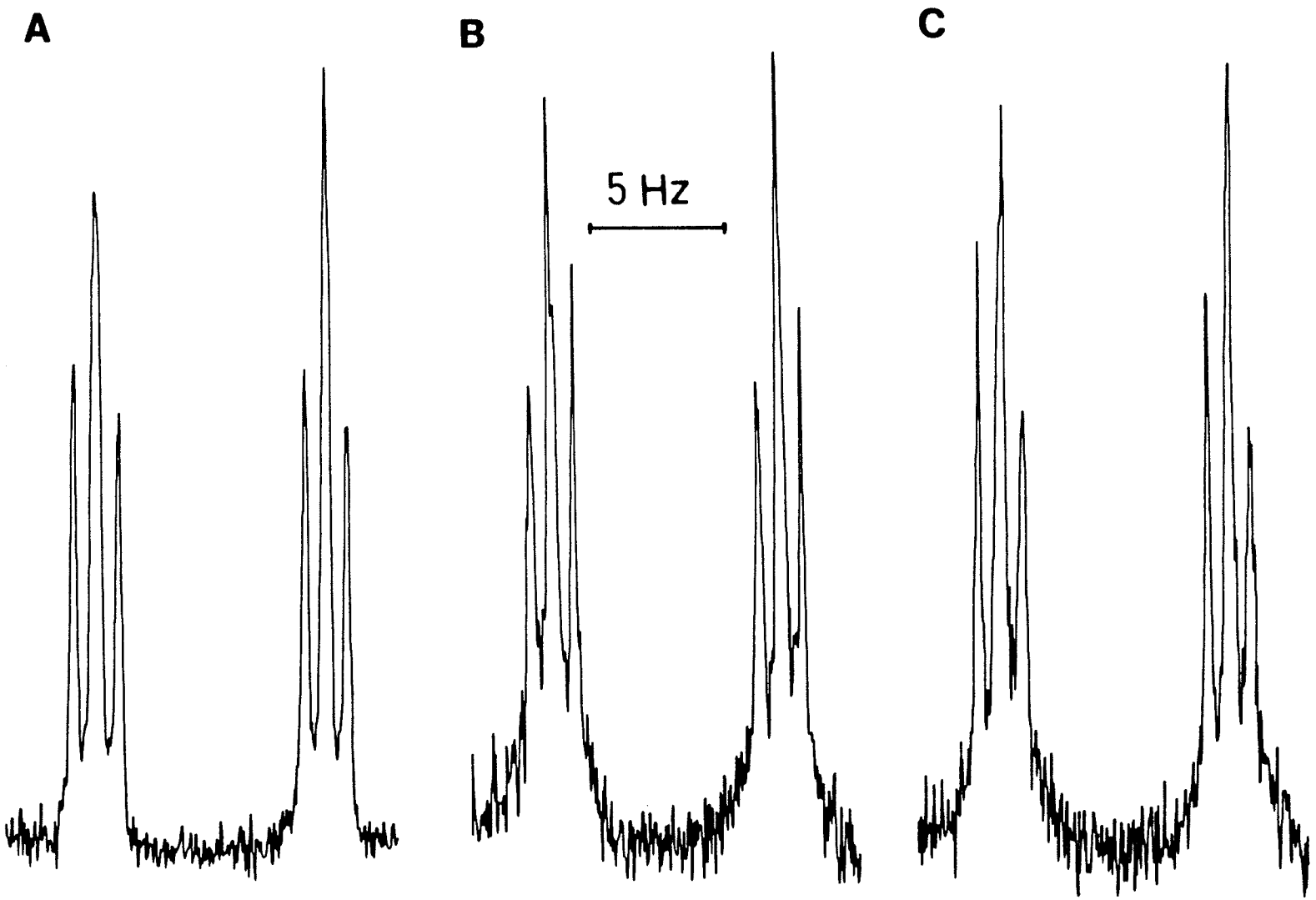
A
B
C
5 Hz

Figure 9

The proton decoupled ^{13}C nmr spectra of the <u>para</u> methyl carbon in

A) 2,6-dibromo-4-methylanisole

B) 4-methyanisole

C) 4-methylthioanisole.

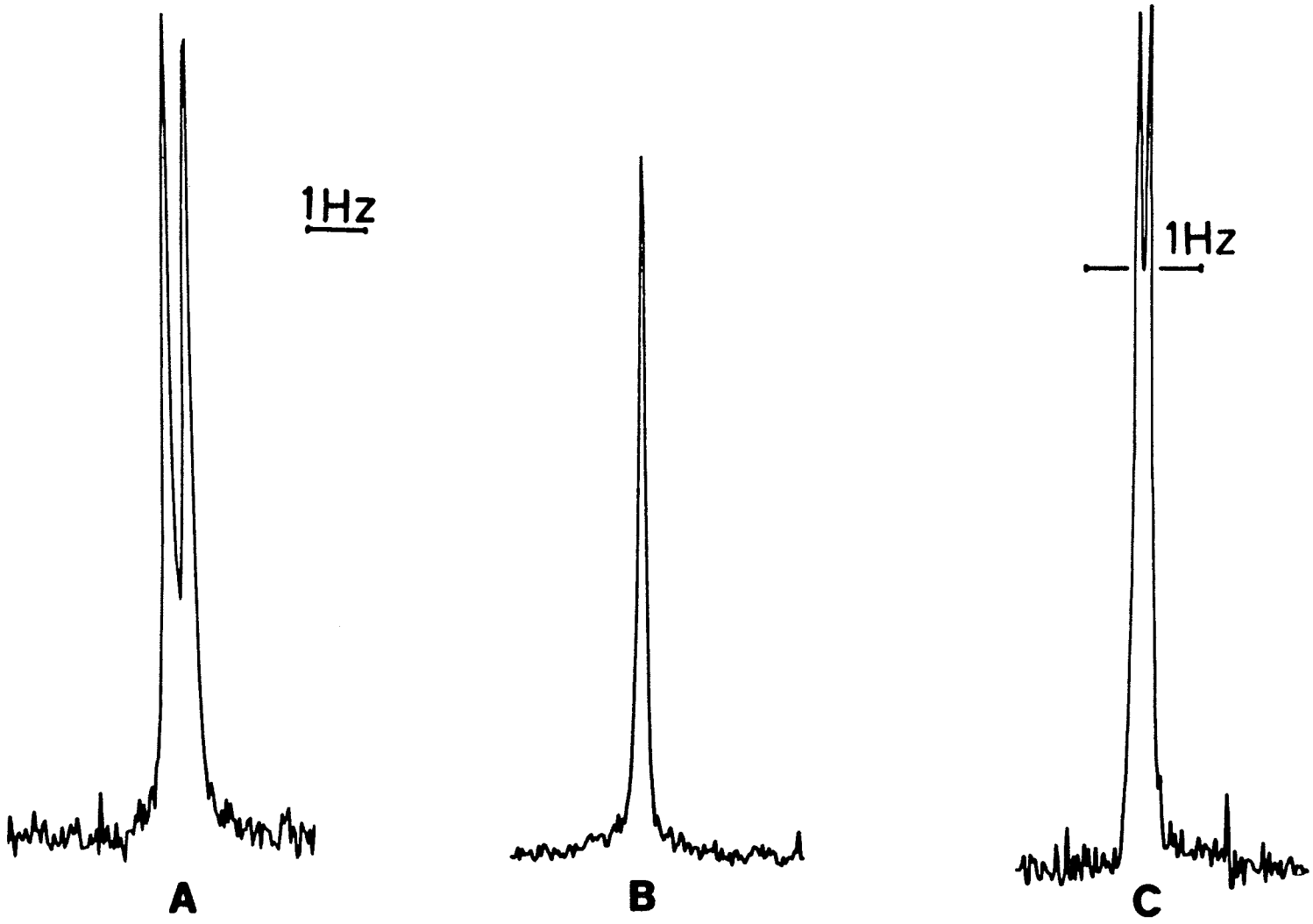
1Hz
1Hz
A
B
C

Figure 10

A The proton decoupled ^{13}C nmr spectrum of C_1 (outer doublet) and C_4 (inner doublet) of 1,4-dimethoxybenzene-^{13}C (1-methoxy carbon is ^{13}C enriched).

B The proton decoupled ^{13}C nmr spectrum of C_2 and C_3 of 1,4-dimethoxybenzene-^{13}C.

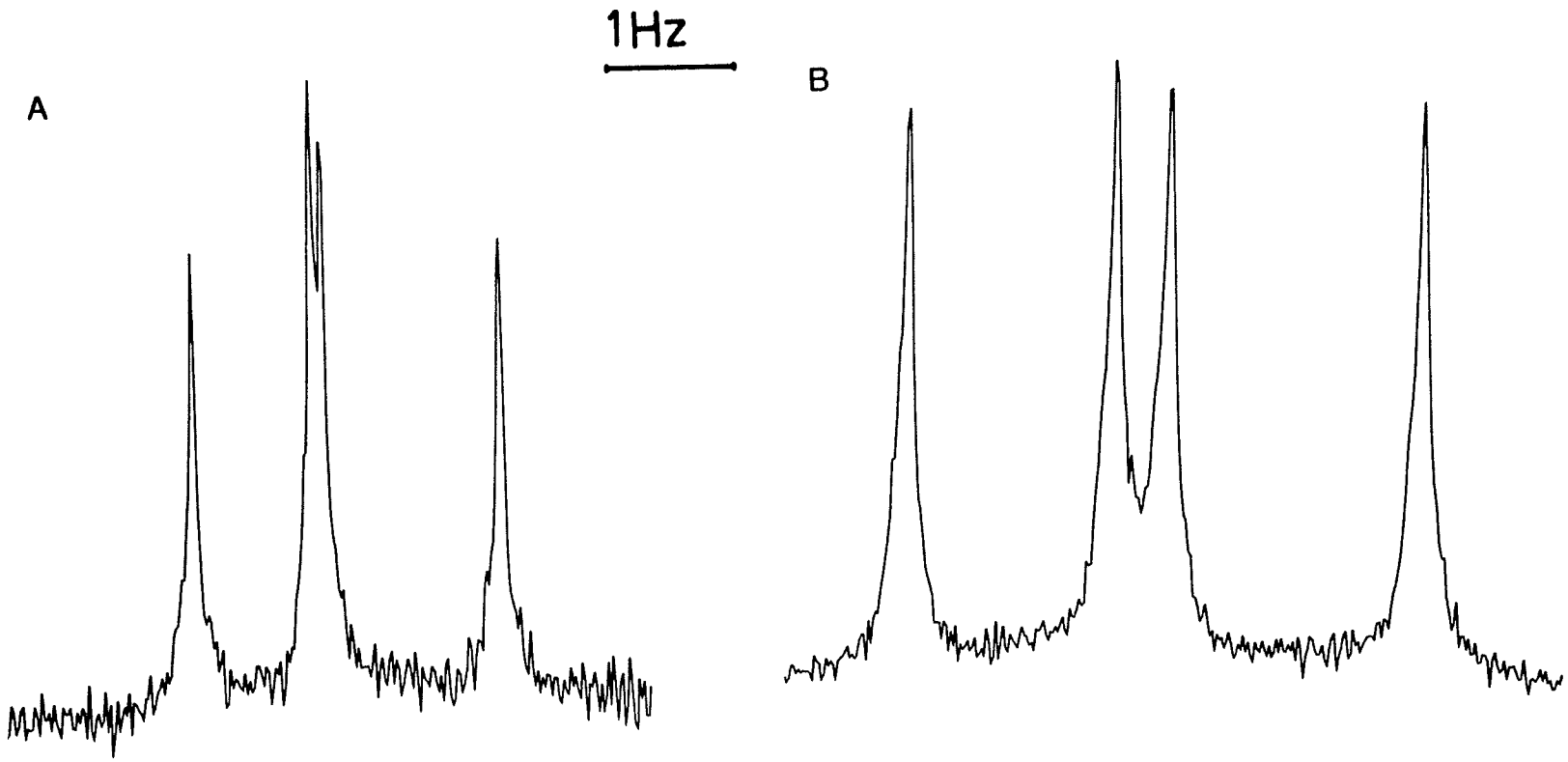
1Hz
A
B

Figure 11

A Part of the ^{13}C nmr spectrum of the 2-methoxy carbon in 1,2,3-trimethoxybenzene. There is no observed coupling to the 1,3-methoxy protons.

B Part of the ^{13}C nmr spectrum of the 1 and 3 methoxy carbons in 1,2,3-trimethoxybenzene. Note that there is no observed coupling to the ring or 2-methoxy protons.

C Part of the ^{13}C nmr spectrum of the methoxy carbon for 2,6-dimethylanisole with decoupling of the ortho methyl protons.

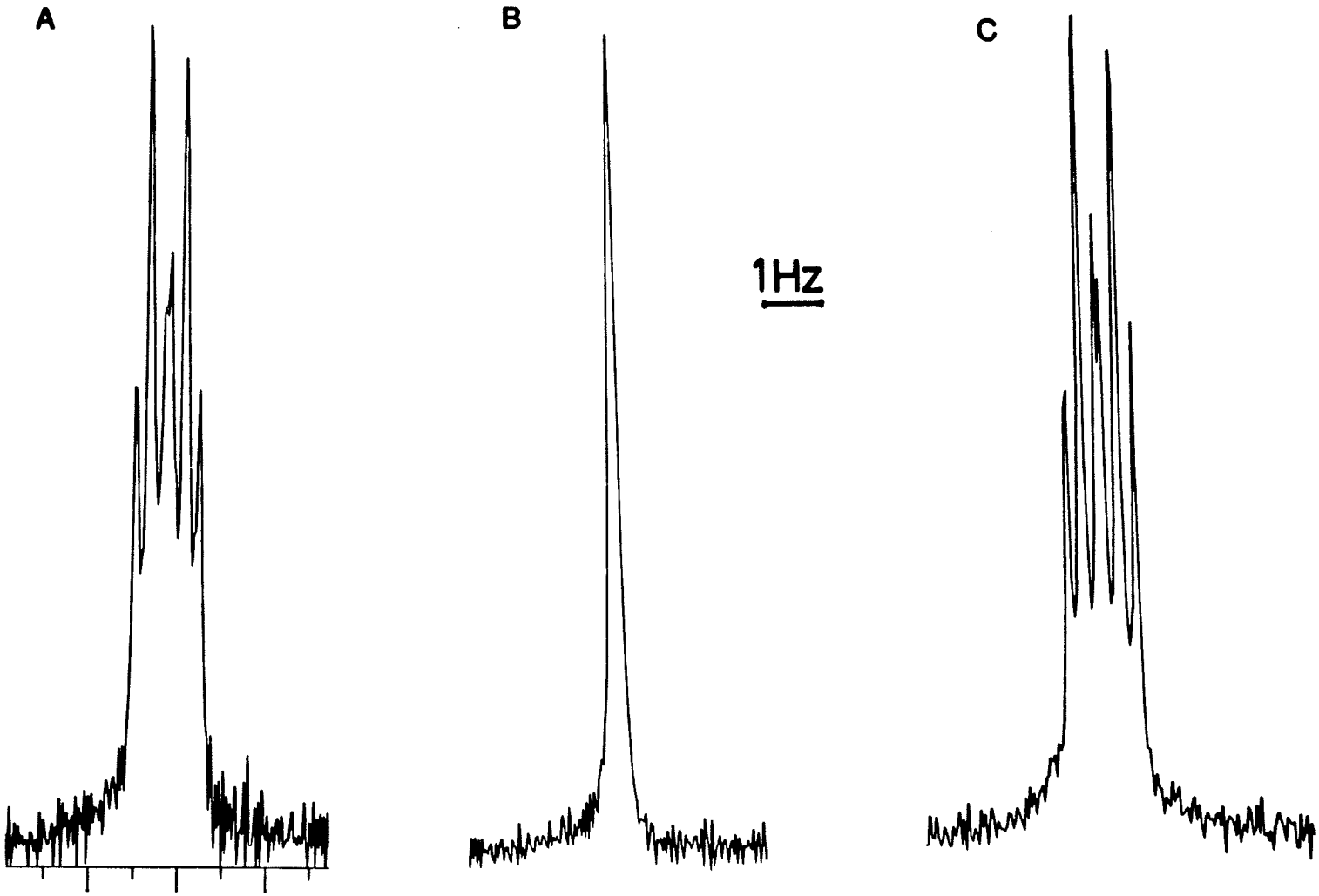
A
B
C
1Hz

Figure 12

A The proton decoupled ^{13}C nmr spectrum of C_1 and C_2 in 1,2-dimethoxybenzene ^{13}C enriched at both methoxy carbons.

B The proton decoupled ^{13}C nmr spectrum of C_4 and C_5 in doubly enriched 1,2-dimethoxybenzene.

C The proton decoupled ^{13}C nmr spectrum of C_3 and C_6 in doubly enriched 1,2-dimethoxy benzene.

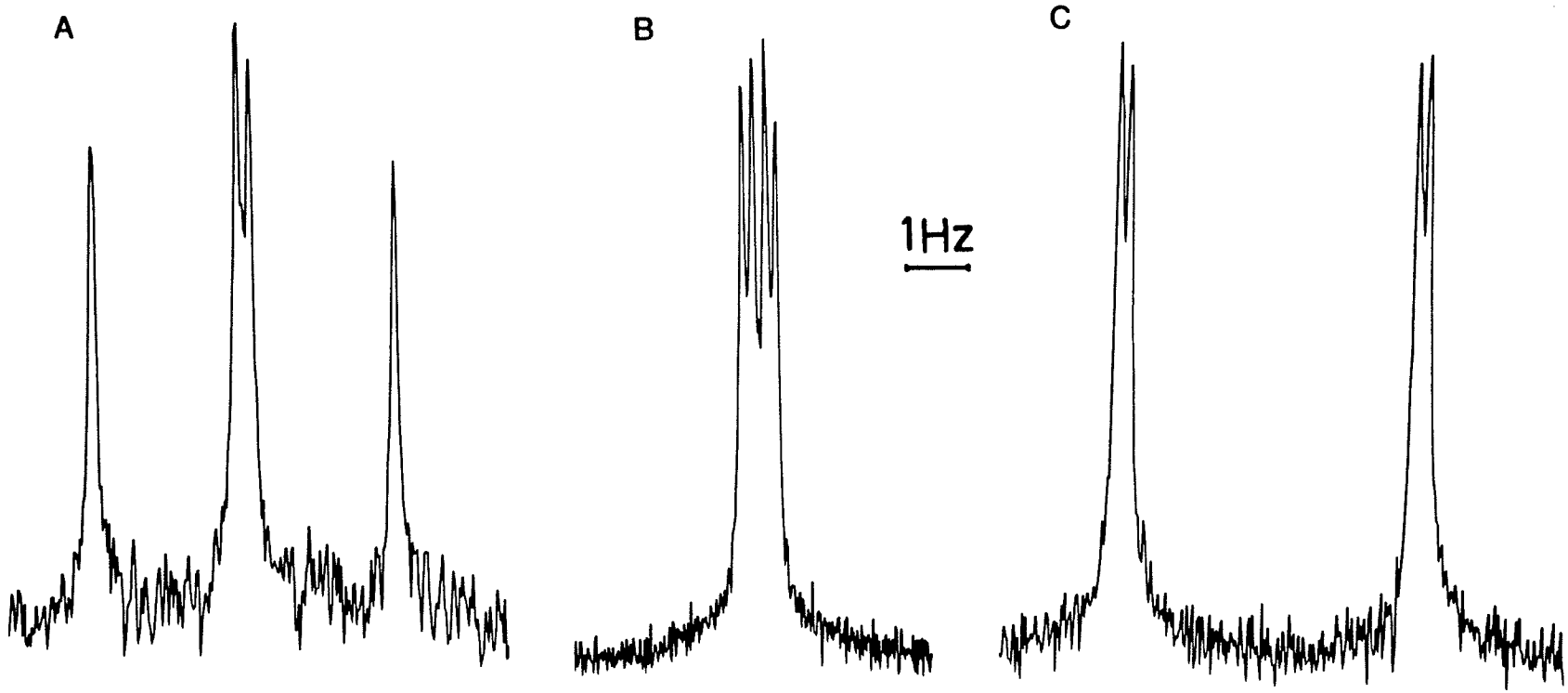
A
B
C
1Hz

Figure 13

The C_2, C_3 and C_4 portions of the proton decoupled ^{13}C nmr spectrum of 2,6-difluoro-N-methylaniline-^{13}C in acetone-d_6. Splittings are due to the ortho fluorine-19 nuclei and the methyl-^{13}C nucleus.

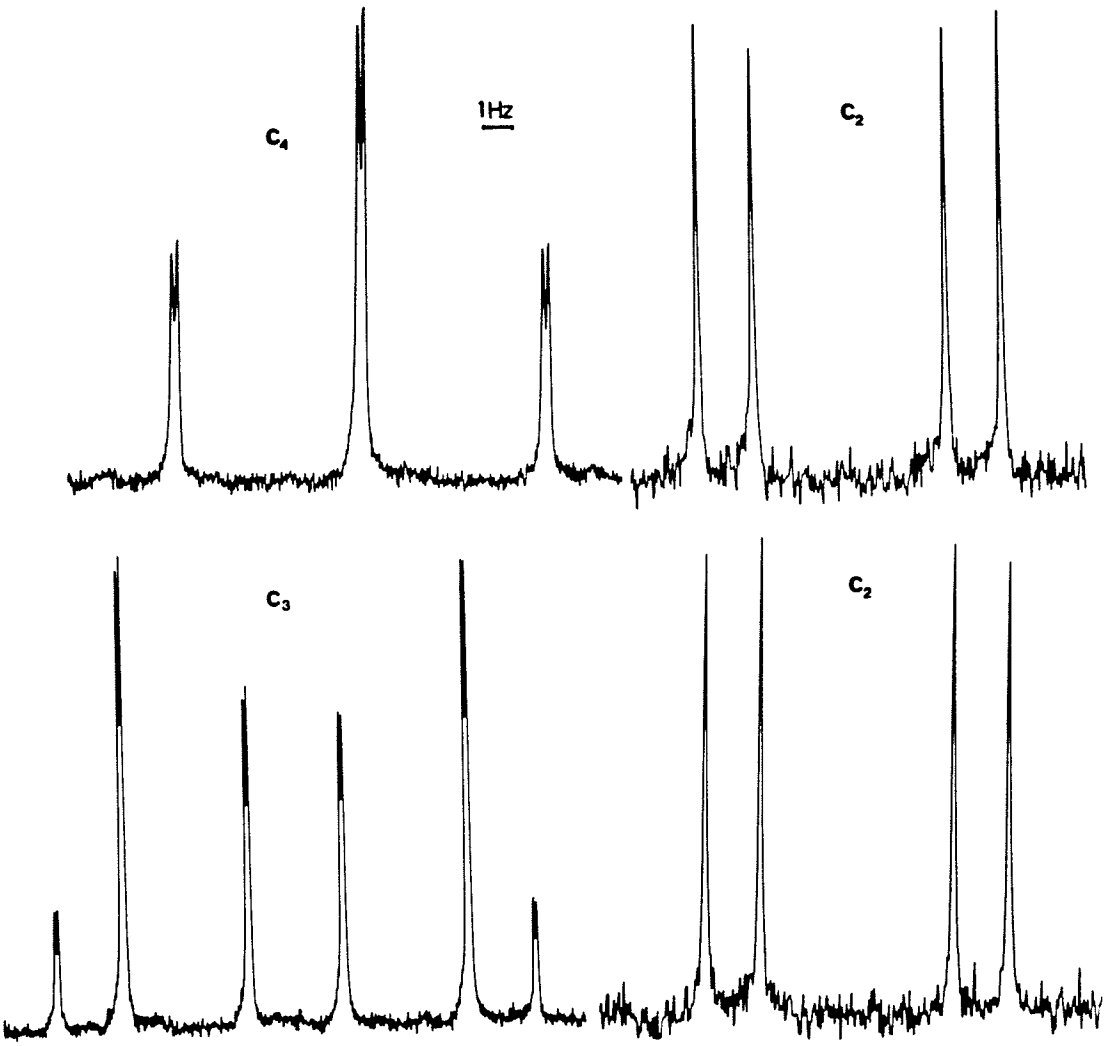
C4
1Hz
C2
C3
C2

Figure 14

A Half of the ^{13}C nmr spectrum of C_3 in 2,6-dichlorobenzyl cyanide-8-^{13}C.

B While decoupling the low frequency multiplet of the methylene protons (assigned to the positive spin state of ^{13}CN, since $^{2}J(CH_2, {}^{13}CN) = -11.1$ Hz). The multiplets of C_3 at low frequency collapse. Hence $^{4}J(^{13}CN, C_3)$ has the same sign as $^{2}J(CH_2, {}^{13}CN)$.

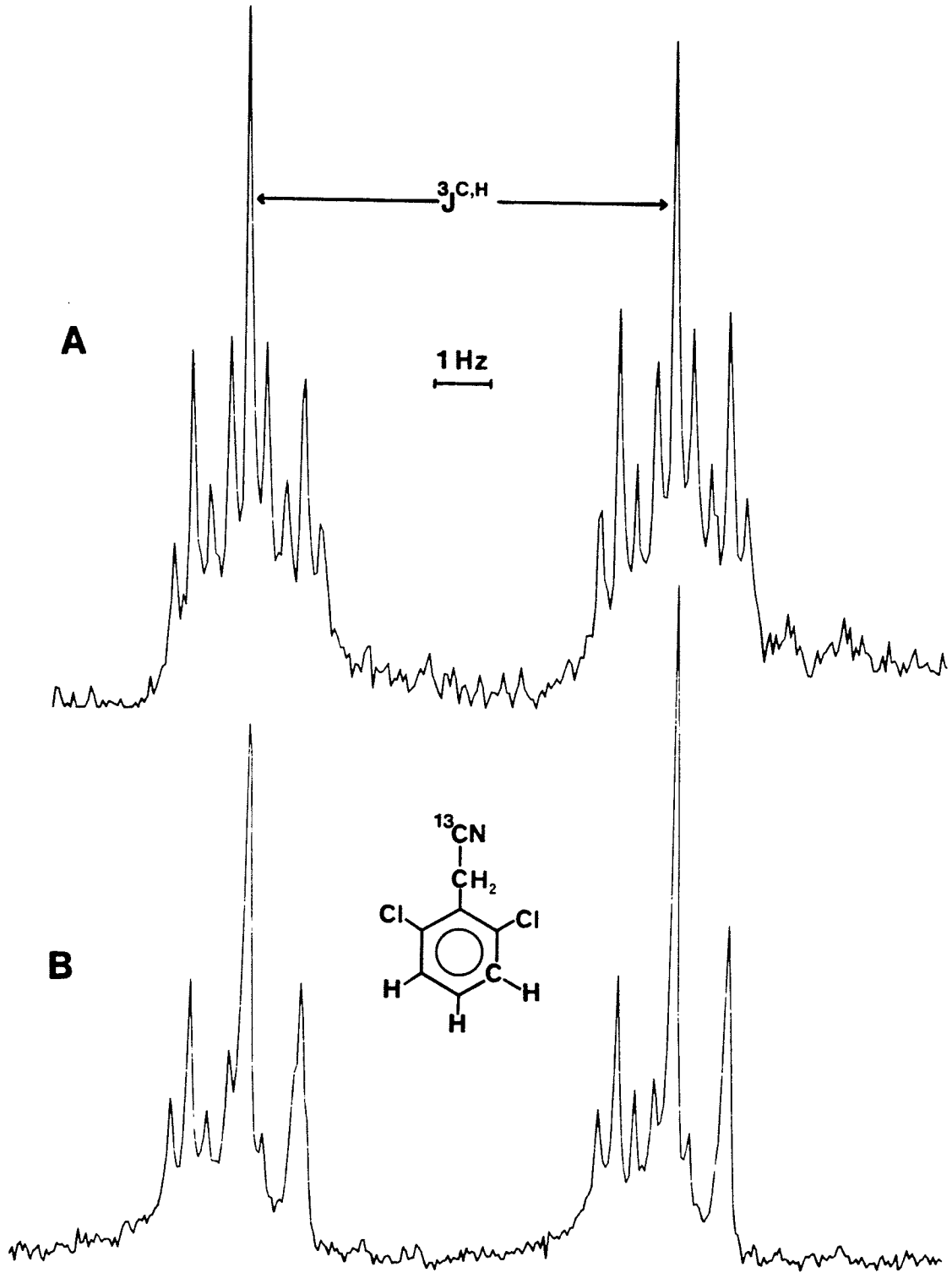
$^3J_{C,H}$
A
1 Hz
B
^{13}CN
CH$_2$
Cl
Cl
H
C
H
H

Figure 15

The ring proton region of the ^{1}H nmr spectrum of benzylcyanide-8-^{13}C.

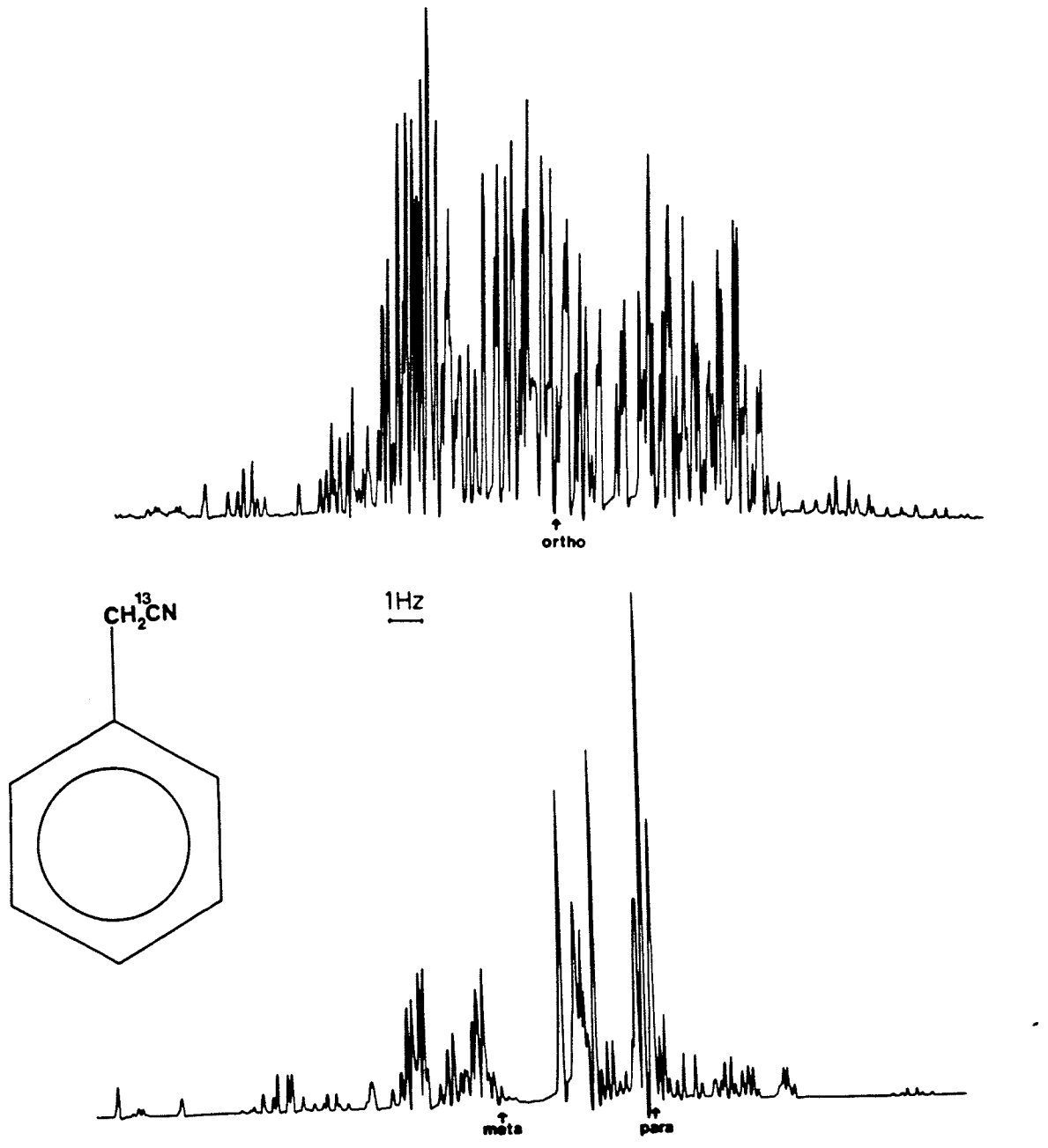
ortho
1Hz
$CH_2^{13}CN$
meta
para

Figure 16

A The proton decoupled ^{13}C nmr spectrum of the <u>para</u> carbon in methyl phenyl selenide-^{13}C.

B The proton decoupled ^{13}C nmr spectrum of the <u>para</u> carbon in methyl phenyl telluride-^{13}C.

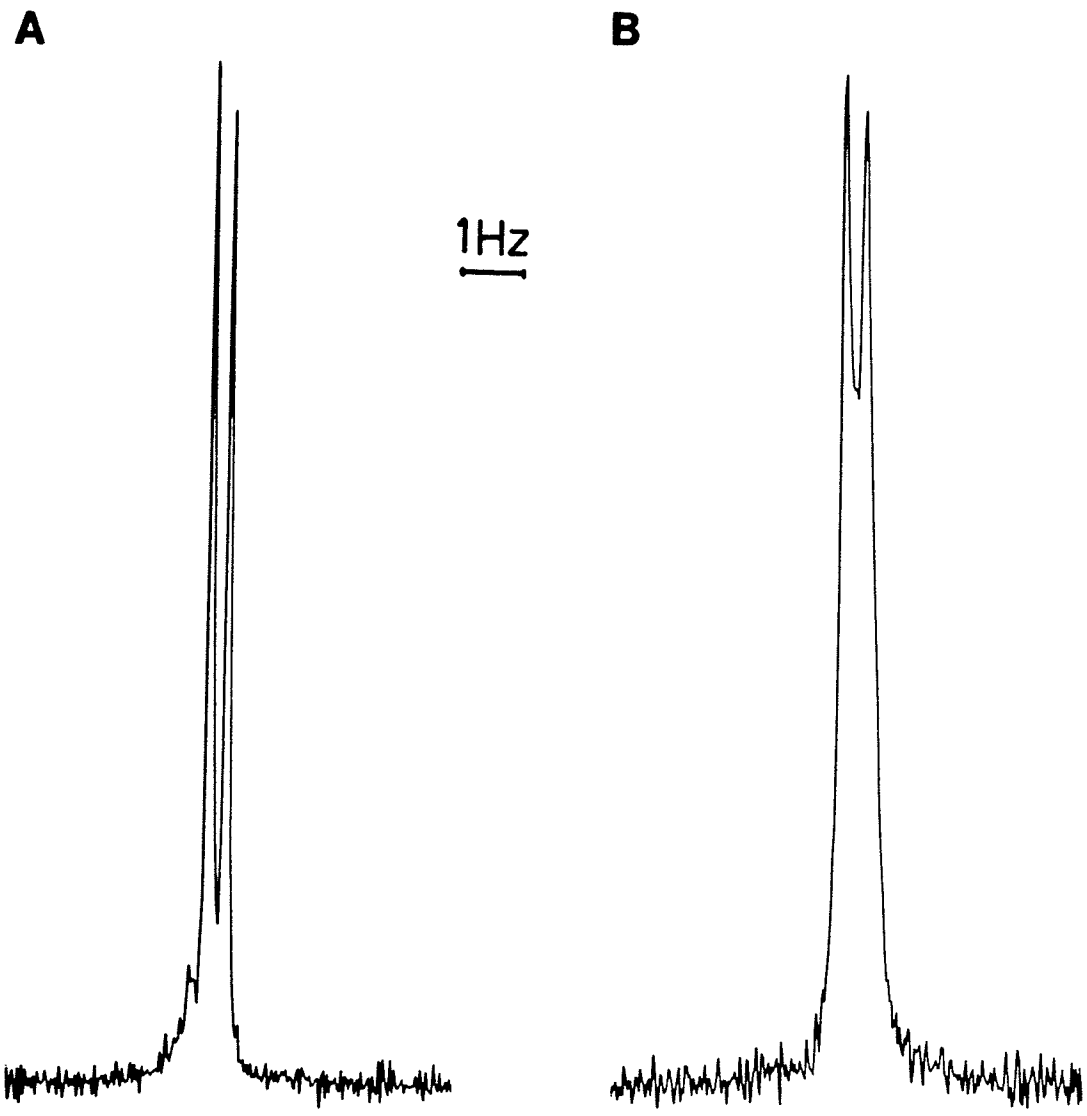
A
B
1Hz

Figure 17a

The proton decoupled ^{13}C nmr spectra of the <u>para</u> carbon in

a) acetophenone-α-^{13}C

b) 2,6-dichloroacetophenone-α-^{13}C.

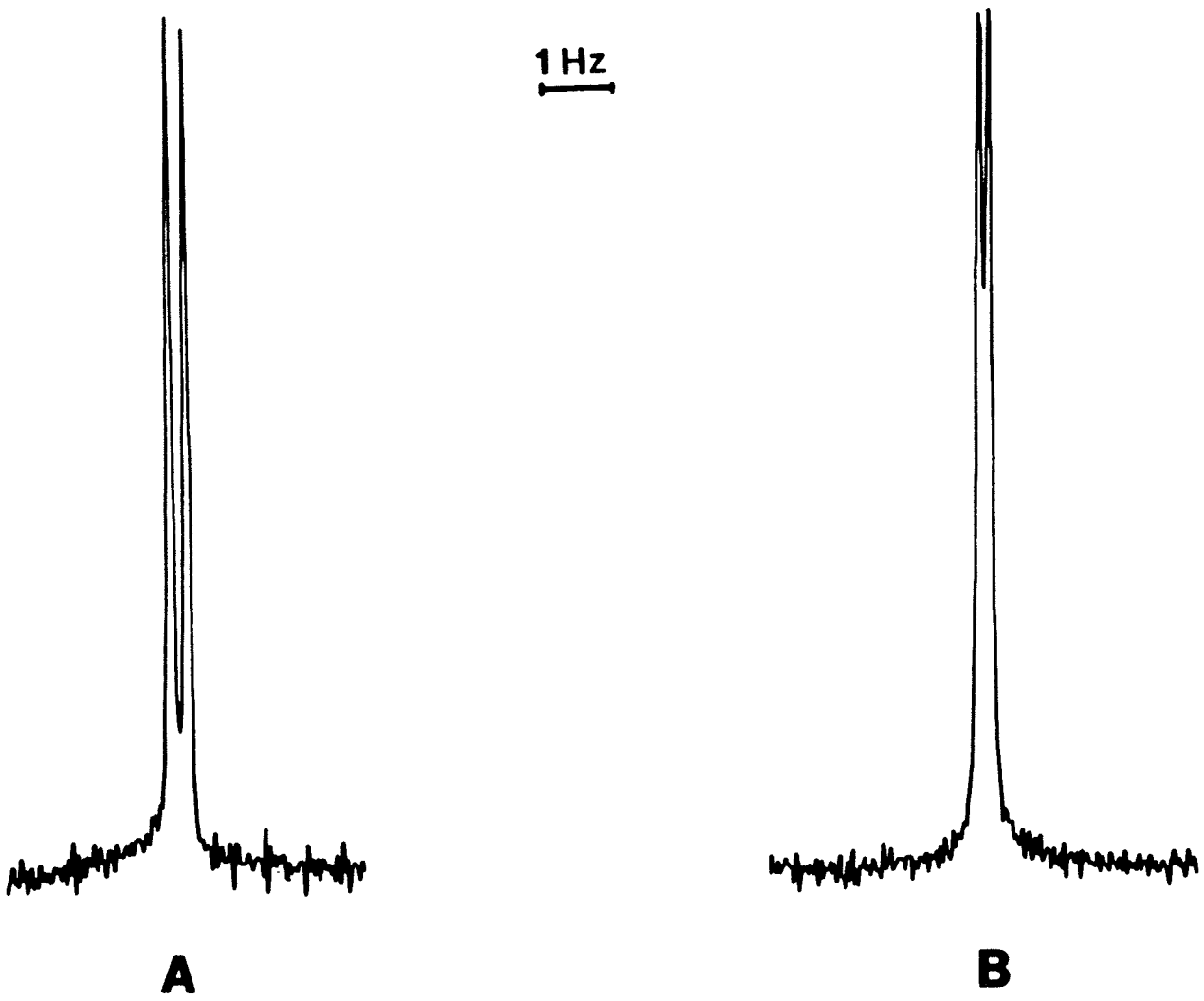
1 Hz
A
B

Figure 17b

The two halves of the proton coupled ^{13}C nmr spectrum of the <u>para</u> carbon in 2,6-difluoroacetophenone are shown in A and B.

The two halves of the proton coupled ^{13}C nmr spectrum of the <u>para</u> carbon in 2,6-difluoroacetophenone-α-^{13}C are shown in C and D.

Comparison of A and B with C and D suggests that there is no splitting or broadening of the <u>para</u> carbon peaks due to coupling to the α ^{13}C nucleus.

Inability to completely decouple the ring protons made it necessary to run a proton coupled ^{13}C spectrum.

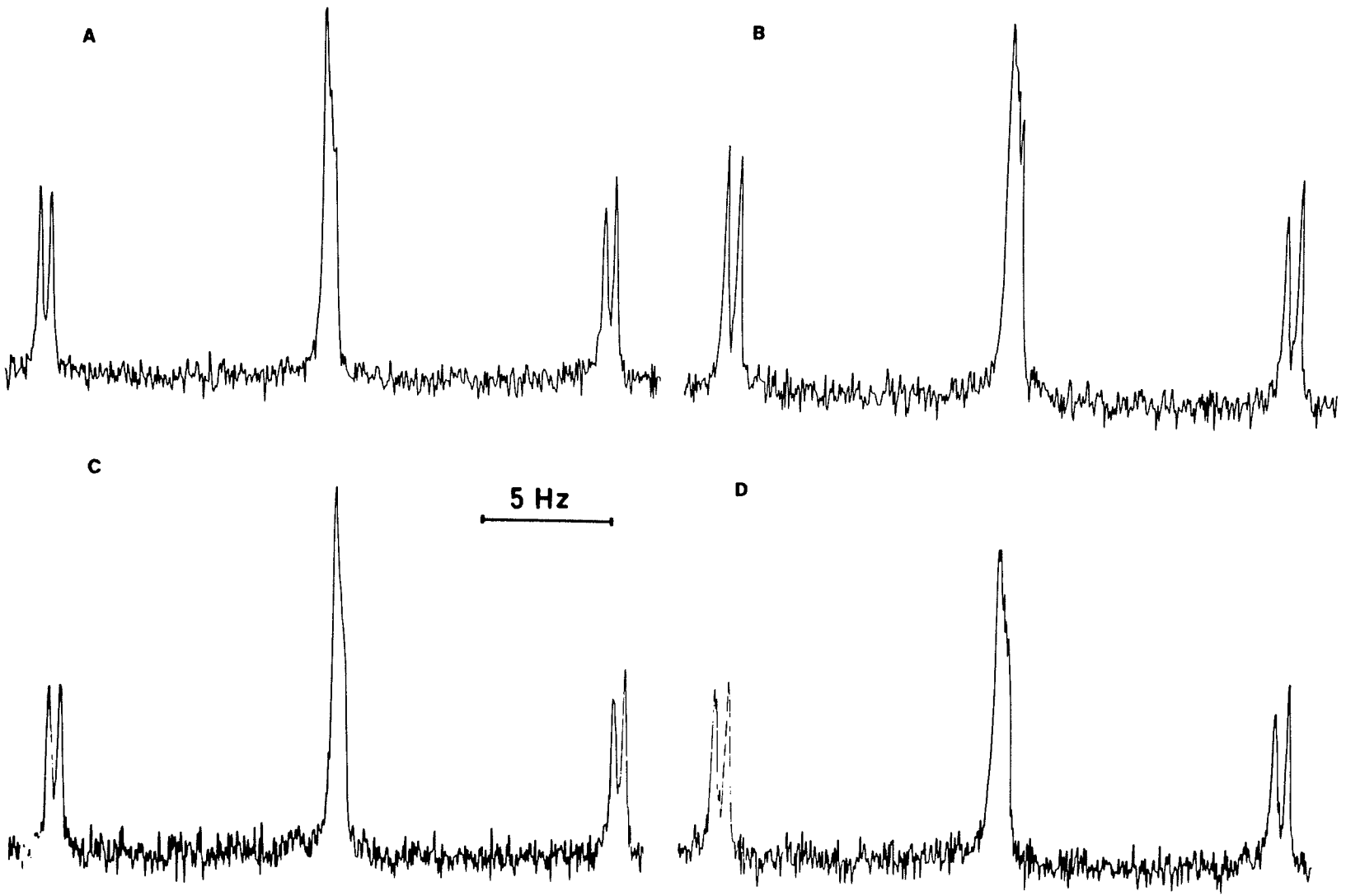
A
B
C
5 Hz
D

Figure 18

A The proton coupled ^{13}C nmr spectrum of the <u>para</u> carbon of 2,6-dichloroacetophenone-α-^{13}C.

B The ^{13}C nmr spectrum of the <u>para</u> carbon of 2,6-dichloroacetophenone-α-^{13}C while decoupling the methyl protons for the positive spin state of the α ^{13}C. The high field half of the unresolved doublet due to $^{5}J(C_{\alpha}, C_{4})$ collapses. $^{5}J(C_{\alpha}, C_{4})$ is therefore negative.

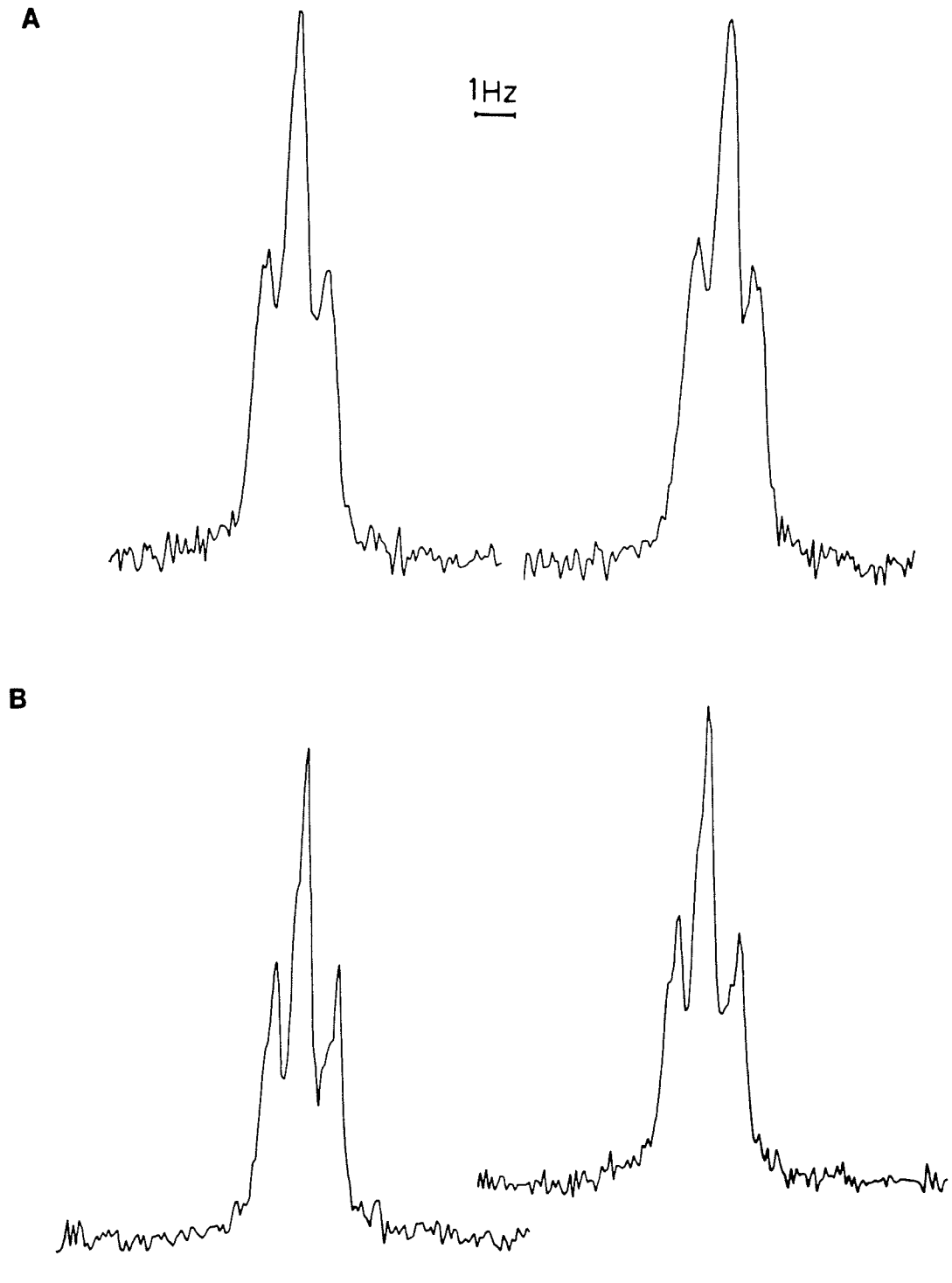
A
1Hz
B

Figure 19

A Part of the ^{13}C nmr spectrum of the <u>para</u> methyl carbon in 2,6-dibromo-4-methylanisole-^{13}C.

B With decoupling of the methoxy protons for positive spin state (low field) of the methyl ^{13}C nucleus. The high field halves of the doublets due to $^{6}J(O^{13}C, \underline{C}H_3)$ sharpen. This implies a negative $^{6}J(O^{13}C, \underline{C}H_3)$.

C With decoupling of the methoxy protons for negative spin state of ^{13}C (high field half). The low field halves of the doublets due to $^{6}J(O^{13}C, \underline{C}H_3)$ sharpen. This confirms that $^{6}J(O^{13}C, \underline{C}H_3)$ is negative.

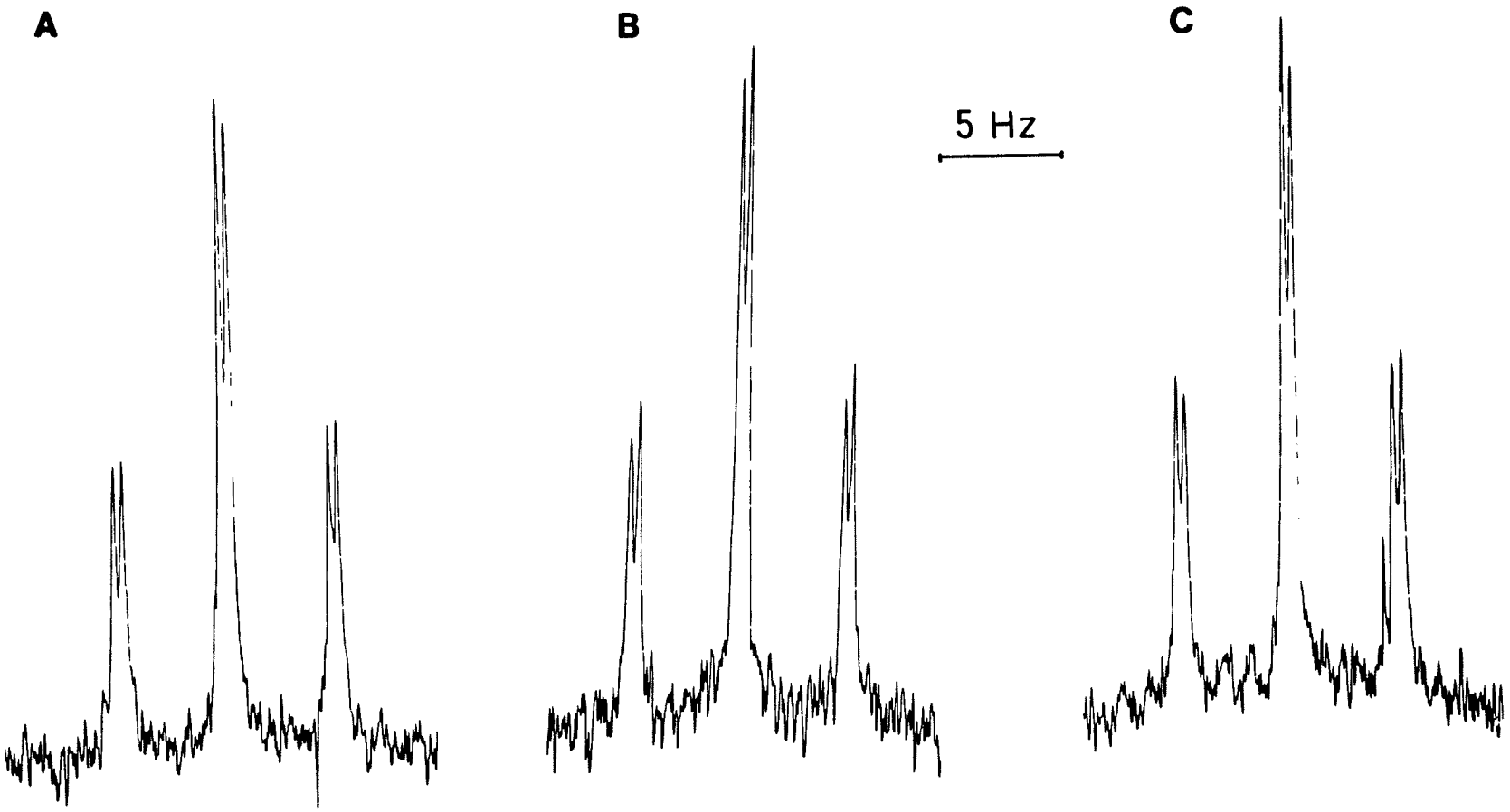
A
B
C
5 Hz

D. DISCUSSION

1. Thioanisoles

a) The conformational dependences of long-range coupling constants between the ring and methyl ^{13}C nuclei.

i) $^5J(S^{13}C, C_4)$

The INDO MO FPT computations (see table 21) can be empirically fit to the equation

$$^5J(S^{13}C, C_4) = 0.05(2) + 1.67(4) \sin^2\theta \qquad (87)$$

The INDO MO FPT formulation usually gives the correct qualitative θ dependence for long-range coupling constants between sidechain nuclei and nuclei in the ortho, meta and para positions in the benzene ring. Quantitative reproduction of the magnitudes of these coupling constants is not expected because of the parameterization of this semiempirical method and because the geometry assumed in the computations may be different from the true geometry. Hence, INDO MO FPT computations support a σ-π mechanism for $^5J(S^{13}C, C_4)$, although the magnitude of $^5J_{90}$ may well be wrong.

Schaefer and co-workers[68] have given evidence that in 2-hydroxybenzenethiol a stereospecific hydrogen bond between the hydroxyl hydrogen and the 3p orbital of the sulfur substituent twists the S-H bond into a plane orthogonal to the benzene ring, as depicted in 6.

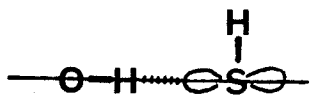

6

Table 21

Coefficients for the decomposition of INDO-MO-FPT ^{n}J values into $J(\theta) = J_o + J_{90}^{\sigma-\pi} \sin^2\theta + J_{180}^{\sigma} \sin^2\theta/2$ for spin-spin couplings between the side-chain carbon-13 nucleus and the ring carbon-13 nuclei in thioanisole, anisole and benzylcyanide.

		$J_{90}^{\sigma-\pi}$	J_{180}^{σ}	J_0
Thioanisole	$^3J(S^{13}C, C_2)$	-0.63(5)[a]	0.50(5)	2.25(4)
	$^4J(S^{13}C, C_3)$	-1.46(2)	0.17(2)	-0.32(2)
	$^5J(S^{13}C, C_4)$	1.67(1)		0.05(0)
Anisole	$^3J(O^{13}C, C_2)$	-0.73(4)	1.47(4)	1.92(3)
	$^4J(O^{13}C, C_3)$	-1.46(1)	0.36(1)	-0.15(1)
	$^5J(O^{13}C, C_4)$	1.54(0)		0.00(0)
N-methylaniline	$^3J(N^{13}C, C_2)$	-0.51(10)	1.41(10)	2.04(7)
	$^4J(N^{13}C, C_3)$	-1.63(5)	0.43(5)	-0.16(4)
	$^5J(N^{13}C, C_4)$	1.67(7)		0.03(4)
Benzyl cyanide	$^3J(^{13}CN, C_2)$	-1.04(6)	2.54(6)	3.07(5)
	$^4J(^{13}CN, C_3)$	-2.19(2)	0.51(2)	-0.32(1)
	$^5J(^{13}CN, C_4)$	2.30(1)		0.18(0)
Acetophenone	$^3J(^{13}C, C_2)$	-0.38(8)	-1.42(7)	3.23(6)
	$^4J(^{13}C, C_3)$	-0.27(5)	-0.58(5)	0.01(4)
	$^5J(^{13}C, C_4)$	0.25(3)		0.74(2)

[a]Numbers in parentheses are standard deviations in the last significant figure after performing a nonlinear regression for 7 points from $\theta = 0$ to 180°. The angle θ for each molecule is defined in the text.

Based on the absence of any through-space coupling between the methyl protons and H_6, Schaefer et al.[69] suggested that the S-C bond in 2-hydroxythioanisole is also orthogonal to the plane of the benzene ring. An analysis of the ^1H nmr spectrum of 2-hydroxythioanisole-^{13}C (see table 6) has $^6J(S^{13}C, H_4)$ as -0.563(2) Hz. This is near the value of -0.541(5) Hz observed by Baleja[70] for 2,6-dibromothioanisole, in which the S-C bond must be nearly perpendicular to the ring plane. Schaefer and Baleja[71] have assumed a $^6J_{90}$ value of -0.56(2) Hz, for thioanisole derivatives, exactly that reported here for 2-hydroxythioanisole-^{13}C. Therefore it is reasonable to assume that 2-hydroxythioanisole has the S-C_α bond perpendicular to the phenyl ring. One may then write equation (88).

$$^6J(S^{13}C, H_4) = -0.563(2) \langle \sin^2\theta \rangle \qquad (88)$$

Assuming that $^5J(S^{13}C, C_4)$ also follows a $\sin^2\theta$ law, as predicted by theoretical computations, one may write (table 5) equation (89).

$$^5J(S^{13}C, C_4) = 0.91(1) \langle \sin^2\theta \rangle \qquad (89)$$

Analysis of the proton decoupled ^{13}C nmr spectrum of ethyl-(2-hydroxyphenyl)-sulfide-^{13}C, enriched at the methylene position yields equation (90).

$$^5J(S^{13}C, C_4) = 0.86 \langle \sin^2\theta \rangle \qquad (90)$$

This suggests a very small reduction of $^5J_{90}$ by an alkyl group in the β position. Evidence for a similar reduction in $^6J_{90}(C, F_4)$ has been observed for alkyl-(2,6-dibromo-4-fluorophenyl) ethers[72] and 4-fluorophenyl alkyl esters[73].

ii) $^4J(S^{13}C, C_3)$

INDO MO FPT computations suggest that $^4J(S^{13}C, C_3)$ has a negative σ−π component, a positive σ component and a negative angle independent term (see table 21). For 2n-fold barriers to internal rotation, $\langle \sin^2\theta/2 \rangle$ is 0.5 and $^4J(S^{13}C, C_3)$ can be written as equation (91).

$$^4J(S^{13}C, C_3) = {}^4J_{90}^{\sigma-\pi}\langle \sin^2\theta \rangle + 0.5\ {}^4J_{180}^{\sigma} + {}^4J_0 \qquad (91)$$

Then, for symmetrically substituted anisoles, $^4J(S^{13}C, C_3)$ is a linear function of $\langle \sin^2\theta \rangle$ with a slope of $^4J_{90}^{\sigma-\pi}$ and an intercept of $^4J_0 + 0.5\ {}^4J_{180}^{\sigma}$. Since $^5J(S^{13}C, C_4)$ is proportional to $\langle \sin^2\theta \rangle$, $^4J(S^{13}C, C_3)$ should be a linear function of $^5J(S^{13}C, C_4)$. In figure 20, $^4J(S^{13}C, C_3)$ is plotted against $^5J(S^{13}C, C_4)$. A linear regression analysis for these points yields a slope of −1.76 and an intercept of 0.65 with a correlation coefficient, r, of −0.991.

Considering the possibility of large substituent perturbations on the coupling mechanism, the fit is rather good. The three points for the ethyl sulfides (table 4), are also included in the regression.

If equation (89) is used to describe the dependence of $^5J(S^{13}C, C_4)$ on $\langle \sin^2\theta \rangle$ then equation (91) may be rewritten as equation (92).

$$^4J(S^{13}C, C_3) = -1.60 \langle \sin^2\theta \rangle + 0.65 \qquad (92)$$

Figure 20

A plot of $^{4}J(S^{13}C, C_3)$ versus $^{5}J(S^{13}C, C_4)$ for some symmetrically substituted thioanisoles. The points are taken from table 2.

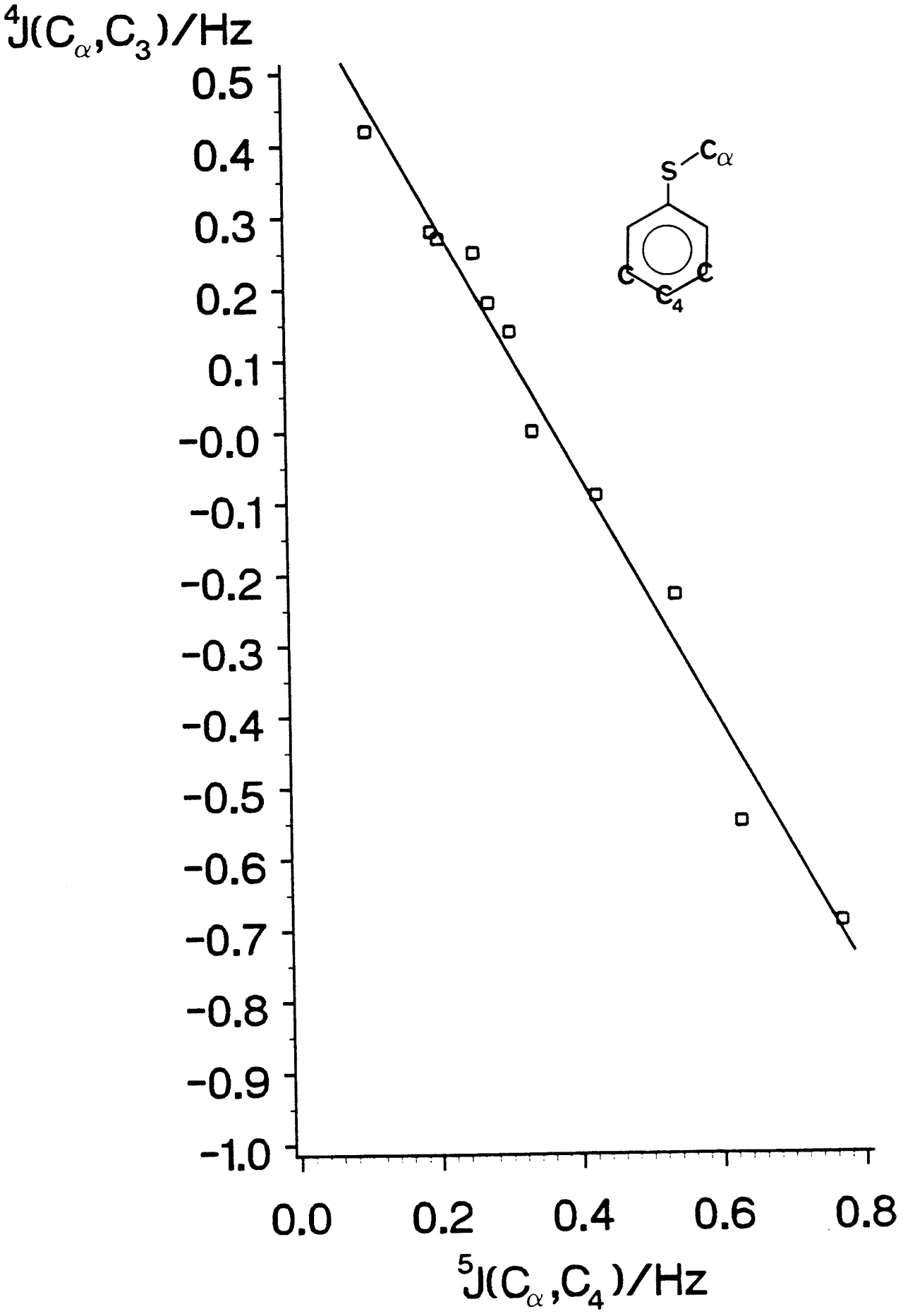
$^4J(C_\alpha,C_3)/Hz$
0.5
0.4
0.3
0.2
0.1
-0.0
-0.1
-0.2
-0.3
-0.4
-0.5
-0.6
-0.7
-0.8
-0.9
-1.0
0.0
0.2
0.4
0.6
0.8
$^5J(C_\alpha,C_4)/Hz$
S
C_α
C
C
C_4

Equation (92) is in agreement with INDO MO FPT computations in that both have a negative σ-π component. At this point the contributions of $^4J^{\sigma}_{180}$ or $^4J_0$ to the intercept in (92) cannot be deduced.

iii) $^3J(S^{13}C, C_2)$

The INDO MO FPT computations of $^3J(S^{13}C, C_2)$ suggest that an equation analogous to (91) can be written, equation (93).

$$^3J(S^{13}C, C_2) = {}^3J^{\sigma-\pi}_{90}\langle\sin^2\theta\rangle + 0.5\ {}^3J_{180} + {}^3J_0 \qquad (93)$$

A plot of $^3J(S^{13}C, C_2)$ against $^5J(S^{13}C, C_4)$ should be a straight line. Such a plot is shown in figure 21. The three points for the ethyl phenyl sulfide derivatives define a line parallel to that for the thioanisoles. These three points fit equation (94).

$$^3J(S^{13}C, C_2) = -3.01\ {}^5J(S^{13}C, C_4) + 3.32 \qquad (94)$$

The nine points for the thioanisole derivatives can be fit by equation (95), with r = -0.994. The point

$$^3J(S^{13}C, C_2) = -2.94\ {}^5J(S^{13}C, C_4) + 3.61 \qquad (95)$$

for 2,6-difluorothioanisole deviates considerably from the best line through the points and is not included in the linear regression.

Using equations (89) and (90) to relate $^5J(S^{13}C, C_4)$ to $\langle\sin^2\theta\rangle$ for the thioanisole and ethyl phenyl sulfides yields equations (96) and (97) respectively.

Figure 21

A plot of $^{3}J(S^{13}C, C_2)$ versus $^{5}J(S^{13}C, C_4)$ for some symmetrically substituted thioanisoles. The points were taken from table 2.

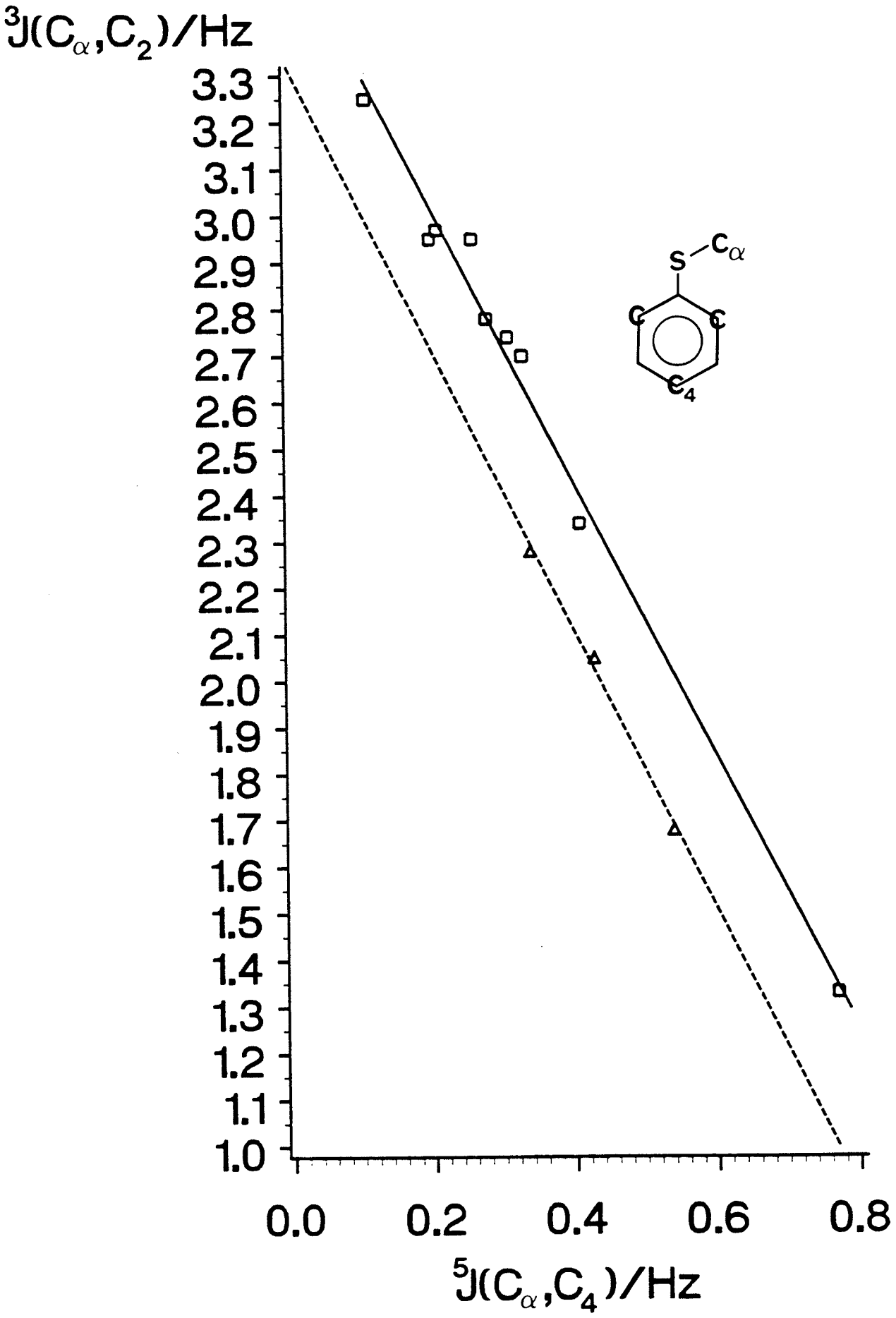
$^3J(C_\alpha,C_2)/Hz$
3.3
3.2
3.1
3.0
2.9
2.8
2.7
2.6
2.5
2.4
2.3
2.2
2.1
2.0
1.9
1.8
1.7
1.6
1.5
1.4
1.3
1.2
1.1
1.0
0.0
0.2
0.4
0.6
0.8
$^5J(C_\alpha,C_4)/Hz$
S
C_α
C
C
C_4

$$^{3}J(S^{13}C, C_2) = -2.68 \langle\sin^2\theta\rangle + 3.61 \quad (96)$$

$$^{3}J(S^{13}C, C_2) = -2.59 \langle\sin^2\theta\rangle + 3.32 \quad (97)$$

Equations (96) and (97) are in qualitative agreement with INDO MO FPT calculations which predict a negative slope and a large positive intercept. Equations (96) and (97) are also consistent with a Karplus relationship.

b) Barriers to internal rotation in some symmetrically substituted thioanisoles.

i) The use of $^{5}J(S^{13}C, C_4)$ to determine barriers in symmetrically substituted thioanisoles

Equations (89) and (90) may be used to relate $^{5}J(S^{13}C, C_4)$ to $\langle\sin^2\theta\rangle$. For symmetrically substituted thioanisoles the barriers to internal rotation are predominantly twofold and, as described in the introduction, $\langle\sin^2\theta\rangle$ can be related to the twofold barrier, V_2. Table 22 gives $\langle\sin^2\theta\rangle$ and V_2 values for a number of symmetrically substituted thioanisoles and ethyl phenyl sulfides. These values are deduced on the assumption of no intrinsic ring-substituent effect on the coupling mechanism for $^{5}J(S^{13}C, C_4)$. In section 2a) of this thesis it is shown that, for anisoles, such an effect is rather small.

Examination of table 22 reveals a trend of decreasing barrier height with increasing electron donating ability of the <u>para</u> substituent. Electron releasing groups in the <u>para</u> position will decrease delocalization of electrons through the C_1-S bond, reducing the bond order and reducing the barrier to rotation about that bond.

Table 22

Values of $^{5}J(S^{13}C, C_4)$[a], $\langle \sin^2\theta \rangle$ and V_2 for some symmetrically substituted thioanisoles.

Substituent	$^{5}J(S^{13}C, C_4)$	$\langle \sin^2\theta \rangle$	V_2(kJ/mol)
H	0.20(1)	0.22(1)	6.9(5)
H[b]	0.22(1)	0.24(1)	6.2(4)
2,6-diF	0.63(1)	0.69(1)	-4.5(4)
2,6-diCl	0.77(1)	0.85(1)	-11.5(8)
3,5-diCl	0.11(1)	0.12(1)	14.5(1.0)
4-Br	0.21(1)	0.23(1)	6.5(4)
4-Cl	0.26(1)	0.29(1)	4.7(3)
4-t-Bu	0.28(1)	0.31(1)	4.2(2)
4-CH_3	0.31(1)	0.34(1)	3.3(3)
4-F	0.33(1)	0.36(1)	2.9(3)
4-OCH_3	0.41(1)	0.45(1)	1.1(2)
β-CH_3	0.34(1)	0.39(1)	2.5(2)
4-CH_3-β-CH_3	0.43(1)	0.49(1)	0.2(2)
4-OCH_3-β-CH_3	0.54(1)	0.59(1)	-2.0(3)

[a] Taken from Table 2.

[b] In CS_2 solution, all other measurements in acetone-d_6.

Nonbonded (steric) interactions between the ortho chlorine or fluorine substituents and the methyl C-H bonds force the methylmercapto group to adopt a perpendicular conformation in the ground state. Negative V_2 values reflect this preference.

The ethyl phenyl sulfides display lower rotational barriers than the corresponding thioanisoles. This is due to steric interactions between the larger ethyl groups and the ortho C-H bonds, destabilizing the planar ground state. In fact, for 4-methoxyphenyl-ethyl-sulfide the perpendicular form is of lowest energy.

The STO-3G MO calculations of Baleja[70] indicate (see figure 1) a predominantly twofold barrier of 6.2 kJ/mol for thioanisole, somewhat lower than the value of 6.9 ± 0.5 kJ/mol reported here. A twofold barrier of 5.4 ± 0.5 kJ/mol was obtained from long-range $^{13}C,^{1}H$ couplings by Schaefer and Baleja[71]. An angle, $\langle\theta\rangle$, of 23 ± 5° has been deduced from dipole moment and induced birefringence data in CCl_4 solution[74]. This corresponds to a twofold barrier of 7.7 ± 1.5 kJ/mol. Electron diffraction patterns in the gas phase can be fit by a θ value of 45 ± 10°[75], suggesting a negligible twofold barrier.

The long-range couplings between the methyl carbon-13 nucleus and the ring carbon-13 nuclei for thioanisole are consistent with a slightly lower barrier to internal rotation in CS_2 solution relative to that in acetone-d_6 solution. The barrier height in CS_2 solution, derived from $^{5}J(S^{13}C, C_4)$ is 6.2 ± 0.4 kJ/mol. The change in rotational barrier in going from highly polar (acetone) solvent to non-polar (CS_2) solvent is just beyond the uncertainty in the experimental measurements.

Long-range $^{13}C,^{1}H$ and $^{13}C,^{19}F$ coupling constants in 4-methylthioanisole and 4-fluorothioanisole[71] yield barriers of 3.3 ±

0.3 and 3.8 ± 0.4 kJ/mol, respectively. These are in reasonable agreement with the present results. The microwave barrier for 4-fluorothioanisole in the gas phase, based on relative intensities[76], is 3.0 ± 1.0 kJ/mol, also in good agreement with the present work. STO-3G MO computations yield barriers of 4.9 and 4.6 kJ/mol for 4-methylthioanisole and 4-fluorothioanisole respectively[71].

The presence of two meta chlorine substituents increases the barrier substantially, from 6.9 ± 0.5 kJ/mol to 12.5 ± 1.0 kJ/mol. Such an increase in barrier height has been confirmed by long-range couplings to the para proton in 3,5-dichlorothiophenol[12] and 3,5-dichlorothioanisole[13].

ii) Use of $^{3}J(S^{13}C, C_2)$ and $^{4}J(S^{13}C, C_3)$

If, for some reason, the ^{13}C nmr spectrum of the para carbon of a thioanisole derivative cannot be observed, it is useful to relate $^{3}J(S^{13}C, C_2)$ or $^{4}J(S^{13}C, C_3)$ to the barrier to internal rotation. Equations (92), (96) and (97) may be used to obtain $\langle \sin^2\theta \rangle$, which may then be used to deduce the twofold barrier.

The rotational barriers in 4-nitrothioanisole and 4-aminothioanisole are of particular interest because they represent the two extremes in substituent π electron withdrawing and donating ability. Unfortunately, in both molecules, relaxation of the quadrupolar ^{14}N nuclei results in broad peaks for the directly bonded para carbon nuclei, precluding observation of any small splittings. The meta and ortho carbon nuclei are not as strongly coupled to the ^{14}N nucleus and therefore yield sharper resonances.

Table 23 shows the long-range coupling constants, $\langle \sin^2\theta \rangle$ and V_2 values for 4-aminothioanisole and 4-nitrothioanisole. The meta carbon peak for 4-aminothioanisole is broad and no splitting to the methyl carbon nucleus is observed.

The $\langle \sin^2\theta \rangle$ values and corresponding barrier heights clearly show a strong stabilization and destabilization of the planar conformation by para nitro and amino groups, respectively.

In table 24 values of $^3J(S^{13}C, C_2)$, $\langle \sin^2\theta \rangle$ and V_2 are presented for 3,5-dichloro-4-hydroxythioanisole, a, 3,5-dichloro-4-methoxythioanisole, b, 3,5-dichlorothioanisole, c, and 4-methoxythioanisole, d. In these compounds the ^{13}C signals of the ortho ^{13}C nuclei are easily observed even in dilute solutions. In a and b all other ring carbon signals are much less intense, lacking the NOE experienced by the ortho carbons, and are obscured by baseline noise. Therefore, for dilute solutions of a and b, $^3J(S^{13}C, C_2)$ is used to deduce V_2.

In d the barrier to rotation of the SCH_3 group is rather low, due to the strong π electron donating ability of the para methoxy group. A para hydroxy substituent would have about the same effect. In a the barrier lies between that for c and d, with the effect of the para hydroxy group dominating. In a the hydroxy group can hydrogen bond to the meta chlorine atoms, allowing maximum delocalization between the oxygen long-pair and phenyl ring π electrons. When the hydroxy group is methylated, to give b, hydrogen bonding is absent and the OCH_3 group is forced to be perpendicular to the benzene ring plane. Delocalization is now minimized and this is reflected in a higher barrier for b relative to a. The barrier in b is not as high as that for c, suggesting that

Table 23

Barriers to internal rotation about the C_1-S bond in 4-nitrothioanisole and 4-aminothioanisole, as deduced from $^3J(S^{13}C, C_2)$ and $^4J(S^{13}C, C_3)$.

	4-NO_2	4-NH_2
$^3J(S^{13}C, C_2)$	3.35(1)	1.94
$\langle\sin^2\theta\rangle$	0.10(1)	0.62(1)
$^4J(S^{13}C, C_3)$	(+)0.47(1)	-
$\langle\sin^2\theta\rangle$	0.11(1)	-
V_2	14.0(2.0)[a]	-2.8(4)[a]

[a]The uncertainty, given here in parentheses, reflects only the uncertainty in the observed couplings. A more rigorous treatment would require consideration of the uncertainties in the slopes and intercepts of equations (92) and (97).

[b]Coupling constants given in Hz. Rotational barriers given in kJ/mol.

Table 24

Barriers to internal rotation in some symmetrically substituted thioanisoles as deduced from $^{3}J(S^{13}C, C_2)$.[a]

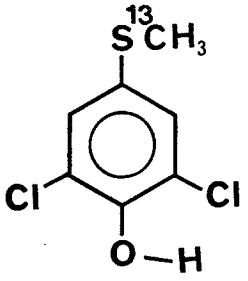

a

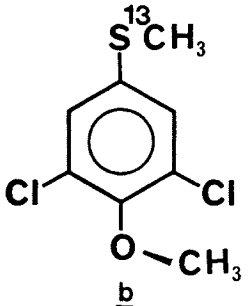

b

	a	b
$^{3}J(S^{13}C, C_2)$	2.67	3.01
$\langle \sin^2\theta \rangle$	0.351	0.224
V_2	3.4	7.5

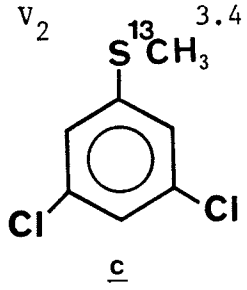

c

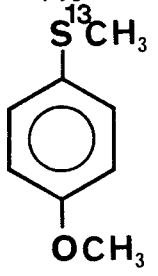

d

	c	d
$^{3}J(S^{13}C, C_2)$	3.25	2.34
$\langle \sin^2\theta \rangle$	0.134	0.474
V_2	13.0	0.6

[a]Coupling constants in Hz. Rotational barriers in kJ/mol.

there is still some donation of π electron density by the orthogonal methoxy group.

c) Ortho substituted thioanisoles.

The rotational potentials for ortho substituted thioanisoles will have large onefold as well as twofold components. For such potential functions, equations (92), (96) and (97) are no longer valid.

If the SCH_3 group in 2-hydroxythioanisole is taken as orthogonal to the benzene ring, as previously assumed, and if 2-bromothioanisole is taken as rigid with the SCH_3 group in the ring plane and trans to the ortho bromine substituent, then the values of J_0, J_{90} and J_{180} can be estimated for $^3J(S^{13}C, C_2)$ and $^4J(S^{13}C, C_3)$. This is a crude approximation since there may exist substantial torsional motion of the SCH_3 group about the C_1-S bond in 2-bromothioanisole. From table 5, the estimated values are: $^3J_{90}^{\sigma-\pi} \simeq -2.10$, $^3J_{180}^{\sigma} \simeq -2.0$, $^3J_0 \simeq 4.2$, $^4J_{90}^{\sigma-\pi} \simeq -1.0$, $^4J_{180}^{\sigma} \simeq -0.6$ and $^4J_0^{\sigma} \simeq 0.6$ Hz. Considering the nature of the approximation, these values are in reasonable agreement with the $J_{90}^{\sigma-\pi}$ and $[0.5\ J_{180}^{\sigma} + J_0]$ values in equations (92) and (97).

In 2-fluorothioanisole and 2-methoxythioanisole $^5J(S^{13}C, C_4)$ is 0.29 and 0.25 Hz, respectively. Equation (89) yields 0.32 and 0.27 for $\langle \sin^2\theta \rangle$ in 2-fluorothioanisole and 2-methoxythioanisole respectively. The size of $\langle \sin^2\theta \rangle$ for these two molecules suggests that non-planar conformations are significantly populated. The fluoro and methoxy substituents are both π electron donating, and, in the ortho position, will reduce the 3p...π conjugation through the C_1-S bond, allowing large amplitude libration of the SCH_3 group.

It is likely that in 2-aminothioanisole hydrogen bonding between an amino N-H bond and the sulfur 3p orbital holds the SCH_3 group rigidly as is proposed for 2-hydroxy thioanisole. Aniline is nonplanar and, in the gas phase, the N-H bonds make an angle of 21° with the phenyl ring[77]. If the amino group is also nonplanar in 2-aminothioanisole, then the 3p orbitals will not be held exactly in plane and the SCH_3 group will twist about the C_1-S bond so as to optimize the N-H...S hydrogen bond. This situation is depicted in 7.

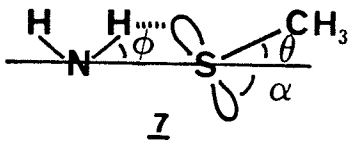

7

ϕ = 21°*

θ = 60°, 66°

α = 30°, 24°

If the molecule is taken as rigid, then $^5J(S^{13}C, C_4)$ in CCl_4 solution and $^6J(S^{13}C, H_4)$ in acetone-d_6 solution give angles, θ, of 66° and 60°, respectively. In acetone-d_6 solution the N-H bond not hydrogen bonding to the 3p sulfur orbital can form an intermolecular hydrogen bond to a solvent molecule, perhaps changing the conformation of the amino group and the stereospecific hydrogen bond to sulfur.

For 2-hydroxythioanisole the intramolecular O-H...S hydrogen bond must be broken if there is to be intermolecular hydrogen bonding to the solvent. In acetone-d_6 solution the ^{13}C nmr peaks broaden and the long-range $^{13}C,^{13}C$ couplings change from those in the CCl_4 solution. When the hydroxyl group is hydrogen bonded to the solvent the effect of this group on the conformation of the SCH_3 moiety will resemble that of a methoxy group. Now assume that, in acetone solution,

*This is the value for unsubstituted aniline in the gas phase.

2-hydroxythioanisole exists as an equilibrium mixture of 8a and 8b. In 8a $^{5}J(S^{13}C, C_4)$ is taken as 0.25 Hz and in 8b as 0.91 Hz. Then

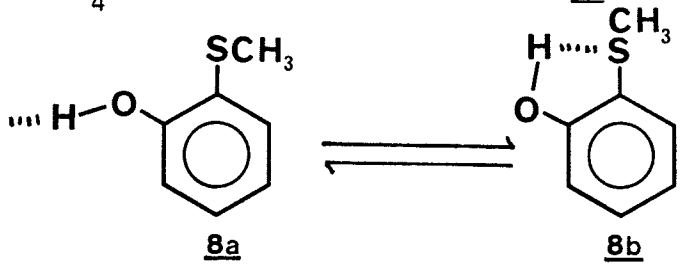

8a 8b

the populations of 8a and 8b are 0.682 and 0.318, respectively, with an equilibrium constant of 0.47 at 300K. The corresponding free energy difference is 1.9 kJ/mol. A variable temperature study of this equilibrium would be of considerable interest.

2. Anisoles

a) Substituent effects on the long-range coupling constants between the sidechain and ring carbon-13 nuclei in anisole derivatives.

It is of interest, at this point, to investigate the magnitude of the effect of substituents on the long-range $^{13}C,^{13}C$ coupling constants between sidechain and ring carbon nuclei.

In ortho dichloro- and dibromoanisoles, the $O\text{-}C_\alpha$ bond of the methoxy moiety is taken as effectively perpendicular to the plane of the phenyl ring. Then any changes in $^{13}C,^{13}C$ coupling constants for meta and para derivatives of these molecules may be assigned to intrinsic perturbations of the coupling mechanism involved and not to changes in conformation.

i) Effects on $^{5}J(0^{13}C, C_4)$

Consider the $^{5}J(0^{13}C, C_4)$ values reported for the molecules depicted in figure 22a-h. Comparison of a with d and of b with e shows that interchange of ortho bromine and chlorine substituents has very little effect on $^{5}J(0^{13}C, C_4)$. Compound b has a $^{5}J(0^{13}C, C_4)$ value of 0.92 Hz. This value does not change upon meta substitution to give c, suggesting that $^{5}J(0^{13}C, C_4)$ is also insensitive to a change in meta substituent. Comparison of the values for a and b shows that the presence of a para fluorine substituent increases $^{5}J(0^{13}C, C_4)$ by 0.08 Hz. This increase is also observed for the corresponding ortho dibromo derivatives, d and e. A similar increase is induced by a para methyl substituent, as in f. A para ester group, as in g, does not change the coupling constant significantly, relative to the parent compound e. The presence of a β-methyl substituent also appears to have little effect on $^{5}J(0^{13}C, C_4)$.

In summary, it appears that $^{5}J(0^{13}C, C_4)$ is significantly perturbed only by the presence of a substituent on C_4.

ii) Effects on $^{4}J(0^{13}C, C_3)$

The observed $^{4}J(0^{13}C, C_3)$ for a through h (as shown in figure 23) are nearly equal, with two exceptions. The presence of meta chlorine substituents increases the coupling from 0.86 Hz in b to 1.02 Hz in c and the presence of a β methyl group, as in h, decreases $^{4}J(0^{13}C, C_3)$, but by only 0.05 Hz.

Again, as for $^{5}J(0^{13}C, C_4)$, only directly bonded substituents have a significant effect on $^{4}J(0^{13}C, C_3)$.

Figure 22

The structure of some substituted anisoles together with the corresponding values of $^{5}J(O^{13}C, C_4)$, the coupling constant between the methyl carbon-13 nucleus and the <u>para</u> ring carbon nucleus.

1.00

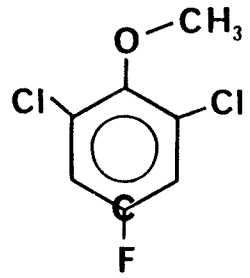

a

0.92

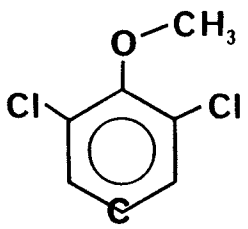

b

0.92

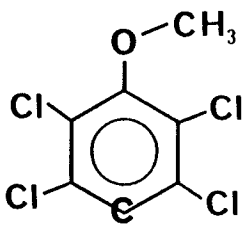

c

1.02

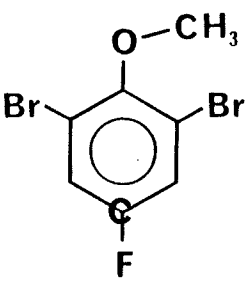

d

0.94

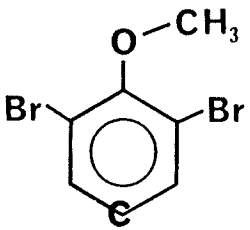

e

1.01

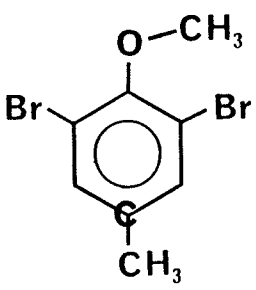

f

0.92

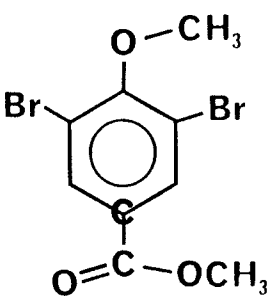

g

0.95

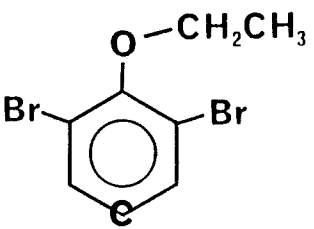

h

Figure 23

The structures of some substituted anisoles together with the corresponding values of $^{4}J(O^{13}C, C_3)$, the coupling constant between the methyl carbon-13 nucleus and the <u>meta</u> ring nuclei.

0.86

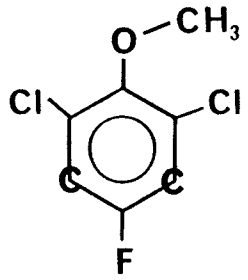

a

0.86

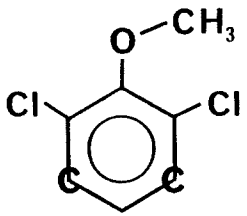

b

1.02

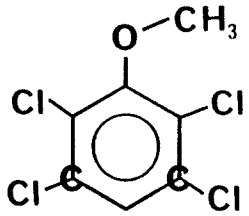

c

0.87

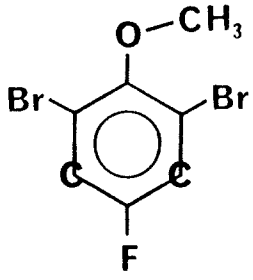

d

0.87

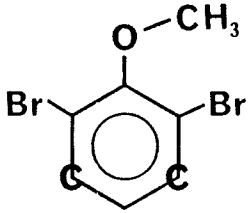

e

0.89

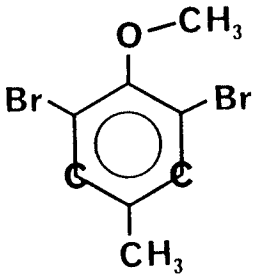

f

0.85

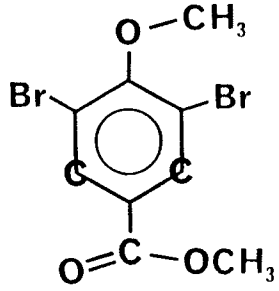

g

0.82

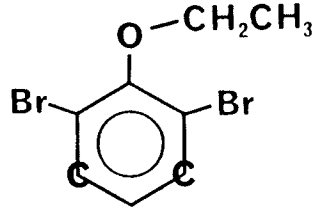

h

iii) Effects on $^{3}J(O^{13}C, C_2)$

It is not possible to hold the methoxy group orthogonal to the benzene ring in the absence of bulky ortho groups. It is possible, though, to compare $^{3}J(O^{13}C, C_2)$ for two different bulky substituents. Comparison of a with d and b with e (see figure 24) suggests that chlorine substituents in the ortho positions increase $^{3}J(O^{13}C, C_2)$ slightly with respect to bromine substituents. $^{3}J(O^{13}C, C_2)$ remains the same for the 2,6-dibromo-4-X-anisoles, where X=F (d), H(e), CH_3(f) or O=C-OCH_3 (g). Placing meta substituents on 2,6-dichloroanisole, b, to give 2,3,5,6-tetrachloroanisole, c, only changes $^{3}J(O^{13}C, C_2)$ slightly. The presence of a β methyl group decreases $^{3}J(O^{13}C, C_2)$ slightly, as seen by comparison of e with h. $^{3}J(O^{13}C, C_2)$ appears to be perturbed by substituents in the β or ortho positions.

In summary, it can be deduced that the long-range coupling constants between the α-carbon-13 nucleus and the ring carbon-13 nuclei in anisoles are only significantly perturbed by the presence of substituents directly connected to either or both of the coupled nuclei. In anisoles this intrinsic perturbation is usually rather small.

b) Stereospecific $^{3}J(O^{13}C, C_2)$ in meta and para symmetrically substituted anisoles.

$^{3}J(O^{13}C, C_2)$ values for several anisoles symmetrically substituted in the meta and para positions are presented in table 25. A range of 0.29 Hz is evenly covered by the six compounds. Considering the small intrinsic effect on $^{3}J(O^{13}C, C_2)$ expected from meta or para substituents, such a range in coupling constants is probably due to changes in conformation.

Figure 24

The structures of some substituted anisoles together with the corresponding values of $^{3}J(O^{13}C, C_2)$, the coupling constant between the methyl carbon-13 nucleus and the ortho ring carbon nuclei.

1.53

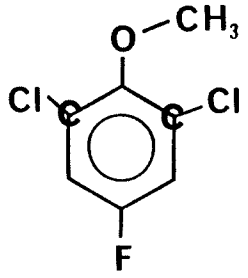

a

1.58

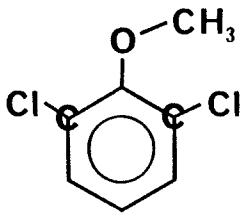

b

1.55

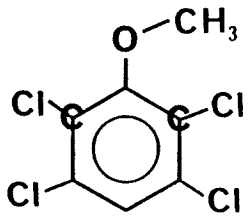

c

1.60

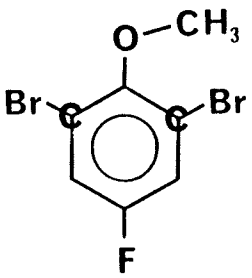

d

1.62

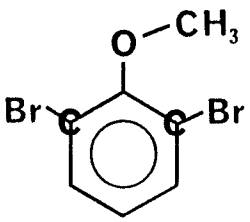

e

1.61

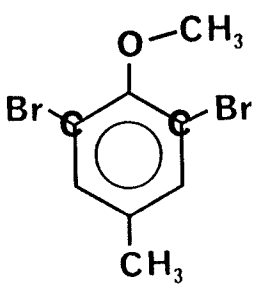

f

1.61

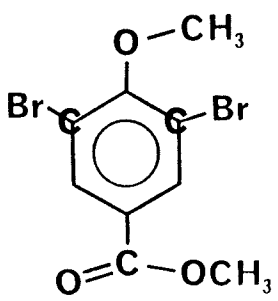

g

1.56

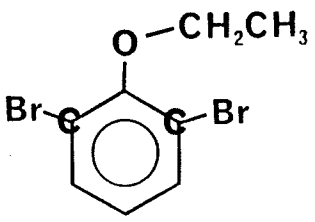

h

If $^{3}J(O^{13}C, C_2)$ is taken as about 4.4 Hz for a rigid planar molecule and as about 1.7 Hz for a rigid molecule with $\theta = 90°$, an approximate equation analogous to equation (96) can be written

$$^{3}J(O^{13}C, C_2) = -2.7\langle\sin^2\theta\rangle + 4.4 \qquad (98)$$

Equation (98) predicts that, as the methoxy group twists away from the plane of the benzene ring via large amplitude vibration about the C_1-O bond, $^{3}J(O^{13}C, C_2)$ should decrease. Table 25 shows a definite trend of decreasing $^{3}J(O^{13}C, C_2)$ with strong π electron donating ability of the <u>para</u> substituent, as expected.

A higher value of $^{3}J(O^{13}C, C_2)$ in 3,5-dichloroanisole implies a decrease in $\langle\sin^2\theta\rangle$. This is consistent with experiments on 3,5-dichlorothioanisole[71] and 3,5-dichlorothiophenol[12].

It has been suggested that for strongly conjugated π systems, as in anisole, a π mechanism can contribute a term in $J_0\langle\cos^2\theta\rangle$ to the observed coupling between sidechain and ring nuclei. If such a term does contribute, it will be absorbed into equation (98), (recall that $\cos^2\theta = 1 - \sin^2\theta$).

c) Stereospecific $^{4}J(O^{13}C, C_3)$ in <u>ortho</u> and <u>para</u> symmetrically substituted anisoles.

$^{4}J(O^{13}C, C_3)$ values for some <u>ortho</u> and <u>para</u> symmetrically substituted anisoles are presented in table 26. As in the corresponding thioanisoles, $^{4}J(O^{13}C, C_3)$ is taken as positive for the <u>para</u> substituted anisoles and as negative for the <u>ortho</u> disubstituted anisoles. From

Table 25

$^{3}J(O^{13}C, C_2)^{a}$ in some meta and para substituted anisoles.

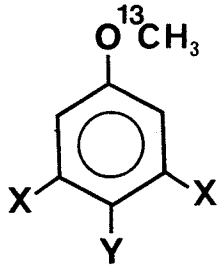

Substituent	$^{3}J(O^{13}C, C_2)$
3,5-diCl	4.26(1)
4-O=C-H	4.19(1)
4-H	4.12(1)
4-F	4.06(1)
4-CH_3	4.05(1)
4-OCH_3	3.97(1)

[a]Coupling constants in Hz.

table 26 an approximate analogue to equation (92) may be written as equation (99)

$$^{4}J(O^{13}C, C_3) = -1.52\langle\sin^2\theta\rangle + 0.65 \qquad (99)$$

INDO MO FPT computations predict a negative $^{4}J^{\sigma-\pi}_{90}$ and a positive $^{4}J^{\sigma}_{180}$ (see table 21).

The trend of decreasing $^{4}J(O^{13}C, C_3)$ (increasing $\langle\sin^2\theta\rangle$) with increasing π electron donating ability of the para substituent is apparent from table 26.

$^{4}J(O^{13}C, C_3)$ is larger in 2,6-difluoroanisole than in 2,6-dichloroanisole or 2,6-dibromoanisole. This suggests that $\langle\sin^2\theta\rangle$ has decreased and that the barrier to rotation about the C_1-O bond is lower in 2,6-difluoroanisole. This is supported by $\langle\sin^2\theta\rangle$ and V_2 derived from $^{5}J(O^{13}C, C_4)$.

d) Ortho substituted anisoles.

Long-range $^{13}C,^{13}C$ coupling constants between sidechain and ring carbon-13 nuclei for three ortho substituted anisoles are given in table 27. Examination of table 27 reveals that those over n bonds slowly approach $^{n}J_{90}$ as the electron donating ability of the ortho substituent increases.

If 0.94 is taken as $^{5}J_{90}$, then $\langle\sin^2\theta\rangle$ is 0.19 for the two methoxy groups in 1,2-dimethoxy benzene. It has been suggested that 1,2-dimethoxybenzene is in an equilibrium between two conformations, one with both methoxy groups in plane, 10, and one with one methoxy group perpendicular to the benzene ring, shown as 11 and 12.

Table 26

$^4J(O^{13}C, C_3)^a$ in some ortho and para symmetrically substituted anisoles.

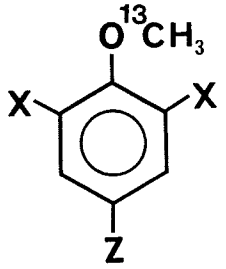

Substituent	$^4J(O^{13}C, C_3)$
4-H	(+)0.54(1)
4-CH_3	(+)0.49(1)
4-F	(+)0.45(1)
4-OCH_3	(+)0.41(1)
2,6-diF	-0.62(1)
2,6-diCl	-0.86(1)
2,6-diBr	-0.87(1)

[a]Coupling constants in Hz.

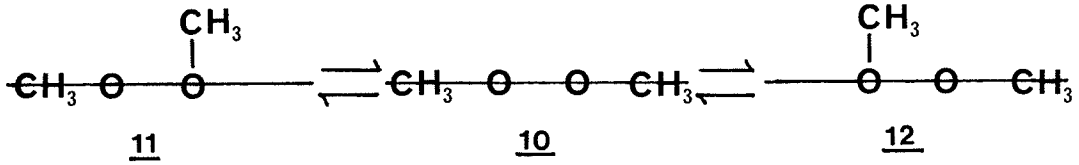

11 10 12

If 10, 11 and 12 are equally populated, then $\langle \sin^2\theta \rangle$ is 0.25. A value of 0.19 suggests that, for this model, 10 is slightly preferred.

On the basis of through-space coupling between methyl protons and ortho protons in several anisole derivatives, Schaefer and Laatikainen[79] interpreted $^5J(H_{ortho},CH_3)$ in 1,2-dimethoxybenzene in terms of a planar molecule undergoing large out-of-plane torsions. It seems possible that the two methoxy groups are undergoing large amplitude libations while maintaining the C_2 symmetry of the molecules, as shown by 13 rather than jumping between two rigid conformations. If the molecule were rigid, yet maintaining C_2 symmetry, $^5J(O^{13}C, C_4)$ would be consistent with with an angle, θ, of 26°. The average amplitude of oscillation would therefore be rather less than 26°.

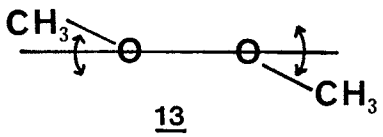

13

e) Stereospecific $^6J(O^{13}C, H_4)$ in ortho disubstituted anisoles.

Table 28 lists $^6J(O^{13}C, H_4)$ for several 2,6-disubstituted anisoles. In 2,6-dibromoanisole and 2,6-dibromo-4-methylanisole it is assumed that the methoxy group is perpendicular to the benzene ring. Then for a σ-π mechanism, in which the coupling is transmitted via the π orbitals of the benzene ring, $^7J(O^{13}C, \underline{C}H_3)$ in 2,6-dibromo-4-methylanisole should be

Table 27

Long-range $^{13}C,^{13}C$ coupling constants[a] in some ortho substituted anisoles.

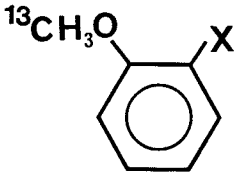

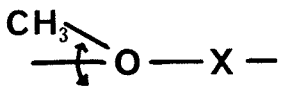

X	$^3J(O^{13}C,C_6)$	$^3J(O^{13}C,C_2)$	$^4J(O^{13}C,C_5)$	$^4J(O^{13}C,C_3)$	$^5J(O^{13}C,C_4)$
Br	4.94(1)	3.26(1)	0.55(1)	0.28(1)	>0.05
F	4.74(1)	2.76(1)	0.42(1)	0.23(1)	0.07(3)[b]
OCH_3	4.77(1)	2.52(1)	0.38(1)	0.17(1)	0.175
limit $\theta\rightarrow 90°$[c]		+1.60		-0.87	+0.94

[a]Coupling constants are in Hz.

[b]Lines for C_4 are broad.

[c]Couplings are those for 2,6-dibromoanisole.

equal to $-{}^{6}J(O^{13}C, H_4)$ in 2,6-dibromoanisole. The signs of these two couplings are unknown. However, these magnitudes are equal to within experimental error.

In 2,6-dichloroanisole ${}^{6}J(O^{13}C, H_4)$ is 0.602 Hz, slightly smaller than in 2,6-dibromoanisole, and may be due to a slight deviation of the methoxy group from a perpendicular conformation due to torsional motion, although ${}^{5}J(O^{13}C, C_4)$ shows no evidence of this.

${}^{6}J(O^{13}C, H_4)$ in 2,6-dimethylanisole is consistent with a perpendicular conformation of the methoxy group. The repulsive interaction between the C-H bonds of the methoxy and methyl groups may be aided by the π electron donating ability of the ortho methyl substituents in destabilizing the planar conformation.

The π electron releasing ability of the 1 and 3 methoxy groups in 1,2,3-trimethoxybenzene probably plays a significant role in destabilizing the planar conformation of the central methoxy group. Through-space coupling between methoxy protons and ortho protons indicates planar conformations for the 1- and 3-methoxy substituents[79]. In this conformation the methoxy oxygens will not greatly hinder the rotation of the 2-methoxy moiety and one might expect ${}^{6}J(O^{13}C, H_5)$ to be closer to that for 2,6-difluoroanisole. For such a conformation oxygen may be taken as approximately as large as a fluorine substituent. However, when the 1- and 3-methoxy groups are in the plane of the benzene ring maximum donation of electrons from the oxygen lone pair to the phenyl system is allowed. This will destabilize a conformation with the central methoxy in the ring plane. In 1,2,3-trimethoxybenzene, ${}^{6}J(O^{13}C, H_5)$ is 0.601(2) Hz, consistent with the conformation shown as 14.

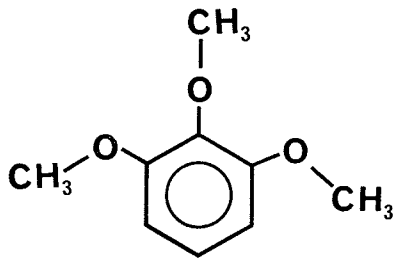

14

In 2,6-difluoroanisole $^{6}J(O^{13}C, H_4)$ is 0.473(1) Hz. Taking $^{6}J_{90}$ as 0.63(1) Hz, one has $\langle \sin^2\theta \rangle$ as 0.75(1). This number corresponds to a V_2 of 6.6 ± 0.3 kJ/mol. The twofold barrier in 2,3,5,6-tetrafluoroanisole derived from $^{6}J(O^{13}C, H_4)$ is 0.4 ± 0.4 kJ/mol[37]. A planar conformation is stabilized by meta fluorine substituents, as in thiophenols[12] and thioanisoles[71].

Table 28

^{6}J ($O^{13}C,H_4$) in some ortho disubstituted anisoles.[a]

Substituent	$^{6}J(O^{13}C,H_4)$[b]
2,6-diBr	(-)0.625(7)
2,6-diCH_3	(-)0.622(3)
2,6-diCl	(-)0.603(5)
2,6-diOCH_3	0.601(2)
2,6-diF	(-)0.473(1)
H	≤0.03

[a] In acetone-d_6 solution

[b] Coupling constants in Hertz

3. Alkyl Phenyl Selenides and Alkyl Phenyl Tellurides

The investigation of phenyl selenides and phenyl tellurides seems a natural extension of the work done on anisoles and thioanisoles and completes the series of molecules depicted as 15.

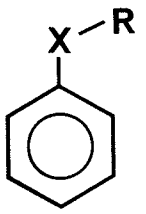

15

X = O, S, Se, Te

R = alkyl

In these molecules, stabilization of the planar ground state by p-π conjugation between lone-pair p-orbitals on the X atom and the aromatic π-system is expected to decrease in the order O > S > Se > Te. This decrease is partly due to an increase in C_1-X bond length in the series, leading to a decrease in the effective p-π orbital overlap.

The difficulty in applying the J method to alkyl phenyl selenides and alkyl phenyl tellurides is in the deduction of a $^5J_{90}$ value. The synthesis of a methyl phenyl selenide-^{13}C or methyl phenyl telluride-^{13}C derivative with bulky ortho substituents, so as to force the side chain to lie orthogonal to the phenyl ring plane, poses some problems. An alternative method, based on a linear relationship between $^5J(X^{13}C, C_4)$ and δC_4, is employed. In part D7) of this thesis it is shown that a linear relationship exists between δC_4 and $^6J(S\underline{C}, F_4)$ for alkyl 4-fluorophenyl sulfides. If only the points for methyl-4-fluorophenyl sulfide and ethyl-4-fluorophenyl sulfide are used to derive the equation

relating $^{6}J(S\underline{C}, F_4)$ to δC_4, then δC_4 for t-butyl-4-fluorophenyl sulfide may be substituted into this equation and $^{6}J(S\underline{C}, F_4)$ can be predicted. The predicted value, 1.40 Hz, is very near the observed value of 1.38 Hz. Since the t-butyl group is a very bulky group, $^{6}J(S\underline{C}, F_4)$ in t-butyl-4-fluorophenyl sulfide may be taken as an approximation to $^{6}J_{90}$. The $^{6}J_{90}$ value used in this laboratory, taken from 2,6-dibromo-4-fluorothioanisole, is 1.47 Hz, fairly close to that predicted. The lower value for t-butyl-4-fluorophenyl sulfide may be due to the presence of the β-methyl groups.

A similar treatment of the data for thioanisole-^{13}C and ethyl phenyl sulfide-^{13}C predicts a $^{5}J(S^{13}C, C_4)$ value of 0.92 Hz for t-butyl phenyl sulfide. The $^{5}J_{90}$ value established earlier in this thesis is 0.91 Hz.

All the δC_4 values used here are taken from the literature, where these values have been reported in the same solvent for all the alkyl-4-fluorophenyl sulfides[80] and alkyl phenyl sulfides[81].

The success of the two examples given above suggests that, if $^{5}J(X^{13}C, C_4)$ and δC_4 are known for two alkyl phenyl derivatives of selenium or tellurium and if a δC_4 value is known for an alkyl phenyl derivative in which the alkyl group sits perpendicular to the phenyl ring (t-butyl group), then $^{5}J_{90}$ $(X^{13}C, C_4)$ may be deduced.

a) Alkyl phenyl selenides.

$^{5}J(Se^{13}C, C_4)$ is 0.27 Hz and 0.38 Hz in methyl phenyl selenide-^{13}C and ethyl phenyl selenide-^{13}C, respectively. For the neat compounds δC_4 is 125.55 ppm and 126.24 ppm, respectively[82]. The assumption of a linear relationship between $^{5}J(Se^{13}, C_4)$ and δC_4 yields two equations in

two unknowns. Solution of this set of linear equations yields equation (100). δC_4 for neat t-butyl phenyl selenide is 128.10 ppm[82].

$$^5J(Se^{13}C, C_4) = -19.745 + 0.1594\ \delta C_4 \qquad (100)$$

Substitution of this number into equation (100) gives an estimated $^5J_{90}$ of 0.68 Hz and equation (101) may be written

$$^5J(Se^{13}C, C_4) = 0.68 \langle \sin^2\theta \rangle \qquad (101)$$

$^5J(Se^{13}C, C_4)$ values for methyl phenyl selenide-^{13}C and ethyl phenyl selenide-^{13}C can now be substituted into equation (101) to yield $\langle \sin^2\theta \rangle$ and hence apparent V_2 values may be deduced. These are provided in table 28. The barrier in the ethyl derivative is the lower one, reflecting the greater steric requirement of an ethyl group. A twofold barrier of 2.2 ± 1.0 kJ/mol for methyl phenyl selenide has $\langle\theta\rangle$ as 38 ± 5°, in good agreement with the angles of 40 ± 13° and 40 ± 5° deduced from electron diffraction[83] and nematic phase nmr experiments[84].

The values of $^3J(Se^{13}C, C_2)$ and $^4J(Se^{13}C, C_3)$ for methyl phenyl selenide-^{13}C and ethyl phenyl selenide-^{13}C allow an estimation of the conformational dependences of these coupling constants.

$$^3J(Se^{13}C, C_2) \simeq -3.34 \langle \sin^2\theta \rangle + 3.52 \qquad (102)$$

Solution of the set of equations for $^4J(Se^{13}C, C_3)$ only give reasonable coefficients if $^4J(Se^{13}C, C_3)$ is taken as positive in methyl phenyl

selenide-^{13}C and negative in ethyl phenyl selenide^{13}C. Equation (103) may then be written

$$^{4}J(Se^{13}C, C_3) \simeq -1.20\langle\sin^2\theta\rangle + 0.56 \qquad (103)$$

Equations (102) and (103) agree well with analogous equations for thioanisole and anisole derivatives.

b) Alkyl phenyl tellurides.

The $^{5}J(Te^{13}C, C_4)$ and δC_4[85] values for methyl phenyl telluride-^{13}C and ethyl phenyl telluride-^{13}C may be used to obtain equation (104)

$$^{5}J(Te^{13}C, C_4) = -16.20 + 0.1304\,\delta C_4 \qquad (104)$$

A δC_4 value for t-butyl phenyl telluride is not available. δC_4 in t-butyl phenyl selenide (128.10 ppm) is nearly that of unsubstituted benzene (128.40 ppm)[82]. These two shift values may be taken as estimates of that for t-butyl phenyl telluride. The former assumes that a small degree of 5p-π conjugation still exists when θ is 90°, the latter assumes that there is no 5p-π overlap. Now, by substitution of either of these shift values into equation (104) one may write equation (105)

$$^{5}J(Te^{13}C, C_4) = 0.54(4)\,\langle\sin^2\theta\rangle \qquad (105)$$

Substitution of the $^{5}J(Te^{13}C, C_4)$ values for methyl phenyl telluride-^{13}C and ethyl phenyl telluride-^{13}C into equation (105) yields $\langle\sin^2\theta\rangle$ values

of 0.574 and 0.685, respectively. The corresponding V_2 values are -1.7 ± 1.0 kJ/mol and -4.0 ± 1.0 kJ/mol, respectively. These numbers together with $\langle\theta\rangle$ values are collected into table 28.

The $^3J(Te^{13}C, C_2)$ values for methyl phenyl telluride-^{13}C and ethyl phenyl telluride-^{13}C may be used to deduce the conformational dependence of this coupling constant. Equation (106) can be written

$$^3J(Te^{13}C, C_2) \simeq -3.15 \langle\sin^2\theta\rangle + 3.32 \qquad (106)$$

Unfortunately, splittings due to $^4J(Te^{13}C, C_3)$ were not observed and an equation analogous to equation (105) could not be written.

Note that equations (102), (103) and (106) assume that there is no perturbation of the $^{13}C,^{13}C$ coupling mechanism due to the presence of a β methyl group (i.e. in the ethyl derivatives); such a perturbation is known to alter $^3J(S^{13}C, C_2)$.

In anisole the barrier height, V_2, is just beyond the range of the J method (>20 kJ/mol). In thioanisole the apparent V_2 ranges from 5.4(5) to 7.6(5) kJ/mol. Based on assumptions put forward in sections a) and b), the twofold barriers in methyl phenyl selenide and methyl phenyl telluride are 2.5 ± 1.0 kJ/mol and -1.7 ± 1.0 kJ/mol, respectively. As expected, the apparent twofold barriers to rotation about the C_1-X bond decrease in the order O > S > Se > Te.

It is also worth noting that the sizes of the $^5J_{90}$ values deduced so far decrease in the order O > S > Se > Te. This is quite reasonable, given that $^5J(X^{13}C, C_4)$ is dominated by a σ−π mechanism. The σ−π mechanism can be visualized as a hyperconjugative transmission of spin state information from the π electron system of the phenyl group to the

$X-C_{\alpha}$ bond electrons. An increase in C_1-X bond length, which follows the series Te > Se > S > O, should reduce effective overlap of the $X-C_{\alpha}$ bond and the $p\pi$ orbital on C_1, in turn reducing transmission of spin state information.

In summary, as predicted, the stabilization of the planar ground state of molecules of type 15 decreases in the order O > S > Se > Te. This is reflected in the apparent twofold barriers to rotation about the C_1-X bond which also decrease in that order. In methyl phenyl selenide, the barrier agrees quite well with those obtained from electron diffraction and nematic phase nmr experiments. The $^5J_{90}$ values also decrease in the above mentioned order, as expected, if transmission of spin information is less effective over a greater C_1-X bond length.

Table 28

$^{5}J(X^{13}C, C_4)$, $\langle \sin^2\theta \rangle$, V_2[a] and $\langle \theta \rangle$ values for some alkyl phenyl derivatives of selenium and tellurium.

X-R	$^{5}J(X^{13}C, C_4)$/Hz	$\langle \sin^2\theta \rangle$	V_2/kJ . mol^{-1}	$\langle \theta \rangle$
$Se^{13}CH_3$	0.27	0.397	2.2 ± 1.0	38 ± 5°
$Se^{13}CH_2CH_3$	0.38	0.559	-1.2 ± 1.0	50 ± 5°
$Te^{13}CH_3$	0.31	0.574	-1.7 ± 1.0	52 ± 5°
$Te^{13}CH_2CH_3$	0.37	0.685	-4.0 ± 1.0	58 ± 5°

[a]Recall that a negative barrier indicates a perpendicular (θ = 90°) conformation is preferred.

4. N-methylanilines

Like anilines, N-methylanilines may undergo both torsion about the C_1-N bond and nitrogen inversion. Vapor phase infrared experiments, together with an assumption of a twofold potential yield 14.5 ± 2.0 kJ/mol as the magnitude of the rotational barrier[86]. Dynamic nmr experiments in $CHFCl_2/CHF_2Cl$[87] and dimethyl ether[88] solutions yield 25.5 kJ/mol and 30.3 kJ/mol, respectively, for $\Delta G^{\ddagger}$.

INDO MO FPT computations of $^5J(N^{15}C, C_4)$ as a function of the angle, θ , between the N-C bond and the plane of the benzene ring (see table 21) can be fit by equation (107).

$$^5J(N^{13}C, C_4) = 0.03 + 1.67 \sin^2\theta \qquad (107)$$

The angle independent term is likely an artefact of the parameterization of the computations. The $\sin^2\theta$ dependence of $^5J(N^{13}C, C_4)$ suggests that a σ-π mechanism is involved. Equation (107) implies that $^5J_{90}^{\sigma-\pi}$ for N-methylanilines is of a similar magnitude to those in thioanisole and anisole. If this is true, then 0.93 ± 0.03 Hz might be a reasonable estimate of $^5J_{90}$ in N-methylaniline, yielding equation (108).

$$^5J(N^{13}C, C_4) = 0.93(3) \langle\sin^2\theta\rangle \qquad (108)$$

Microwave experiments have θ as 18° in the minimum energy conformation[89]. If N-methylaniline were rigid, $\langle\sin^2\theta\rangle$ then would be 0.10. The inversion barrier in N-methylaniline is only 2.3 ± 0.5

kJ/mol[86]. If the inversion barrier in solution is similar to that for N-methylaniline vapor, then $\sin^2\theta$ averaged over such a barrier is likely to be less than 0.10. This, together with equation (108) predicts a $^5J(N^{13}C, C_4)$ value of less than 0.09 Hz. No coupling between the methyl and para carbon-13 nuclei is observed for N-methylaniline in acetone-d_6, benzene-d_6 or CS_2 solutions (see table 14). Based on the linewidth of the para carbon peak, an upper limit of 0.05 Hz can be placed on $^5J(N^{13}C, C_4)$. This is consistent with a small θ value and high rotational barrier in solution.

In N-methylaniline, $^3J(N^{13}C, C_2)$ appears to increase with increasing polarity or hydrogen-bond accepting ability of the solvent (see table 14). $^3J(N^{13}C, C_2)$ is 3.38 Hz in CS_2 solution and 3.48 Hz in acetone-d_6 solution. If it is assumed that $^3J_{90}^{\sigma-\pi}$ is negative, as it is in thioanisole and anisole, and as indicated by INDO MO FPT computations, then the change is consistent with an increase of rotational barrier height with increasing polarity or hydrogen-bond accepting ability.

$^4J(N^{13}C, C_3)$ is less sensitive to change in $\langle\sin^2\theta\rangle$ but, given a negative $^4J_{90}^{\sigma-\pi}$, the smaller $^4J(N^{13}C, C_3)$ in acetone-d_6 solution relative to that in CS_2 or C_6D_6 solutions is consistent with an increase in barrier height. Dimethyl ether is a more polar, better hydrogen-bond accepting solvent than $CHFCl_2/CHF_2Cl$ and, indeed, the $\Delta G^{\ddagger}$ for internal rotation for N-methylaniline is higher in the former.

The free energy barrier to internal rotation about the C_1-N bond in 4-bromo-2,6-difluoro-N-methylaniline in dimethyl ether solution is 23.1 ± 0.4 kJ/mol, as determined by ^{19}F dynamic nmr experiments. The

rotational barrier in 2,6-difluoro-N-methylaniline may be slightly lower; an estimate of 21.0 ± 0.7 kJ/mol was made[90].

In acetone-d_6 solution, $^5J(N^{13}C, C_4)$ is 0.27(1) Hz in this compound. Equation (108) gives a $\langle \sin^2\theta \rangle$ of 0.29 (1). Now, if the heavy atom skeleton in 2,6-difluoro-N-methylaniline is assumed to be rigid then θ is 33 ± 2° (θ = arcsin $\langle \sin^2\theta \rangle^{\frac{1}{2}}$). This assumption is reasonable because the rotational barrier in acetone-d_6 solution will probably be rather high (>20 kJ/mol) and the inversion barrier also will be high since the nitrogen must invert via a transition state depicted as 17. Repulsive interaction between the methyl and ortho fluorine groups in 17 will yield a rather high inversion barrier.

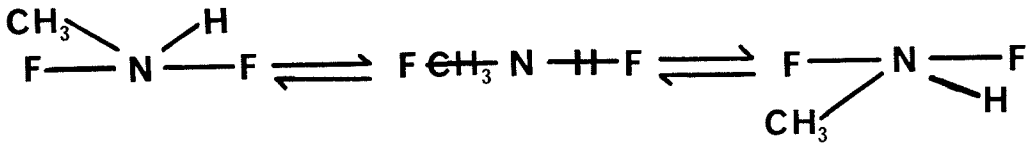

16 17 18

$^3J(N^{13}C, C_2)$ and $^4J(N^{13}C, C_3)$ are lower in 2,6-difluoro-N-methylaniline than in N-methylaniline. These are consistent with negative $^3J_{90}^{\sigma-\pi}$ and $^4J_{90}^{\sigma-\pi}$ components in the associated coupling mechanisms, as implied by the solvent dependent $^3J(N^{13}C, C_2)$ values in N-methylaniline.

Attempts to synthesize the 2,6-dibromo and 2,6-dichloro derivatives were unsuccessful. The ^{13}C spectrum of 2,6-dimethyl-N-methylaniline could not be analyzed due to very broad peaks (incomplete decoupling and large couplings to ^{14}N), the presence of several reaction products and due to very closely spaced ^{13}C signals for the ring carbon nuclei.

In summary, $^5J(N^{13}C, C_4)$ values are consistent with a nearly planar N-methylaniline molecule (θ < 10°) and a non-planar 2,6-difluoro-N-methylaniline molecule ($\theta \simeq 33°$) in solution. $^3J(N^{13}C, C_2)$ values are

consistent with a higher barrier to rotation about the C_1-N bond in more polar, better hydrogen bond accepting solvents.

5. Benzyl Cyanides

a) Stereospecific $^{13}C,^{13}C$ coupling constants

i) $^{5}J(^{13}CN, C_4)$

In 2,6-dichlorobenzyl cyanide, repulsive interactions between the cyano group and the two ortho chlorine substituents will force the C≡N group into a plane perpendicular to the benzene ring. The barrier to rotation about the C_1-C_α bond is expected to be rather high. Ab initio computations at the STO-3G level of molecular orbital theory yield energies as a function of θ that are best fit by a twofold potential of 29.6(5) kJ/mol[92] (θ is defined in 19). At 300K a

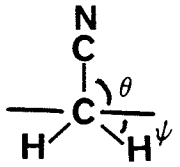

19

hindered rotor model[9] yields $\langle\sin^2\theta\rangle$ as 0.955 for a V_2 of 29.6 kJ/mol. $^{5}J(^{13}CN, C_4)$ is 1.08 Hz for 2,6-dichlorobenzylcyanide in benzene-d_6 solution. This implies a $^{5}J_{90}$ of 1.13 Hz and one may write equation (109).

$$^{5}J(^{13}CN, C_4) = 1.13 \langle\sin^2\theta\rangle \qquad (109)$$

A σ-π coupling mechanism for $^{5}J(^{13}CN, C_4)$ is supported by INDO MO FPT computations (see table 21).

For benzyl cyanide in benzene-d_6 solution $\langle\sin^2\theta\rangle$ is 0.51(1)/1.13(1) or 0.45(1), corresponding to an apparent twofold barrier

of 1.0(3) kJ/mol. Ab initio molecular orbital calculations of the energies of benzyl cyanide, as a function of θ, with different basis sets, are statistically fit to potentials composed of twofold and fourfold components (see table 29 and figure 25). These computations suggest that the potential function for internal rotation in benzyl cyanide may have a substantial fourfold component. Unfortunately, different combinations of V_2 and V_4 may yield the same $\langle \sin^2\theta \rangle$ and the J method cannot discriminate between these combinations.

For the 2,6-difluoro derivative, $^5J(^{13}CN, C_4)$ corresponds to an apparent V_2 of 9.6 ± 1.2 kJ/mol, but again, its value cannot descriminate between this estimate and a combination of V_2 and V_4. STO-3G computations give V_2 and V_4 as -9.86(3) and -2.35(3) kJ/mol, respectively.

ii) $^4J(^{13}CN, C_3)$

The experimental values of $^4J(^{13}CN, C_3)$ and $^5J(^{13}CN, C_4)$ for the benzyl cyanides in benzene solution are related by equation (110)

$$^4J(^{13}CN, C_3) = 0.55 - 1.48\ ^5J(^{13}CN, C_4) \qquad (110)$$

Statistically, a better fit is obtained with a negative value of $^4J(^{13}CN, C_3)$, -0.19 Hz, for benzyl cyanide in benzene-d_6 solution. Equation (110) predicts a $^4J(^{13}CN, C_3)$ value of -0.30 Hz for benzyl cyanide-8-^{13}C in acetone-d_6 solution, rather close to the observed value of -0.29 Hz. The success of equation (110) in reproducing the experimental values of $^4J(^{13}CN, C_3)$ suggests rather minor intrinsic

Table 29

Results of a statistical fit of the relative energies of the optimized geometries of benzyl cyanide to a potential of the form $V(\theta) = V_2 \sin^2\theta + V_4 \sin^2 2\theta$.[a]

	V_2[b]	V_4[b]
STO-3G	-2.597(6)	-0.477(6)
4-21G	-1.634(4)	0.266(4)
4-31G	-1.312(5)	-0.131(5)
6-31G	-1.076(3)	-0.293

[a]Numbers in parentheses are standard deviations.

[b]V_2 and V_4 are given in units of kJ/mol.

Table 30

Internal rotational potentials in benzyl cyanide-8-^{13}C and its two derivatives in benzene-d_6 solution.

parameter	2,6-diCl	2,6-diH	2,6-diF
$^6J(CH_2, H_4)$/Hz	-0.334(4)	-0.585(3)	-0.390(2)
$^2J_{90}$	-1.20(2)	-1.20(2)	-1.20(2)
$\langle\sin^2\psi\rangle$	0.278(7)	0.488(1)	0.325(7)
V_2/kJ mol^{-1}	-24(6)	-0.4(4)	-10.3(9)
$^6J(^{13}CN, H_4)$/Hz	-0.718(5)	-0.364(4)	-0.656(2)
$^6J_{90}$	-0.752(5)[a]	-0.752(5)	-0.752(5)
$\langle\sin^2\theta\rangle$	0.955[a]	0.484(8)	0.872(8)
V_2/kJ mol^{-1}	-29.6(5)[a]	0.3(1)	-11.8(6)
$^5J(^{13}CN, C_4)$/Hz	1.08(1)	0.51(1)	0.95(1)
$^5J_{90}$	1.13(1)[a]	1.13(1)	1.13(1)
$\langle\sin^2\theta\rangle$	0.955[a]	0.45(1)	0.84(2)
V_2/kJ mol^{-1}	-29.6(5)[a]	-1.0(3)	-9.6(1.2)

[a]The theoretical value of V_2 is used for $^5J_{90}$, $^6J_{90}$, and $\langle\sin^2\theta\rangle$.

Figure 25

The relative energies of the optimized geometries of benzyl cyanide are plotted against the dihedral angle, θ, which is zero when the cyano group lies in the benzene plane.

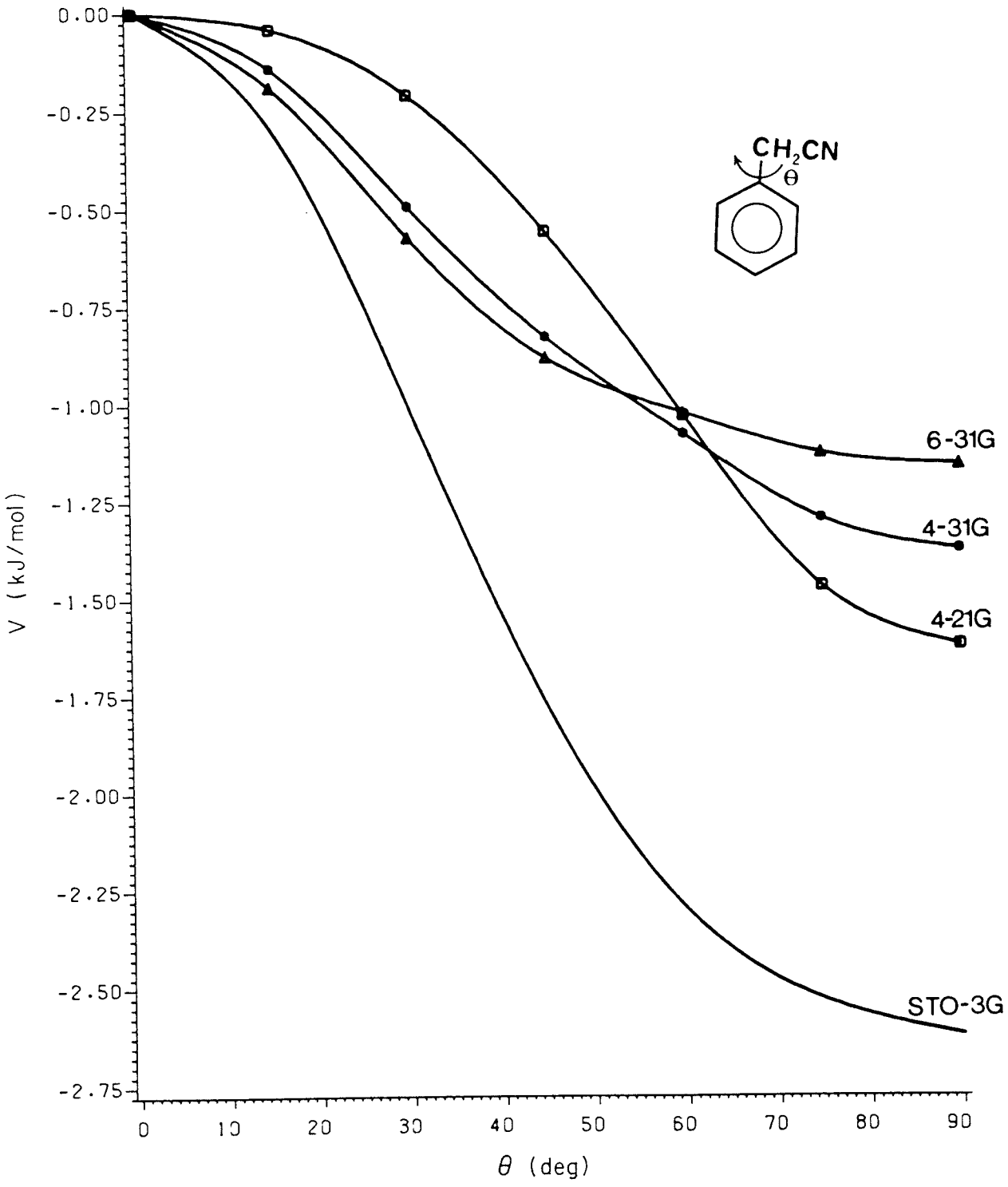
0.00
-0.25
-0.50
-0.75
-1.00
-1.25
-1.50
-1.75
-2.00
-2.25
-2.50
-2.75
V (kJ/mol)
0
10
20
30
40
50
60
70
80
90
θ (deg)
CH2CN
θ
6-31G
4-31G
4-21G
STO-3G

perturbations of the coupling mechanism due to ortho ring substituents. Equation (109) may be substituted into equation (110) to yield (111).

$$^{4}J(^{13}CN, C_3) = 0.55 - 1.67 \langle \sin^2\theta \rangle \quad (111)$$

Equation (111) implies a negative $^{4}J_{90}^{\sigma-\pi}$ for benzyl cyanides, as predicted by INDO MO FPT computations (see table 21).

iii) $^{3}J(^{13}CN, C_2)$

$^{3}J(^{13}CN, C_2)$ for 2,6-dichlorobenzyl cyanide differs from that for 2,6-difluorobenzyl cyanide by only 0.01 Hz whereas $^{5}J(^{13}CN, C_4)$ values suggest that $\langle \sin^2\theta \rangle$ differs significantly for these two molecules. In light of the deviation of $^{3}J(S^{13}C, C_2)$ in 2,6-difluorothioanisole from the best straight line through a plot of $^{3}J(S^{13}C, C_2)$ versus $\langle \sin^2\theta \rangle$ for thioanisoles (see equation 96), it is likely that there is an intrinsic perturbation of $^{3}J(^{13}CN, C_2)$ by the ortho fluorine substituents in 2,6-difluorobenzyl cyanide. The experimental values of $^{3}J(^{13}CN, C_2)$ and $^{5}J(^{13}CN, C_4)$ for benzyl cyanide and 2,6-dichlorobenzyl cyanide in benzene-d_6 solution are related by equation (112).

$$^{3}J(^{13}CN, C_2) = 4.51 - 2.07\ ^{5}J(^{13}CN, C_4) \quad (112)$$

Equation (112) predicts a $^{3}J(^{13}CN, C_2)$ value of 3.31 Hz for benzyl cyanide in acetone-d_6 solution, exactly that observed. Substitution of equation (109) into (112) yields equation (113).

$$^{3}J(^{13}CN, C_2) = 4.51 - 2.34 \langle \sin^2\theta \rangle \quad (113)$$

Equation (113) implies a negative $^3J_{90}^{\sigma-\pi}$ and a large positive (^3J_o + 0.5 $^3J_{180}^{\sigma}$), as predicted by INDO MO FPT computations (see table 21).

iv) Solvent effects

In benzyl fluoride[91] the perpendicular conformer (θ = 90° for the C-F bond) is stabilized by approximately 2 kJ/mol when the solvent is changed from CS_2 to acetone-d_6, qualitatively as expected from electrostatic considerations because this conformer has a higher computed dipole moment than the one with θ = 0°.

The dipole moments of benzyl cyanide are computed as 3.17 and 3.26 D for θ = 0 and 90°, respectively, at the STO-3G level of MO theory. The observed dipole moment in benzene solution is 3.50 D at 298 K, that of methyl cyanide also being 3.5 D in the same solvent. Qualitatively, the perpendicular conformer should be more stable in acetone than in CS_2 solution.

Qualitatively, $^3J(^{13}CN, C_2)$ and $^4J(^{13}CN, C_3)$ should decrease if the perpendicular conformer is stabilized, as indicated by equations (113) and (111), respectively. Equation (109) implies an increase in $^5J(^{13}CN, C_4)$.

The $^nJ(^{13}CN, C_{n-1})$ values (n = 3, 4, 5) of benzyl cyanide in CS_2/C_6D_{12}, benzene-d_6 and acetone-d_6 solution do indeed indicate increased stability of the more polar (θ = 90°) conformer in polar solvent.

Quantitatively, based on $^nJ(^{13}CN, C_{n-1})$, $\langle\sin^2\theta\rangle$ changes from 0.45(1) in C_6D_6 to 0.51(1) in acetone-d_6 solutions. Therefore the apparent V_2 changes from 1.0(4) kJ/mol in benzene-d_6 solution to -0.2(2) in acetone-d_6 solution. Qualitatively, $^3J(^{13}CN, C_2)$ and $^4J(^{13}CN, C_3)$

have the planar form slightly more stable in CS_2 than in benzene solution. Based on $^5J(^{13}CN, C_4)$, $\langle\sin^2\theta\rangle$ is 0.44(1) in CS_2 solution, corresponding to an apparent V_2 of 1.3(4) kJ/mol, which is within the uncertainty range of the barrier in benzene solution.

Comparison of $^nJ(^{13}CN, C_{n-1})$ values, n = 2-5, for 2,6-dichlorobenzyl cyanide in benzene-d_6 and acetone-d_6 solutions in table 8 suggests their insensitivity to solvent polarity. The barrier to internal rotation is rather high and this molecule may be considered as rigid, so that significant differences in the magnitudes of these coupling constants in the two solvents would be attributable to an intrinsic perturbation of coupling mechanisms by solvent molecules. Consequently, the solvent dependence of these coupling constants in benzyl cyanide can be assigned to conformational changes, that is, to perturbations of the internal rotational potential.

b) $^6J(^{13}CN, H_4)$

$^6J(^{13}CN, H_4)$ in 2,6-dichlorobenzyl cyanide is -0.718(5) Hz. If $\langle\sin^2\theta\rangle$ is taken as 0.955 then one may write equation (114).

$$^6J(^{13}CN, H_4) = -0.752 \langle\sin^2\theta\rangle \qquad (114)$$

This is in excellent agreement with the $^6J_{90}$ value of -0.756 Hz predicted by INDO MO FPT computations.

Based on $^6J(^{13}CN, H_4)$, $\langle\sin^2\theta\rangle$ in benzyl cyanide is 0.484(8), implying an apparent V_2 of 0.3(1) kJ/mol. Similarly $\langle\sin^2\theta\rangle$ in 2,6-difluorobenzyl cyanide is 0.872(8) with a corresponding V_2 of -11.8(6) kJ/mol.

c) $^{6}J(CH_2, H_4)$

Results of analyses of the ^{1}H spectra of benzyl cyanide, 2,6-difluorobenzyl cyanide and 2,6-dichlorobenzyl cyanide are given in tables 11, 10 and 9, respectively.

For toluene $^{6}J_{90}(CH_2, H_4)$ is -1.20 Hz[8]. In a benzyl derivative, an electronegative substituent[10] will polarize the C-H bonds in the methylene group, thereby decreasing the hyperconjugative interaction and reducing the magnitude of $^{6}J^{\sigma-\pi}$. Qualitatively the INDO MO FPT formulation agrees with this reduction[11]. Such calculations for benzyl cyanide indicate no reduction of $^{6}J^{\sigma-\pi}$ relative to toluene, perhaps an increase of 0.005 Hz at $\theta = 90°$. Confirmatory evidence comes from a plot $^{6}J(CH_2, H_4)$ against the electronegativity of the substituent, X, in a series of 2,6-dichlorobenzyl X compounds. For X = CN the smallest deviation from the roughly linear plot occurs if the cyano group is taken to have the same electronegativity as hydrogen. If $^{6}J_{90}$ is taken as -1.20 Hz, $\langle \sin^2\psi \rangle$ (see 19 for angle ψ) is 0.488(10) for benzyl cyanide, corresponding to a V_2 of 0.4(4) kJ/mol. Similarly, in 2,6-difluorobenzyl cyanide $\langle \sin^2\theta \rangle$ is 0.325(7) corresponding to a V_2 of -10.3(9) kJ/mol. In 2,6-difluorotoluene in CS_2 solution, $^{6}J(CH_2, H_4)$ is 0.623(4) Hz[32], implying a $^{6}J_{90}$ of -1.25(2) Hz, a $\langle \sin^2\psi \rangle$ of 0.312(7) and an apparent V_2 of 12.1(9) kJ/mol for 2,6-difluorobenzyl cyanide.

In the 2,6-dichloro derivative, $^{6}J(CH_2, H_4)$ is -0.334(3) Hz, corresponding to a $\langle \sin^2\psi \rangle$ of 0.278(7) if $^{6}J_{90}$ is -1.20(2) Hz. An analysis of the ^{1}H spectrum of 2,6-dichlorotoluene in CS_2 solution gave $^{6}J(CH_3, H_4)$ as -0.630 Hz, implying $^{6}J_{90}$ as -1.26(2) Hz in the presence of two ortho chlorine substituents. Then $\langle \sin^2\psi \rangle$ becomes 0.263(7).

One might also expect ortho substituent perturbations on $^{6}J(^{13}CN, H_4)$ and $^{5}J(^{13}CN, C_4)$. There is no clear way to establish such perturbations.

In summary, long-range coupling constants are consistent with a rather small barrier to rotation about the C_1-C_α bond in benzyl cyanide, in agreement with ab initio mo computations and Kerr constant measurements in CCl_4 solution[93]. The rotational barrier is slightly dependent on solvent. The $\theta = 90°$ conformation is stabilized in more polar solvent.

6. Acetophenones

Examination of table 21 reveals rather small $J_{90}^{\sigma-\pi}$ components of $^5J(^{13}C_\alpha, C_4)$, $^4J(^{13}C_\alpha, C_3)$ and $^3J(^{13}C_\alpha, C_2)$ for acetophenone. Schaefer *et al.*[94] conclude that the $\sigma-\pi$ contributions to spin-spin coupling constants over six bonds, between *para* protons or ^{19}F nuclei, and protons or ^{13}C nuclei in the sidechain of benzaldehyde and phenyl ketones amount to only about 25% of those in toluene derivatives. In addition, the six-bond coupling constants for ^{19}F nuclei contain substantial negative components in planar conformations. It is of interest to see if similar anomalous carbon-carbon coupling constants are observed in acetophenone derivatives.

In solution, the free energy of activation for rotation about the Csp^2-Csp^2 bond in acetophenone is 22.4 kJ/mol[95]. STO-3G MO computations with geometry optimization indicate a planar ground state and a twofold barrier to rotation[94]. For a twofold barrier of 22.4 kJ/mol, $\langle \sin^2\theta \rangle$ is 0.06 (θ is defined in 20). If

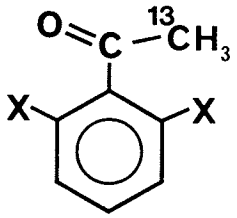

$\theta = 0°$

20

a $\sigma-\pi$ mechanism, following a $\sin^2\theta$ law, dominates $^5J(^{13}C_\alpha, C_4)$ and if $^5J_{90}^{\sigma-\pi}$ is between 0.9 and 1.0 Hz, as in anisoles and thioanisoles, then the five-bond coupling constant should be 0.05 to 0.06 Hz. If $^5J_{90}^{\sigma-\pi}$ is smaller, as indicated by INDO MO FPT computations, $^6J(^{13}C_\alpha, C_4)$ should be much less than 0.06 Hz. The measured coupling constant is ±0.23 Hz. This value indicates that another mechanism is contributing to $^5J(^{13}C_\alpha, C_4)$.

Schaefer et al.[94] propose that a π mechanism contribution to $^{6}J(CHO, F_4)$ in 4-fluorobenzaldehyde (planar conformation preferred by 34 kJ/mol[95]) accounts for the measured value of -0.442, where a σ-π mechanism would have a very small positive value. Therefore, it is possible that a π mechanism also contributes to $^{5}J(^{13}C_{\alpha}, C_4)$ in acetophenone.

Turning to 2,6-dichloroacetophenone-^{13}C, $^{5}J(^{13}C_{\alpha}, C_4)$is +0.13 Hz. Geometry-optimized STO-3G MO computations find the conformation with θ = 90° as 47.0 kJ/mol more stable than the planar conformation. Analysis of the X-ray diffraction pattern of a single crystal of 4-t-butyl-2,6-dichloroacetophenone yields θ as 80.6° [96]. It seems reasonable to assume that $\langle\sin^2\theta\rangle$ is near unity in 2,6-dichloroacetophenone.

The π contribution to $^{6}J(CHO, F_4)$ in 4-fluorobenzaldehyde is taken to be of opposite sign to the σ-π contribution and to follow a $\cos^2\theta$ law[94]. In certain paramagnetic nickel II aminotropeneimineate derivatives[97], the hyperfine parameter, Q_{CH}, for an aldehyde group attached to a π electron system is negative, unlike the effective Q_{CH} for a methyl group, which is really a Q_{CCH} originating in a θ dependent hyperconjugative interaction. The π contribution to $^{5}J(^{13}C_{\alpha}, C_4)$ is also taken as negative and to go as $\cos^2\theta$. One may now write

$$^{5}J(^{13}C_{\alpha}, C_4) = 0.13 \langle\sin^2\theta\rangle - 0.23 \langle\cos^2\theta\rangle \qquad (115)$$

Equation (115) suggests that $^{5}J_{90}^{\sigma-\pi}$ is 0.13 Hz and that $^{5}J_{0}^{\pi}$ is -0.23 Hz. Equation (115) may be rewritten as equation (116)

$$^{5}J(^{13}C_{\alpha}, C_4) = -0.23 + 0.36 \langle\sin^2\theta\rangle \qquad (116)$$

The energies of 2,6-difluoroacetophenone as a function of θ yield equation (117) at the STO-3G level of molecular orbital theory.

$$V(\theta) = 2.95(8)\ \sin^2\theta - 3.44(8)\ \sin^2 2\theta \qquad (117)$$

When averaged over this potential, $\sin^2\theta$ is 0.400. If this value of $\langle\sin^2\theta\rangle$ is substituted into equation (117), then a $^5J(^{13}C_\alpha, C_4)$ value of -0.08 Hz is predicted. The observed value is <0.05 Hz. The V_2 component is likely to be larger for a molecule in solution than for an isolated molecule, as is the case for benzaldehyde[98] and acetophenone[94,95], yielding a larger $\langle\sin^2\theta\rangle$ value and a higher $^5J(^{13}C_\alpha, C_4)$, in better agreement with the predicted value.

In acetophenone, $^4J(^{13}C_\alpha, C_3)$ and $^3J(^{13}C_\alpha, C_2)$ will each be averaged out to $^4J_0^\pi + 0.5\,^4J_{180}^\sigma$ and $^3J_0^\pi + 0.5J_{180}^\sigma$, respectively. Similarly in 2,6-dichloroacetophenone, with the assumption of a rigid molecule (θ = 90°), $^4J(^{13}C_\alpha, C_3)$ and $^3J(^{13}C_\alpha, C_2)$ will be $^{4,3}J_{90}^{\sigma-\pi} + 0.5\,^{4,3}J_{180}^\sigma$. Therefore, the difference in $^3J(^{13}C_\alpha, C_2)$ or $^4J(^{13}C_\alpha, C_3)$ values between the two molecules is the difference between the corresponding $J_{90}^{\sigma-\pi}$ and J_0^π values.

The increase in $^4J(^{13}C_\alpha, C_3)$ in going from acetophenone to 2,6-dichloroacetophenone is consistent with $^4J_{90} > {}^4J_0$. This is rather unusual since $^4J_{90}$ is expected to be negative and $^4J_0$ is expected to be positive, based on the analogous couplings in anisole, thioanisole, N-methylaniline and benzyl cyanide.

$^3J(^{13}C_\alpha, C_2)$ in acetophenone and 2,6-dichloroacetophenone, assuming the coupling constants are positive in both molecules, is consistent with a negative $^3J_{90}$ and a positive $^3J_0$.

In 2,6-difluoroacetophenone, $^{3}J(^{13}C_{\alpha}, C_2)$ is less than 0.05 Hz and probably cannot be used to aid in the decomposition of $^{3}J(^{13}C_{\alpha}, C_2)$ because a large substituent effect is expected. $^{4}J(^{13}C_{\alpha}, C_3)$ in the same molecule could not be measured due to incomplete proton decoupling by the WALTZ16 pulse sequence.

In summary, $^{5}J(^{13}C_{\alpha}, C_4)$ in acetophenones appears to have a negative π component as well as the expected positive σ-π component. The very small values of $^{5}J_{90}^{\sigma-\pi}$ and $^{5}J_{0}^{\pi}$ render $^{5}J(^{13}C_{\alpha}, C_4)$ of little use in conformational analysis. The conformational dependence of $^{4}J(^{13}C_{\alpha}, C_3)$ and $^{3}J(^{13}C_{\alpha}, C_2)$ could not be deduced. The possibility of a π contribution to $^{3}J(^{13}C_{\alpha}, C_2)$ and $^{4}J(^{13}C_{\alpha}, C_3)$ cannot be confirmed.

7. Some Additional Long-Range Couplings Between the Side-Chain ^{13}C Nucleus and Ring Nuclei

a) $^{6}J(X^{13}C, F_4)$ versus δC_4.

i) $^{6}J(S^{13}C, F_4)$ in some alkyl-4-fluorophenyl sulfides

Early studies have demonstrated good correlations of the para-carbon chemical shifts of monosubstituted benzene with the Hammett σp parameter[99]. Lauterbur[100] has shown that the shielding of the aromatic carbons appear to be simply related to the ground state electronic distributions of these molecules and that it appears likely that the π electron densities are a major factor determining ^{13}C shielding in aromatic molecules. If there is a resonance interaction between the aromatic π-system and the p orbitals or π-system of the substituent, evidence of steric inhibition of resonance may be obtained from studies of the chemical shifts of aromatic carbon nuclei.

Katritzky et al.[101] have related σ_R^0 values to the twist angle θ for alkyl phenyl ketones by equation (118).

$$(\sigma_R^0)_{tw} = (\sigma_R^0)_0 \cos^2\theta \qquad (118)$$

Therefore it is reasonable to relate the chemical shift of the para carbon-13 nucleus to $\cos^2\theta$. This has been done by Dhami and Stothers[102] for alkyl phenyl ketones. The relationship they proposed can be recast into the form

$$\delta(\theta) = \delta^0 C_4 + \delta C_4 \langle \sin^2\theta \rangle \qquad (119)$$

Recall that $\sin^2\theta = 1-\cos^2\theta$ and that, since these molecules are not rigid, the concern is with average or expectation values. Equation (118) should be extendable to other molecules, for example, alkyl phenyl ethers or alkyl phenyl sulfides, where the size of the alkyl group will increase the twist angle θ and change the p-π conjugation with a resulting change in δC_4. In this thesis, long-range couplings between the alpha sidechain carbon-13 nucleus and a para proton, carbon-13 or fluorine-19 nuclei have been taken as proportional to $\langle \sin^2\theta \rangle$. Hence one should find a linear relationship between δC_4 and $^6J(S\underline{C}, F_4)$ in alkyl 4-fluorophenyl sulfides. Theoretical evidence for such relationships comes from INDO MO FPT computations of $^6J(S\underline{C}, F_4)$[70] (see equation 119) and STO-3G MO computations of π electron density on C_4 (see equation 120) in 4-fluorothioanisole as a function of θ.

$$^6J(S\underline{C}, F_4) = 0.89 \sin^2\theta - 0.35 \qquad (119)$$

$$\rho(C_4) = 5.87144 - 0.01036 \sin^2\theta \qquad (120)$$

A plot of experimental $^6J(S\underline{C}, F_4)$ vs δC_4 values for several alkyl-4-fluorophenyl sulfides yields equation (121), with a correlation coefficient of 0.9997.

$$^6J(S\underline{C}, F_4) = -69.42 + 0.434\,\delta C_4 \qquad (121)$$

This plot is depicted in figure 26. Equation (121) is in excellent agreement with experimental values.

Figure 26

A plot of $^{6}J(S\underline{C}, F_4)$ versus δC_4 for some alkyl-4-fluorophenyl sulfides.

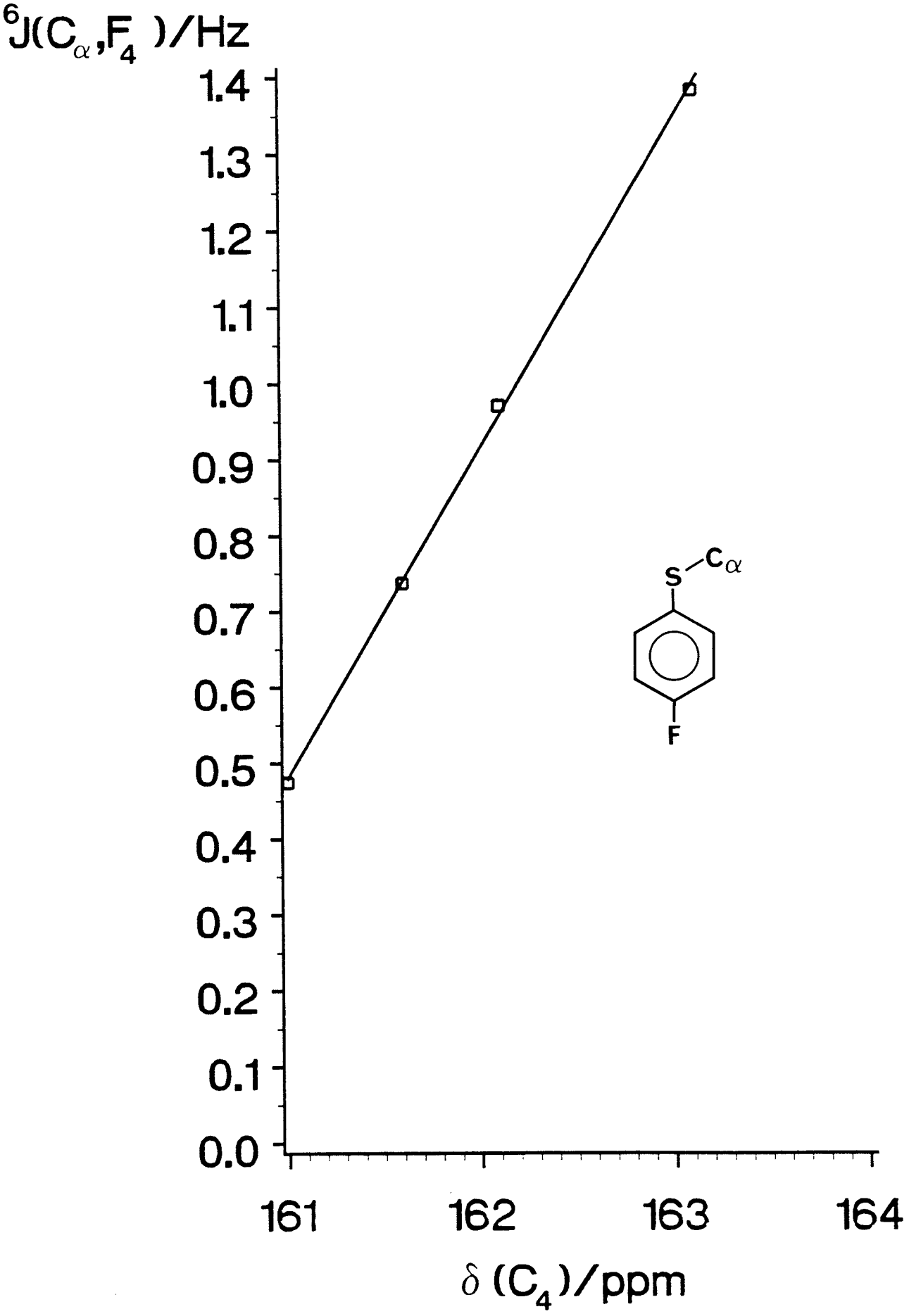
$^6J(C_\alpha,F_4)$/Hz
1.4
1.3
1.2
1.1
1.0
0.9
0.8
0.7
0.6
0.5
0.4
0.3
0.2
0.1
0.0
161
162
163
164
δ (C_4)/ppm
S
C_α
F

In 2,6-dibromo-4-fluorophenylthioanisole, $^{6}J(S\underline{C}, F_4)$ is 1.47 Hz. If this is taken as $^{6}J_{90}$, apparent V_2 values can be deduced for the alkyl-4-fluorophenyl sulfides. These values are given in table 31. t-Butyl-4-fluorophenyl sulfide may be considered as having $\theta = 90°$ with perhaps large amplitude torsion about the C_1-S bond.

ii) $^{6}J(O^{13}C, F_4)$ in some alkyl-4-fluorophenyl ethers

In alkyl phenyl ethers, δC_4 for 21a-c covers a range of less than 0.4 ppm[103], but increases by over 2 ppm for the t-butyl derivative, 21d. This

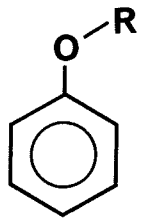

a R = CH_3
b R = CH_2CH_3
c R = $CH(CH_3)_2$
d R = $C(CH_3)_3$

21

suggests that in 21a-c the repulsive (steric) interaction between the alkyl and ortho C-H bonds is not strong enough to twist the O-R group out of the benzene ring plane but that in 21d, the t-butyl group has sufficient "bulk" to twist the sidechain and significantly reduce the 2p-π conjugation and increase δC_4.

This hypothesis is born out by $^{6}J(O\underline{C}, F_4)$ values in the corresponding para fluoro derivatives of 21a-d. In 2,6-dibromo-4-fluoroanisole, $^{6}J(O\underline{C}, F_4)$ is 1.48 Hz. If $^{6}J(O\underline{C}, F_4)$ follows a $\sin^2\theta$ law then one may write

$$^{6}J(O\underline{C}, F_4) = 1.48 \langle\sin^2\theta\rangle. \qquad (122)$$

Table 31

$^{6}J(S\underline{C}, F_4)$, δC_4, $\langle \sin^2\theta \rangle$ and V_2 values for some alkyl-4-fluorophenyl sulfides.

R	$^{6}J(S\underline{C}, F_4)^{a}$	$C_4{}^{b}$	$\langle \sin^2\theta \rangle^{c}$	$V_2{}^{d}$
CH_3	0.474	161.0	0.322	4.2
CH_2CH_3	0.737	161.6	0.501	0.0
$CH(CH_3)_2$	0.921	162.1	0.661	-3.7
$C(CH_3)_3$	1.384	163.1	0.941	-33.5

[a]Coupling constants in Hertz, taken from 50 mol% solutions in acetone-d_6.

[b]Chemical shifts in ppm, taken from neat samples with a small amount of TMS added. Taken from reference 103.

[c]These values deduced from $^{6}J(S\underline{C}, F_4)$ using 1.47 Hz as $^{6}J_{90}$.

[d]In kJ/mol.

The values of $\langle \sin^2\theta \rangle$ may now be deduced and, based on the assumption of twofold barriers to rotation about the C_1-O bond, rotational barrier heights, V_2, may be obtained. These are collected in table 32.

The 4-fluoro derivatives of 21a-c strongly prefer to have the O-C_α bond in the plane of the phenyl ring, whereas t-butyl-4-fluorophenyl ether prefers the perpendicular conformation. If twofold barriers to internal rotation about the C_1-O bond are assumed, then a t-butyl group stabilizes the perpendicular conformation by at least 15 kJ/mol relative to the methyl, ethyl or isopropyl ethers.

In summary, the excellent linear correlation between $^6J(S\underline{C}, F_4)$ and δC_4 in alkyl-4-fluorophenyl sulfides together with computations of $^6J(S\underline{C}, F_4)$ and para carbon π-electron density give strong evidence that both parameters are related to $\sin^2\theta$. If $^6J(O\underline{C}, F_4)$ in alkyl-4-fluorophenyl ethers is proportional to $\sin^2\theta$, then, based on an assumed twofold barrier about the C_1-O bond, the t-butyl group stabilizes the $\theta = 90°$ conformation by over 15 kJ/mol with respect to the other alkyl groups.

b) $^5J(X^{13}C, C_4)$ versus $^6J(X^{13}C, H_4)$.

Throughout this thesis $^5J(X^{15}C, C_4)$ has been taken to vary as $^5J_{90}^{\sigma-\pi} \sin^2\theta$, where $^5J_{90}^{\sigma-\pi}$, a positive quantity, changes with X. The assumption of a $\sin^2\theta$ functional form and the positive sign of $^5J_{90}^{\sigma-\pi}$ are confirmed by INDO MO FPT computations. Evidence has also been presented in this thesis and in earlier work[37,38] to support the $^6J_{90}^{\sigma-\pi} \sin^2\theta$ form for $^6J(S^{13}C, H_4)$. If both $^5J(S^{13}C, C_4)$ and $^6J(X^{13}C, H_4)$ obey the aforementioned angular relationships, they must be proportional to each other when measured in the same molecule, unsubstituted in the para position. A plot of $^5J(X^{13}C,$

C_4) versus $^6J(X^{13}C, H_4)$ for several benzene derivatives is shown in figure 27. The data used to obtain this plot are presented in table 33. A linear regression analysis of the points yields equation (123).

$$^5J(X^{13}C, C_4) = -1.50\ ^6J(X^{13}C, H_4) + 0.02 \qquad (123)$$

The fit is very good, having a correlation coefficient of -0.9995.

The proportionality of $^5J(X^{13}C, C_4)$ to $^6J(X^{13}C, H_4)$ appears to be independent of the nature of the sidechain, as is expected if spin state information is transmitted via a σ-π mechanism. If this is the case, then for benzene derivatives one may write

$$Q_{CH}^{C} = -1.5\ Q_{CH}^{H} \qquad (124)$$

where Q_{CH}^{C} is the hyperfine coupling parameter representing the transmission of unpaired spin density from the π-type orbitals of the aromatic ring carbon to the <u>para</u> carbon-13 nucleus. Q_{CH}^{H} represents transmission of unpaired spin density to the <u>para</u> proton. Early work agrees that Q_{CH}^{C} and Q_{CH}^{H} are of opposite sign[104,105].

c) $^5J(X^{13}C, C_4)$ versus $^6J(X^{13}C, C')$.

Several $^6J(X^{13}C, C')$ values have been reported in this thesis and are collected in table 34. (for C' see <u>22</u>).

Table 32

$^{6}J(O\underline{C}, F_4)$, $\langle \sin^2\theta \rangle$ and V_2 values for some alkyl-4-fluorophenyl ethers[9].

R	$^{6}J(OC, F_4)$[b]	$\langle \sin^2\theta \rangle$	V_2[c]
CH_3	0.108[d]	0.073	25.5
CH_2CH_3	0.123	0.083	21.5
$CH(CH_3)_2$	0.268	0.181	9.5
$C(CH_3)_3$	1.035	0.699	-4.5

[a]All samples are 50 mol% in acetone-d_6, except R = $C(CH_3)_3$, which is 5 mol%.

[b]In Hertz.

[c]In kJ/mol.

[d]This value is taken from the enriched (R = $^{13}CH_3$) sample.

Table 33

Values of $^{5}J(X^{13}C, C_4)$ and $^{6}J(X^{13}C, H_4)$ for some derivatives of anisole, thioanisole and benzyl cyanide[a].

Substituents	$^{5}J(X^{13}C, C_4)$[b]	$^{6}J(X^{13}C, H_4)$[b]
$O^{13}CH_3$	<0.03	<0.03
$S^{13}CH_3$	0.20	-0.15
$CH_2{}^{13}CN$	0.51	-0.36
2,6-diF-$S^{13}CH_3$	0.62	-0.42
2,6-diCl-$S^{13}CH_3$	0.77	-0.52
2,6-diBr-$O^{13}CH_3$	0.94	-0.63
2,6-DiF-$CH_2{}^{13}CN$	0.95	-0.65
2,6-DiCl-$CH_2{}^{13}CN$	1.08	-0.72

[a]Concentrations and solvents are given in tables 2-19.

[b]In Hertz.

Figure 27

A plot of $^{5}J(X^{13}C, C_4)$ versus $^{6}J(X^{13}C, H_4)$ for some benzene derivatives.

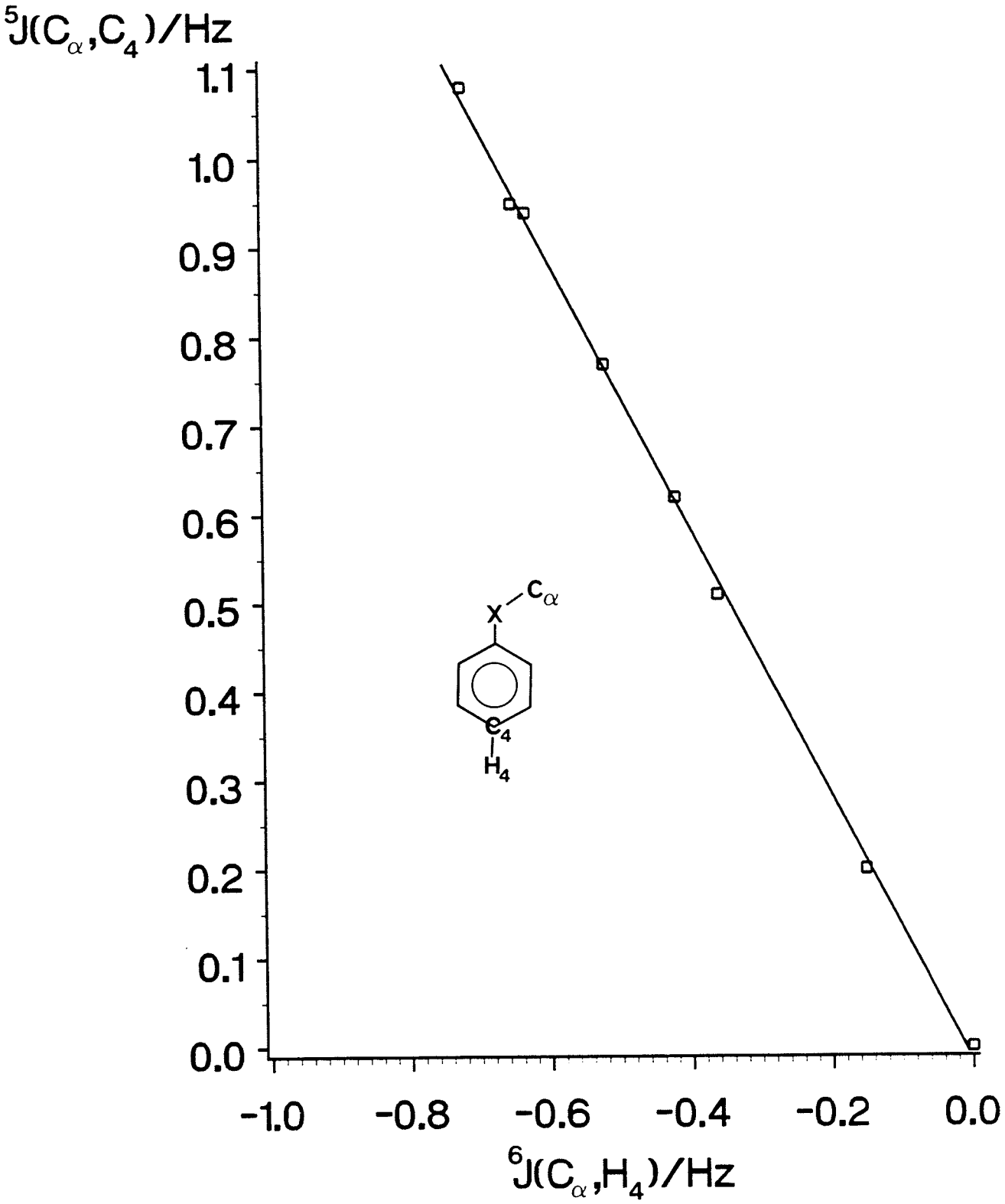
$^5J(C_\alpha,C_4)$/Hz
1.1
1.0
0.9
0.8
0.7
0.6
0.5
0.4
0.3
0.2
0.1
0.0
-1.0
-0.8
-0.6
-0.4
-0.2
0.0
$^6J(C_\alpha,H_4)$/Hz
X
C_α
C_4
H_4

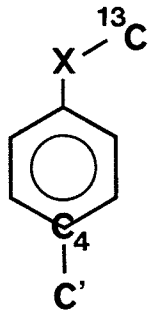

22

It is of interest to determine if $^{6}J(X^{13}C, C')$ is dominated by a σ-π mechanism. If so, $^{6}J(X^{13}C, C')$ should be linearly related to $^{5}J(X^{13}C, C_4)$. A plot of $^{6}J(X^{13}C, C')$ versus $^{5}J(X^{13}C, C_4)$ for several <u>para</u> methyl derivatives of anisole and thioanisole is shown in figure 28. They are related by equation (125), with a correlation coefficient of -0.9990.

$$^{6}J(X^{13}C, C') = -0.35\ ^{5}J(X^{13}C, C_4) \qquad (125)$$

If $^{6}J(O^{13}C, C')$ in 2,6-dibromo-4-methylanisole is taken as that for $\theta = 90°$, then equation (125) becomes

$$^{6}J(X^{13}C, C') = -0.35 \langle \sin^2\theta \rangle . \qquad (126)$$

INDO MO FPT computations on 4-methylanisole yield equation (127), in good qualitative agreement.

$$^{6}J(O^{13}C, \underline{C}H_3) = -0.49 \sin^2\theta \qquad (127)$$

Using the $^{5}J(S^{13}C, C_4)$ value for 4-t-butyl thioanisole, equation (125) predicts a $^{6}J(S^{13}C, C')$ values of -0.09_8 Hz. The lower observed value of (-)0.07 Hz is likely due to the presence of three methyl groups on C'. In methyl 3,5-dibromo-4-methoxybenzoate in which $\theta = 90°$, $^{6}J(O^{13}C, C')$ is slightly larger than that predicted by equation (125). INDO MO FPT computations of $^{6}J(O^{13}C, O=\underline{C})$ in 4-methoxy benzaldehyde and 4-methoxy benzoyl fluoride predict $^{6}J_{90}$ values of -1.22 Hz and -0.98 Hz respectively. These values are in qualitative agreement with experiment in that they predict a larger $^{6}J(O^{13}C, O=\underline{C})$ value but overestimate the increase in magnitude with respect to $^{6}J(O^{13}C, \underline{C}H_3)$.

Figure 28

A plot of $^{6}J(X^{13}C, C')$ versus $^{5}J(X^{13}C, C_4)$ for some derivatives of 4-methyl anisole and 4-methyl thioanisole.

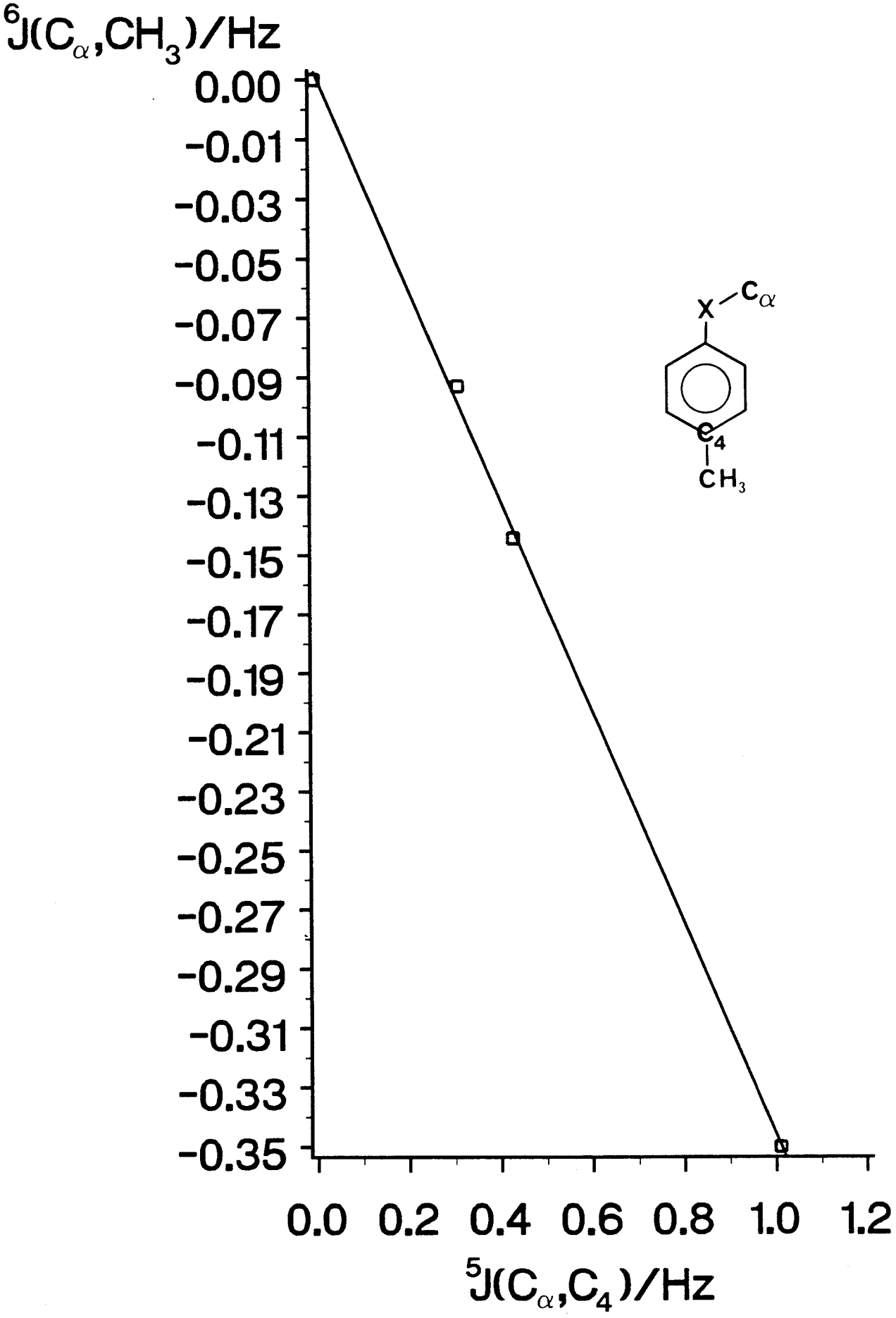
$^6J(C_\alpha,CH_3)/Hz$
0.00
-0.01
-0.03
-0.05
-0.07
-0.09
-0.11
-0.13
-0.15
-0.17
-0.19
-0.21
-0.23
-0.25
-0.27
-0.29
-0.31
-0.33
-0.35
0.0
0.2
0.4
0.6
0.8
1.0
1.2
$^5J(C_\alpha,C_4)/Hz$
X
C_α
C_4
CH_3

Table 34

$^{5}J(X^{13}C, C_4)$ and $^{6}J(X^{13}C, C')$ values for some derivatives of anisole and thioanisole[a].

Substituents		$^{5}J(X^{13}C, C_4)$[b]	$^{6}J(X^{13}C, C')$[b]
$O^{13}CH_3$	4-CH_3	0.03	0.03
2,6-diBr-$O^{13}CH_3$	4-CH_3	(+)1.01	-0.35
$S^{13}CH_3$	4-CH_3	(+)0.31	(-)0.10
$S^{13}CH_2CH_3$	4-CH_3	(+)0.45	(-)0.15
$S^{13}CH_3$	4-t-Bu	(+)0.28	(-)0.07
$O^{13}CH_3$	4-O=C-H	$\leq$0.03	$\leq$0.03
2,6-diBr-$O^{13}CH_3$	4-O=C-OCH_3	(+)0.92	(-)0.42

[a]Concentrations and solvents are given in tables.

[b]In Hertz.

E. SUMMARY AND CONCLUSION

"Would you mind repeating that? It is not yet totally unclear to me."

A large part of this thesis is an attempt to show that couplings between the sidechain carbon-13 nucleus and ring protons, fluorine-19 and carbon-13 nuclei in benzene derivatives obey angular relationship given by equation (128), as predicted by theory, and to relate $\langle \sin^2\theta \rangle$ to a twofold barrier to internal rotation in symmetrically substituted derivatives. In most cases such attempts are quite successful. The following is a brief summary of the results of this work and conclusions based thereon.

$$J = J_{90} \langle \sin^2\theta \rangle + [J_0 + 0.5J_{180}] \qquad (128)$$

In symmetrically substituted thioanisoles, $^5J(S^{13}C, C_4)$, $^4J(S^{13}C, C_3)$ and $^3J(S^{13}C, C_2)$ follow equation (128). Rotational barriers for <u>para</u> substituted thioanisoles range from -2.8 ± 0.4 kJ/mol in 4-aminothioanisole to 16.5 ± 2.0 kJ/mol in 4-nitrothioanisole, reflecting the π-electron donating or accepting ability of the <u>para</u> substituent. <u>Ortho</u> bromo- fluoro- and methoxy-thioanisole demonstrate preferred coplanarity of all heavy atoms. In the latter two, the electron donating ability of the <u>ortho</u> substituent results in large amplitude vibration about the C_1-S bond. Long-range coupling constants are consistent with a S-C_α bond orthogonal to the phenyl ring plane in 2-hydroxythioanisole. The hydroxyl group likely hydrogen bonds to the sulfur 3p orbital, forcing the S-C_α bond into a conformation with $\theta = 90°$. In acetone solution the molecule appears to exist in an equilibrium between intermolecular and intramolecular hydrogen bonded species. Based on the assumption of a rigid molecule, $^5J(S^{13}C, C_4)$ and $^6J(S^{13}C, H_4)$ in 2-aminothioanisole have θ

as 66° and 60°, respectively. The methylthio group likely twists about the C_1-S bond so as to optimize the NH...S hydrogen bond.

Long-range $^{13}C,^{13}C$ coupling constants in a series of anisole derivatives experience small intrinsic substituent effects. These effects are only observed when the substituent is attached to either or both of the coupled ^{13}C nuclei.

Small changes in $^3J(O^{13}C, C_2)$ and in $^4J(O^{13}C, C_3)$ observed in <u>para</u> substituted anisoles are consistent with slight stabilization or destabilization of the planar ground state by π-electron withdrawing or donating substituents, respectively. <u>Meta</u> chlorine substituents appear to stabilize the planar conformation.

$^6J(O^{13}C, H_4)$ values imply a greater stabilization of the orthogonal ground state in 2,6-difluoroanisole relative to 2,3,5,6-tetrafluoroanisole, suggesting that <u>meta</u> fluorine substituents increase the 2p-π conjugation across the C_1-O bond.

$^5J(Se^{13}C, C_4)$ and $^5J(Te^{13}C, C_4)$ have been used to deduce $\langle\sin^2\theta\rangle$ and V_2 values for methyl phenyl selenide, ethyl phenyl selenide, methyl phenyl telluride and ethyl phenyl telluride. Methyl phenyl selenide prefers a planar conformation and methyl phenyl telluride prefers an orthogonal conformation. In the ethyl derivatives, orthogonal conformations are stabilized with respect to the methyl derivatives, presumably due to the greater "steric" requirement of an ethyl group.

In solution, long-range $^{13}C,^{13}C$ coupling constants suggest that N-methylaniline prefers a nearly planar conformation. Small changes in $^3J(N^{13}C, C_2)$ with solvent imply a higher barrier to internal rotation in more polar, better hydrogen-bond accepting solvents. Based on the assumption of a rigid molecule, 2,6-difluoro-N-methylaniline displays a

conformation in which the N-C bond makes an angle of about 33° with the plane of the benzene ring.

Long-range couplings from the cyanide carbon to the para proton or carbon-13 nucleus are consistent with nearly free internal rotation about the Csp^2-Csp^3 bond in benzyl cyanide. $^3J(^{13}CN, C_2)$, $^4J(^{13}CN, C_3)$ and $^5J(^{13}CN, C_4)$ show a solvent dependence that is consistent with a stabilization of the conformation with $\theta = 90°$ in more polar solvent. In 2,6-difluorobenzyl cyanide, $^5J(^{13}CN, C_4)$ and $^6J(^{13}CN, H_4)$ yield barriers of -9.6 ± 1.2 kJ/mol and -11.8 ± 0.9 kJ/mol, respectively. STO-3G computations yield a barrier height, V_2, of -9.86 kJ/mol but also have a V_4 term of -2.35 kJ/mol. Unfortunately, the J method cannot distinguish between different combinations of V_2 and V_4 corresponding to the same $\langle \sin^2\theta \rangle$.

In acetophenone derivatives, $^5J(^{13}C, C_4)$ takes the form $J_{90}^{\sigma-\pi} \langle \sin^2\theta \rangle + J_0^{\pi} \langle \cos^2\theta \rangle$, which can be recast into equation (128). The small value of J_{90} renders $^5J(^{13}C, C_4)$ of little use in conformational analysis. the stereospecificity of $^3J(^{13}C_\alpha, C_2)$ and $^4J(^{13}C_\alpha, C_3)$ could not be deduced.

Theoretical computations imply that both δC_4 and $^6J(S\underline{C}, F_4)$ in alkyl-4-fluorophenyl sulfides should vary as $\sin^2\theta$. A plot of δC_4 versus $^6J(S\underline{C}, F_4)$ in some R-4-fluorophenyl sulfide (R = Me, Et, i-Pr, t-But) is indeed linear. Plots of $^5J(X^{13}C, C_4)$ versus $^6J(X^{13}C, H_4)$ in some derivatives of thioanisole, anisole and benzyl cyanide, as well as of $^5J(X^{13}C, C_4)$ versus $^6J(X^{13}C, \underline{C}H_3)$ in some derivatives of 4-methyl anisoles and 4-methyl thioanisoles, are linear and suggest the hypothesis that these coupling constants are proportional to $\sin^2\theta$.

F. SUGGESTIONS FOR FUTURE RESEARCH

In this thesis stereospecific $^{13}C,^{13}C$ coupling constants have been investigated in thioanisoles, anisoles, selenoanisoles, telluroanisoles, N-methylanilines and benzyl cyanides. The stereospecificity of $^{13}C^{13}C$ coupling constants has yet to be investigated in derivatives of styrene (26, 27 and 30), ethylbenzene (40), isopropyl benzene (29), α-methyl benzyl alcohol (25), α-alkyl-α methyl benzyl alcohol (28), methyl phenyl sulfones (23), methyl phenyl sulfoxides (24), phenyl alkyl ketones (32, 35) and phenethyl-X compounds (33, 34, 37 and 38). Possible routes towards the synthesis of ^{13}C derivatives of these compound are depicted in figure 29.

A study of $^{5}J(CH_2, C_4)$ in some benzyl-X compound has been reported and the effects of ring substituents have been briefly discussed[36]. In ring substituted derivatives of toluene, $\langle \sin^2\theta \rangle$ is 0.5 and any change in $^{5}J(CH_3, C_4)$ should be due to intrinsic substituent perturbations. Toluene derivatives are commercially available. It would be of interest to have a complete study of substituent effects on $^{5}J(CH_3, C_4)$.

In benzaldehyde, $^{5}J(CHO, C_4)$ is reported to be 0.1 Hz[106]. In solution benzaldehyde is planar with a large barrier to internal rotation[95,98]; therefore $\langle \sin^2\theta \rangle$ should be very near zero. A non-zero coupling suggests that in benzaldehyde derivative $^{5}J(CHO, C_4)$ may have a π component, as proposed in this thesis for $^{5}J(^{13}C, C_4)$ in acetophenones and as previously proposed for $^{6}J(CHO, F_4)$ in 4-fluorobenzaldehyde. Many benzaldehyde derivatives are commercially available and a thorough study of $^{5}J(CHO, C_4)$ would be very important in establishing the nature of these couplings.

The introduction of FT NMR spectroscopy and, in particular, of polarization transfer experiments have allowed the observation of rare or insensitive nuclei. NMR spectroscopy of ^{13}C at natural abundance (1.1%) is now routine. Nitrogen-15, with an absolute sensitivity 46 times less than carbon-13, has recently received much attention[107]. For example, with respect to coupling mechanisms, measurement of $^{5}J(CH_3, N)$ in 4-methylpyridine would provide information on the size of $^{5}J_{90}^{\sigma-\pi}$ (CH_3, N). Proton decoupled ^{15}N spectra of 4-fluorobenzylalkyl amines would yield $^{6}J(^{15}N, F_4)$ which, together with measurement of $^{6}J(CH_2, F_4)$, could be used to deduce the conformational preferences and barriers to internal rotation. The ring proton spectra of benzyl alkyl amines are not analyzable, even at 300 MHz. Therefore, measurement of $^{15}N,^{13}C$ coupling constants could provide conformational information not obtainable from the proton spectra. ^{15}N enriched compounds are commercially available and several benzene derivatives may be synthesized for the purpose of measuring long-range couplings between the sidechain ^{15}N nucleus and ring protons, carbon-13 or fluorine-19 nuclei. Figure 30 shows several possible syntheses of ^{15}N enriched benzene derivatives.

Long-range $^{13}C,^{13}C$ and $^{13}C,^{1}H$ coupling constants in 3,5-dichlorothioanisole, 3,5-dichloroanisole and 2,3,5,6-tetrafluoroanisole suggest that chlorine or fluorine substituents in the <u>meta</u> positions increase the barriers to internal rotation about the C_1-O or C_1-S bonds. Dynamic nmr experiments on a series of <u>meta</u> disubstituted N-methylaniline and benzaldehydes would be of great help in examining the effects <u>meta</u> substituents have on rotation of the sidechain.

Figure 29

Possible syntheses of some ^{13}C enriched derivatives of benzene.

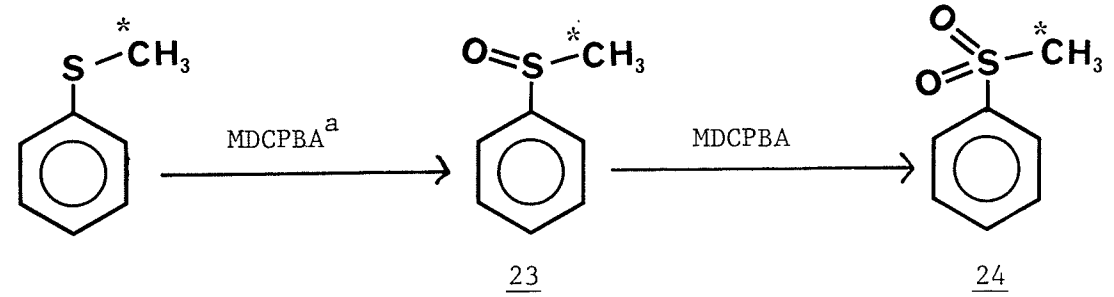

23 24

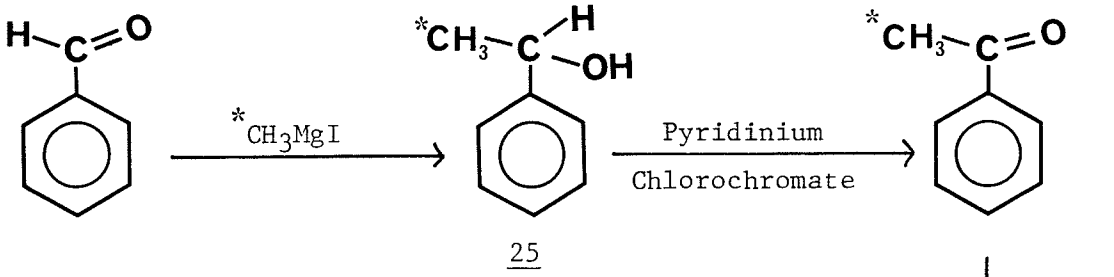

25

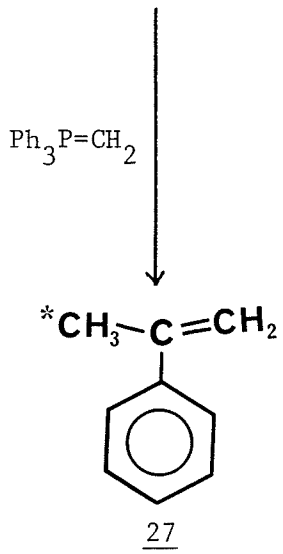

26 27

[a]Meta chloroperoxybenzoic acid

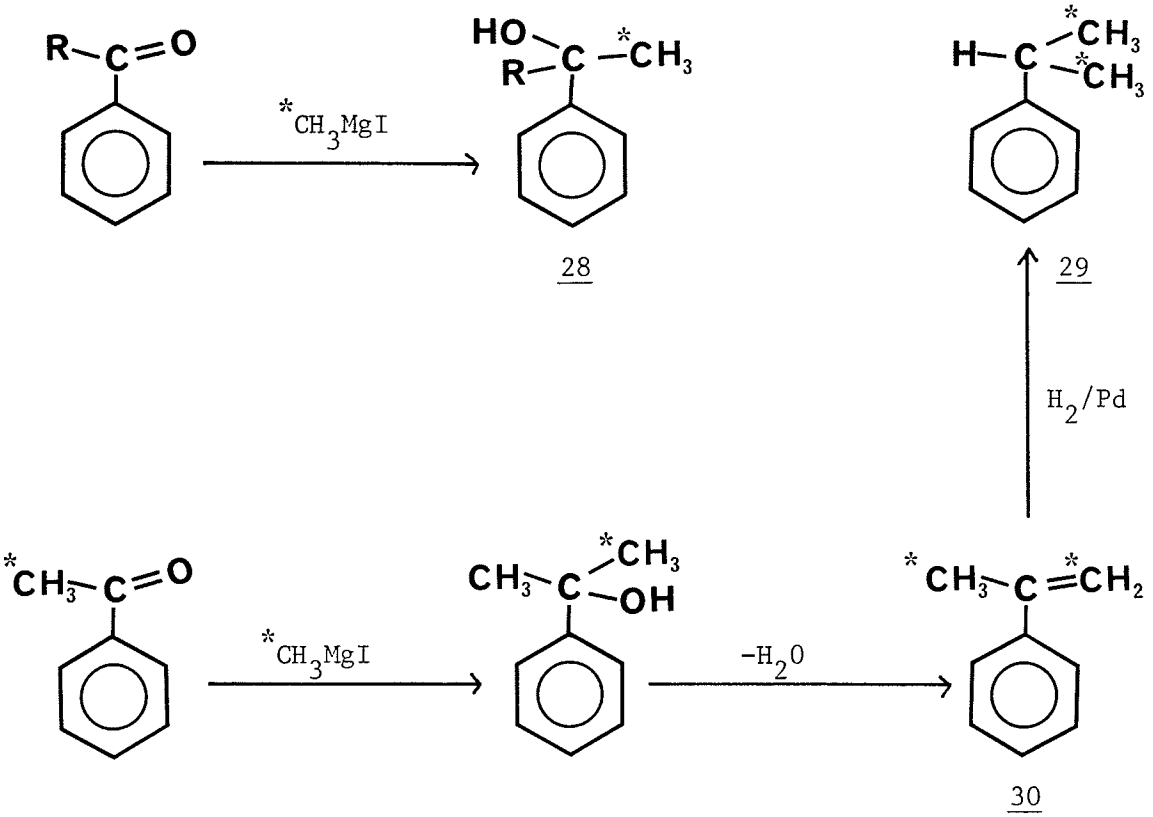
R–C=O
*CH3MgI
HO
R
C
*CH3
28
*CH3
H–C
*CH3
29
H2/Pd
*CH3–C=O
*CH3MgI
CH3
C
*CH3
OH
-H2O
*CH3–C=*CH2
30

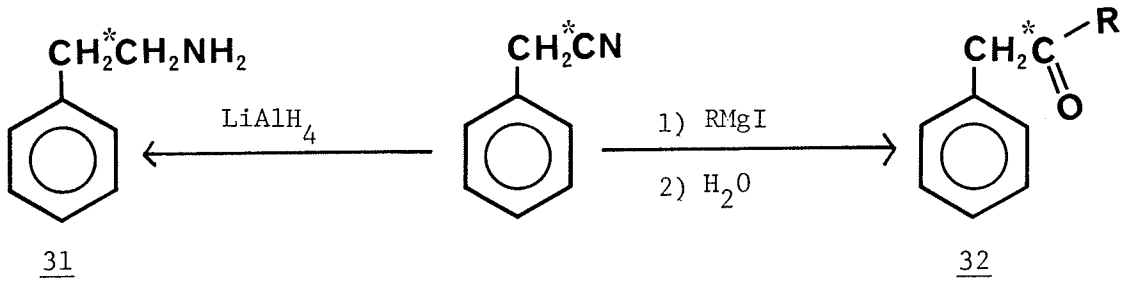
CH2*CH2NH2
LiAlH4
CH2*CN
1) RMgI
2) H2O
CH2*C
R
O
31
32

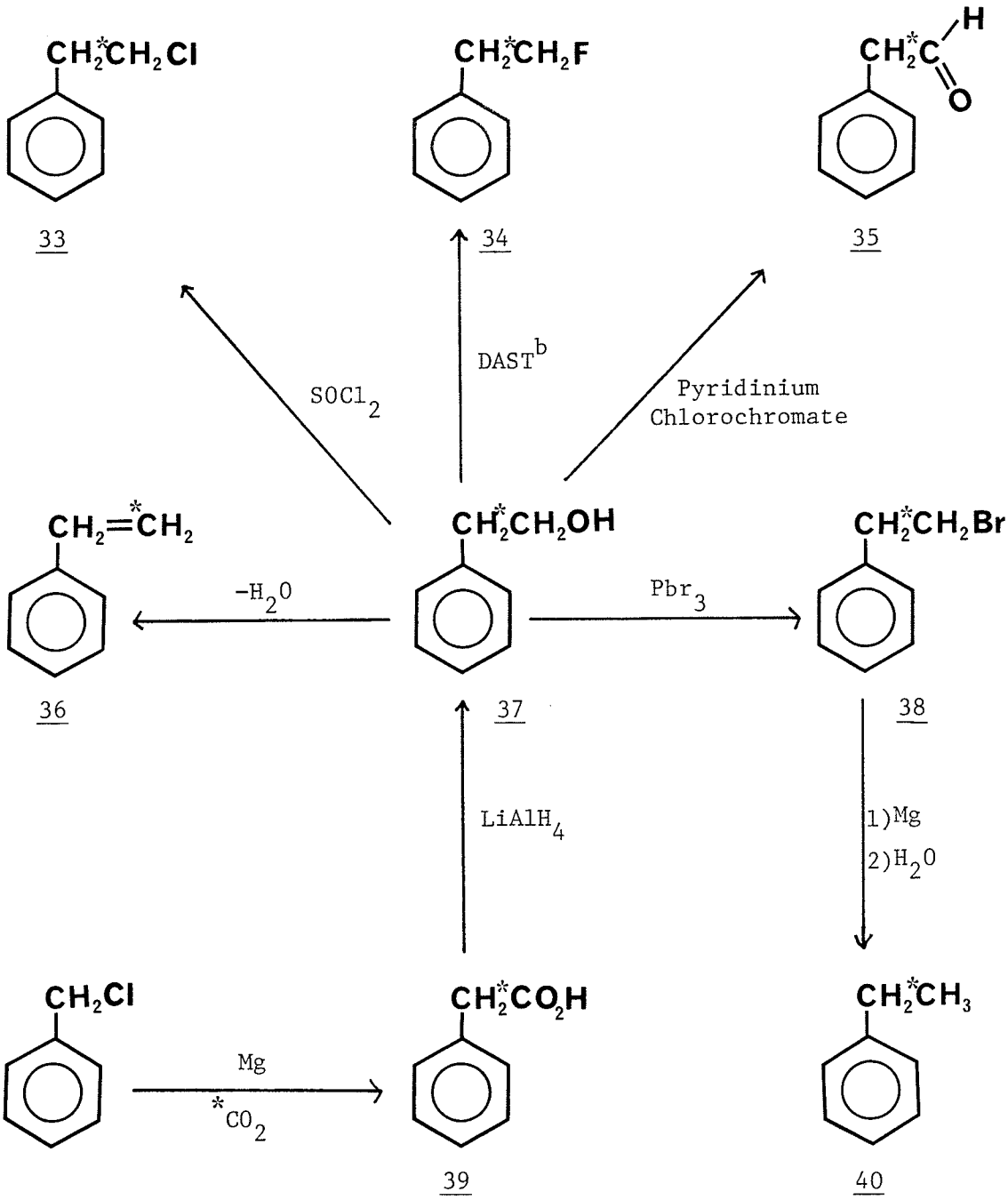

[b]Diaminosulfur trifluoride

Figure 30

Possible syntheses of some ^{15}N enriched derivatives of benzene.

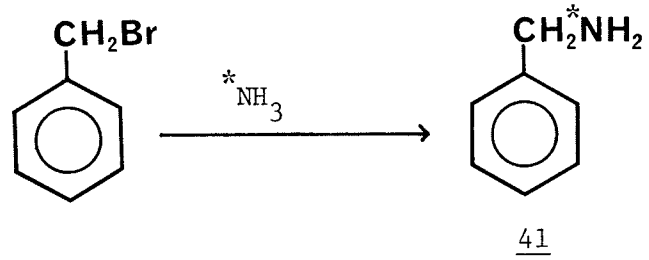
CH2Br
*NH3
CH2*NH2

41

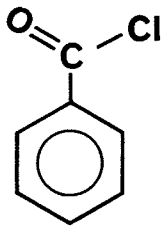
O
C
Cl

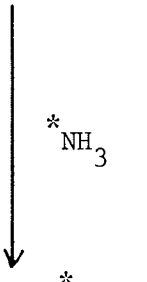
*NH3

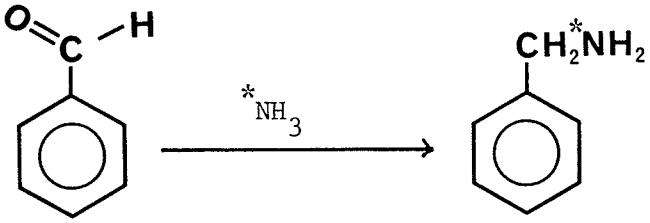
O
C
H
*NH3
CH2*NH2

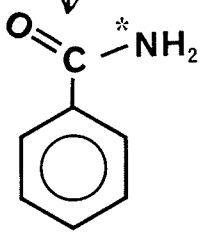
O
C
*NH2

42

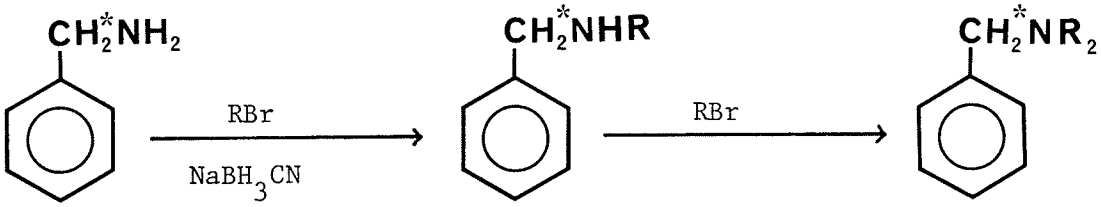
CH2*NH2
RBr
NaBH3CN
CH2*NHR
RBr
CH2*NR2

43

44

REFERENCES

1. M. Karplus. J. Chem. Phys. 30, 11 (1959).
2. R. Wasylishen and T. Schaefer. Can. J. Chem. 50, 1852 (1972).
3. C. Heller and H. M. McConnell. J. Chem. Phys. 32, 1532 (1960).
4. J. Hilton and L. H. Sutcliffe. Spectrochim. Acta. A32, 201 (1976).
5. T. Schaefer, S. R. Salman, T. A. Wildman and G. H. Penner. Can. J. Chem. 63, 782 (1985).
6. M. Barfield, C. J. Fallick, K. Hata, S. Sternhell and P. W. Westerman. J. Am. Chem. soc. 105, 2178 (1983).
7. T. Schaefer and R. Laatikainen. Can. J. Chem. 61, 2785 (1983).
8. T. Schaefer, R. Sebastian and G. H. Penner. Can. J. Chem. 63, 2597 (1985).
9. W. J. E. Parr and T. Schaefer. Acc. Chem. Res. 13, 400 (1980).
10. A. F. Janzen, M.Sc. Thesis, University of Manitoba, (1970).
11. T. Schaefer, J. Peeling and R. Sebastian. Can. J. Chem. 63, 3219 (1985).
12. T. Schaefer, J. D. Baleja and G. H. Penner. Can. J. Chem. 63, 2471 (1985).
13. T. Schaefer, T. A. Wildman and R. Sebastian. Can. J. Chem. 60, 1924 (1982).
14. T. Schaefer and W. J. E. Parr. Can. J. Chem. 55, 552 (1977).
15. T. Schaefer and W. J. E. Parr. Can. J. Chem. 57, 1421 (1979).
16. W. J. E. Parr and T. Schaefer. Can. J. Chem. 55, 557 (1977).
17. J. B. Rowbotham, M. Smith and T. Schaefer. Can. J. Chem. 53, 986 (1975).
18. T. Schaefer and J. B. Rowbotham. Can. J. Chem. 54, 2228 (1976).

19. T. Schaefer and J. B. Rowbotham. Can. J. Chem. 54, 2243 (1976).

20. T. Schaefer, R. Sebastian and T. A. Wildman. Can. J. Chem. 57, 3005 (1979).

21. T. Schaefer, B. M. Addison, R. Sebastian and T. A. Wildman. Can. J. Chem. 59, 1656 (1981).

22. T. Schaefer, R. Sebastian and S. R. Salman. Can. J. Chem. 62, 113 (1984).

23. R. Wasylishen and T. Schaefer. Can. J. Chem. 49, 3216 (1971).

24. T. Schaefer, S. R. Salman and T. A. Wildman. Can. J. Chem. 58, 2364 (1980).

25. T. Schaefer, G. H. Penner, K. J. Davie and R. Sebastian. Can. J. Chem. 63, 777 (1985).

26. M. Barfield, C. J. MacDonald, I. R. Peat and W. F. Reynolds. J. Am. Chem. Soc. 93, 4195 (1971).

27. T. Schaefer and W. J. E. Parr. J. Mol. Spectrosc. 61, 479 (1976).

28. R. Laatikainen and E. Kolehmainen. J. Magn. Reson. 65, 89 (1985).

29. T. Schaefer and G. H. Penner. Chem. Phys. Lett. 114, 526 (1985).

30. J. M. Hollas, H. Musa, T. Ridley, P. H. Turner, K. H. Weisenberger and V. Fawcett. J. Mol. Spectrosc. 94, 439 (1982).

31. T. Schaefer, W. Danchura, W. Niemczura and J. Peeling. Can. J. chem. 56, 2442 (1978).

32. T. Schaefer, R. Sebastian, R. P. Veregin and R. Laatikainen. Can. J. Chem. 61, 29 (1983).

33. T.Schaefer, W. Danchura and W. Niemczura. Can. J. Chem. 56, 2233 (1978).

34. Unpublishable results from this Lab (analysis of 3,5-difluorotoluene).

35. T. Schaefer, J. Peeling, G. H. Penner, A. Lemire and R. Laatikainen. Can. J. Chem. 64, 1859 (1986).

36. T. Schaefer, J. Peeling and G. H. Penner. Can. J. Chem. 61, 2773 (1983).

37. T. Schaefer, R. Laatikainen, T. A. Wildman, J. Peeling, G. H. Penner, J. Belaja and K. Marat. Can. J. Chem. 62, 1592 (1984).

38. T. Schaefer and J. D. Baleja. Can. . Chem. 64, 1376 (1986).

39. T. Schaefer, J. Peeling, G. H. Penner, A. Lemire and R. Sebastian. Can. J. Chem. 63, 24 (1985).

40. T. A. Wildman, Ph.D. Thesis, Department of Chemistry, Unviersity of Manitoba (1982).

41. J. L. Marshall. "Carbon-Carbon and Carbon-Proton NMR Couplings: Applications to Organic Stereochemistry and Conformational Analysis." Verlag Chemie International, Deerfield Beach, Florida (1983).

42. P. B. Ayscough, M. C. Brice and R. E. D. McClung. Mol. Phys. 20, 41 (1971).

43. D. G. Lister, J. N. Macdonald and N. L. Owen. "Internal Rotation and Inversion" Academic Press, London (1978).

44. L. Lunazzi, C. Magagnoli, M. Guerra and D. Dancciantelli. Tet. Lett. 3031 (1979).

45. M. Oki, "Application of Dynamic NMR Spectroscopy". Academic Press, Torotn, 1982.

46. J. Sandstrom, "Dynamic NMR Spectroscopy". Academic Press, Toronto, 1982.

47. D. Mirarchi and G. L. P. Ritchie. Aust. J. Chem. 34, 1443 (1981).

48. M. Camail, A. Proutiere and H. Bodot. J. Phys. Chem. 79, 1966 (1975).

49. M. J. Aroney. Angew. Chem. (Int. Ed.) 16, 663 (1977).

50. P. Diehl, C. L. Khetrapal, W. Niederberger and P. Partington. J. Magn. Reson. 2, 181 (1970).

51. P. Diehl, P. M. Henrichs and W. Niederberger. Mol. Phys. 20, 139 (1971).

52. P. Scharfenberg. J. Chem. Phys. 77, 4791 (1982).

53. A. H. Clark in "Internal Rotation in Molecules" W. J. Orville-Thomas (Ed.), Wiley, Toronto (1974).

54. L. V. Vilkov, V. S. Mastryukov and N. I. Sadova. "Determination of the Geometrical Structure of Free Molecules". Mir, Moscow (1983).

55. J. E. Wollrab. "Rotational Spectra and Molecular Structure" Academic Press. New York, 1967.

56. N. L. Owen in "Internal Rotation in Molecules" W. J. Orville-Thomas (Ed.) Wiley, Toronto, 1974.

57. J. H. Hog, L. Hygaard and G. O. Sorensen. J. Mol. Struct. 7, 111 (1970).

58. D. Christian, D. G. Lister and J. Sheridan. J. Chem. Soc. Faraday II, 70, 1953 (1974).

59. J. R. Durig, H. D. Bist, K. Furic, J. Qui and T. S. Little. J. Mol. Struct. 129, 45 (1985).

60. W. J. Hehre, L. Radom, P. V. R. Schleyer and J. A. Pople. "Ab Initio Molecular Orbital Theory", Wiley, Toronto (1986).

61. G. H. Penner, P. George and C. W. Bock. J. Mol. Struct. (Theochem) in press.

62. P. Pulay in "Molecular Theoretical Chemistry", Vol. 4, H. F. Schaefer III (Ed.), Plenum Press, New York, 1977.

63. A. R. Quirt and J. S. Martin. J. Magn. Reson. 5, 318 (1971); J. S. Martin, A. R. Quirt and K. E. Worvill. The nmr program library. Daresbury Laboratory, Daresbury, U.K.

64. M. R. Petersen and R. A. Poirier. MONSTERGAUSS. Department of Chemistry, University of Toronto, Toronto, Ontario, 1981.

65. J. S. Binkley, R. A. Whiteside, R. Krishnan, R. Seeger, D. J. DeFrees, H. B. Schlegel, S. Topiol, L. R. Kahn, and J. A. Pople. QCPE, 12, 406 (1980).

66. GAUSSIAN82. J. S. Binkley, M. J. Frisch, D. J. DeFrees, K. Raghavachara, R. A. Whiteside, H. B. Schlegel, E. M. Fluder, and J. A. Pople. Department of Chemistry, Carnegie-Mellon University, Pittsburgh, P.A.

67. P. A. Dobosh and N. S. Ostlund. QCPE 11, 281 (1975).

68. T. Schaefer, T. A. Wildman and S. R. Salman. J. Amer. Chem. Soc. 102, 107 (1980).

69. T. Schaefer, S. R. Salman, T. A. Wildman and P. D. Clark. Can. J. Chem. 60, 342 (1982).

70. J. Baleja, M.Sc. Thesis, Department of Chemistry, University of Manitoba (1984).

71. T. Schaefer and J. D. Baleja. Can. J. Chem. 64, 1376 (1986).

72. G. Penner, unpublished results.

73. T. Schaefer and G. Penner. Can. J. Chem. 65 (1987) in press.

74. M. J. Aroney, R. J. W. LeFebre, R. K. Pierens and M. G. N. The. J. Chem. Soc. London, B, 1132 (1971).

75. N. M. Zaripov. Zh. Strukt. Khim. 17, 741 (1976).

76. D. G. Lister, P. Polmieri and C. Zauli. J. Mol. Struct. 35, 299 (1976).

77. D. G. Lister, J. K. Tyler, J. H. Hog and N. W. Larsen. J. Mol. Struct. 23, 253 (1974).

78. G. M. Anderson III, P. A. Kollman, L. N. Domelsmith and K. N. Houk. J. Amer. Chem. Soc. 101, 2344 (1979).

79. T. Schaefer and R. L. Laatikainen. Can. J. Chem. 61, 224 (1983).

80. V. M. Bzhezovskii, V. A. Pestunovich, G. A. Kalabin, I. A. Aliev, B. A. Trofimov, I. D. Kalikhman, M. A. Shakhgel'diev, A. N. Kuliev and M. G. Voronkov. Izv. Akad. Nauk SSR, Ser. Khim. 2004 (1976).

81. L. B. Krivdin, G. A. Kalabin and B. A. Trofimov. Izv. Akad. Nauk SSSR, Ser. Khim., 565 (1982).

82. V. M. Bzhezovskii, G. A. Kalabin, G. A. Chmatova and B. A. Trofimov. Izv. Akad. Nauk SSSR, Ser. Khim., 586 (1977).

83. N. M. Zaripov, A. V. Golubinskii, G. A. Chmutova and L. V. Vilkov. Zh. Strukt. Khimi. 19, 894 (1978).

84. A. G. Avent, J. W. Emsley, M. Longeri, S. G. Murray and P. N. Nickolson. J. Chem. Soc. Perkin Trans. II 487 (1986).

85. V. V. Bairov, G. A. Kalabin, M. L. Al'pert, V. M. Bzhezovskii, I. D. Sadekov, B. A. Trofimov and V. I. Minkin. Zh. Org. Khim. 14, 671 (1978).

86. R. A. Kydd and A. R. C. Dunham. J. Mol. Struct. 98, 39 (1983).

87. F. A. L. Anet and M. Ghiaci. J. Amer. Chem. Soc. 101, 6857 (1979).

88. L. Lunazzi, C. Magagnoli and D. Macciantelli. J. Chem. Soc. Perkin Trans. 2, 1705 (1980).

89. R. Cervellati, A. Dalborgo and F. Scappini. J. Mol. Struct. 56, 69 (1979).

90. T. Schaefer, G. H. Penner, K. Marat and R. Sebastian. Can. J. Chem. 62, 2686 (1984).

91. T. Schaefer, J. Peeling and R. Sebastian. Can. J. Chem. 63, 3219 (1985).

92. T. Schaefer and G. H. Penner. Can. J. Chem. 64, 2013 (1986).

93. K. E. Calderbank, R. J. W. LeFevre and R. Pierens. J. Chem. Soc. B, 1463 (1970).

94. T. Schaefer, J. Peeling, G. H. Penner, A. Lemire and R. Laatikainen. Can. J. Chem. 64, 1859 (1986).

95. T. Drakenberg, J. Sommer and R. Yost. J. Chem. Soc. Perkin Trans. 2, 363 (1980).

96. H. van Koningsveld, J. J. Scheele and J. C. Jansen. Acta Cryst. C43, 294 (1987).

97. D. R. Eaton, A. D. Josey and R. E. Benson. J. Amer. Chem. Soc. 89, 4040 (1967).

98. G. H. Penner, P. George and C. W. Bock. J. Mol. Struct. (Theochem.) in press.

99. H. Spiesecke and W. G. Scheider. J. Chem. Phys. 35, 731 (1961).

100. P. C. Lauterbur, Tetrahedron Lett. 274 (1961).

101. A. R. Katritzky, R. F. Pinzelli and R. D. Topson. Tetrahedron. 28, 3449 (1972).

102. K. S. Dhami and J. B. Stothers. Tetrahedron Lett. 631 (1964).

103. L. B. Krivdin, G. A. Kalabin and B. A. Trofimov. Izv. Akad. Nauk SSSR. Ser. Khim. 570 (1982).

104. H. M. McConnell and D. B. Chestnut. J. Chem. Phys. 28, 107 (1958).

105. M. Karplus and G. K. Fraenkel. J. Chem. Phys. 35, 1312 (1961).

106. L. Ernst, V. Wray, V. A. Chertkov and N. M. Sergeyev. J. Magn. Res. 25, 123 (1977).

107. W. von Philipsborn and R. Mueller. Angew. Chem. Int. Ed. Engl. 25, 383 (1986).

"My God, how we adored this buggering up of our lovely language for we felt that all languages were lifeless if not buggered up a little."

Josef Sknorecky

"Red Music"

LIST OF PUBLICATIONS

1. T. Schaefer, J. Peeling, and G. H. Penner. The spin-spin coupling mechanism for ^{5}J(C-4, CH_{α}) in toluene derivatives and its conformational applications. Can. J. Chem. 61, 2773 (1983).
2. T. Schaefer, R. Laatikainen, T. A. Wildman, J. Peeling, G. H. Penner, J. Baleja and K. Marat. Long range $^{13}C,^{1}H$ and $^{13}C,^{19}F$ coupling constants as indicators of the conformational properties of 4-fluoroanisole, 2,3,5,6-tetrafluoroanisole and pentafluoroanisole. Can. J. Chem. 62, 1592 (1984).
3. T. Schaefer, G. H. Penner, K. Marat and R. Sebastian. The free energy barrier to rotation about the Csp^{2}-N bond in 4-bromo-2,6-difluoro-N-methylaniline. Molecular orbital calculations and experiments. Inversion. Can. J. Chem. 62, 2686 (1984).
4. T. Schaefer, J. Peeling, G. H. Penner, A. Lemire, and R. Sebastian. The conformational dependence of $^{6}J_{p}^{C,F}$ in some 4-fluorophenyl derivatives of methane, ethene, and cyclohexane. Can. J. Chem. 63, 24 (1985).
5. T. Schaefer, G. H. Penner, K. J. Davie and R. Sebastian. Control of the orientation of the aldehyde group in 2-(alkylthio)-benzaldehydes by the directional lone-pair on sulfur. Can. J. Chem. 63, 777 (1985).
6. T. Schaefer, S. R. Salman, T. A. Wildman and G. H. Penner. The range of $^{5}J_{O}^{H,CH}3$ in anisole derivatives. An indicator of torsion and compression of the methoxy group. Can. J. Chem. 63, 782 (1985).

7. T. Schaefer and G. H. Penner. Six-bond $^{1}H,^{1}H$ and $^{1}H,^{19}F$ spin coupling constants as indicators of geometry in aniline and p-fluoroaniline. Can. J. Chem. 63, 2253 (1985).

8. T. Schaefer, G. H. Penner, T. A. Wildman and J. Peeling. The conformational behaviour of 2-fluoro and 2,6-difluoroacetophenone implied by proximate spin-spin coupling constants and MO calculations. Can. J. Chem. 63, 2256 (1985).

9. T. Schaefer, J. D. Baleja and G. H. Penner. An increased rotational barrier in thiophenol caused by meta substituents. Can. J. Chem. 63, 2471 (1985).

10. T. Schaefer, R. Sebastian and G. H. Penner. ^{1}H nuclear magnetic resonance spectral parameters of toluene. Implications for conformational analysis and isotope shifts. Can. J. Chem. 63, 2597 (1985).

11. T. Schaefer and G. H. Penner. Calculations of the C(1)-C(α) torsional barrier in styrene. Comparison with experiment. Chem. Phys. Lett. 114, 526 (1985).

12. T. Schaefer and G. H. Penner. Internal rotation in α,α-dichlorotoluene. J. Raman Spect. 16, 353 (1985).

13. T. Schaefer, G. H. Penner, R. Sebastian and C. S. Takeuchi. Long-range proton coupling constants and molecular orbital calculations as indicators of conformational populations of benzene-1,2- and -1,3-dicarbaldehydes. Can. J. Chem. 64, 158 (1986).

14. J. L. Charlton, M. M. Alauddin and G. H. Penner. E,E- and E,Z-α-phenyl-α'-acetoxyorthoquinodimethane: steric and electronic control of cycloaddition reactions. Can. J. Chem. 64, 793 (1986).

15. G. H. Penner. Ab initio MO calculations on structures and internal rotational barriers of nitroethene and nitrobenzene. J. Mol. Struct. (Theochem) 137, 121 (1986).

16. G. H. Penner. STO-3G MO calculations of the rotational potential function in biphenyl. J. Mol. Struct. (Theochem) 137, 191 (1986).

17. T. Schaefer and G. H. Penner. STO-3G MO computations of six-fold barriers in some toluene derivatives. J. Mol. Struct. Theochem. 138, 305 (1986).

18. T. Schaefer, R. Sebastian and G. H. Penner. The internal rotational potential in benzyl chloride. Can. J. Chem. 64, 1372 (1986).

19. T. Schaefer, R. Sebastian, G. H. Penner and S. R. Salman. The proximate spin-spin coupling, $^{5}J(\underline{F},C\underline{H}_3)$, as a quantitative conformational indicator in alkylfluorobenzenes and related compounds. Can. J. Chem. 64, 1602 (1986).

20. T. Schaefer, J. Peeling and G. H. Penner. The mechanism of long-range $^{13}C,^{19}F$ and $^{19}F,^{19}F$ coupling constants in derivatives of biphenyl and fluorine. Differential isotope effects. Can. J. Chem. 64, 2162 (1986).

21. T. Schaefer, J. Peeling, G. H. Penner, A. Lemire and R. Laatikainen. The carbonyl group as a reluctant transmitter of hyperconjugation or - spin-spin coupling interactions in derivatives of benzaldehyde, acetophenone and benzophenone. Can. J. Chem. 64, 1859 (1986).

22. T. Schaefer and G. H. Penner. Mechanisms of $^{1}H,^{1}H$; $^{1}H,^{13}C$ and $^{13}C,^{13}C$ spin-spin coupling constants in benzyl cyanide and some derivatives. Experimental and theoretical estimates of internal rotational potentials. Can. J. Chem. 64, 2013 (1986).

23. T. Schaefer and G. H. Penner. The STO-3G MO structure and internal rotational potential of benzophenone. J. Chem. Phys. 85, 6249 (1986).

24. T. Schaefer, D. M. McKinnon, R. Sebastian, J. Peeling, G. H. Penner, and R. P. Veregin. Concerning lone-pair stereospecificity of intramolecular OH hydrogen bonds to oxygen and sulfur in solution. Can. J. Chem. 65, in press (1987).

25. T. Schaefer and G. H. Penner. Theoretical twofold and fourfold components of internal rotational barriers for a series of para-substituted derivatives of phenol, thiophenol, anisole and thioanisole. J. Mol. Struct. (Theochem) in press 1987.

26. T. Schaefer, G. H. Penner and R. Sebastian. ^{1}H nmr and molecular orbital studies of the structure and internal rotation of ethylbenzene. Can. J. Chem. 65, 873 (1987).

27. G. H. Penner. Conformational preference and internal rotation about the C_1-C_α bond in phenylacetaldehyde and some benzyl alkyl ketones from ^{1}H nmr and ab initio molecular orbital calculations. Can. J. Chem. 65, 538 (1987).

28. G. H. Penner, P. George and C. W. Bock. A molecular orbital study of the barrier height in benzaldehyde, and the changes in geometry which accompany the rotation of the formyl group. J. Mol. Struct. (Theochem) in press, 1987.

29. T. Schaefer and G. H. Penner. The structure and internal rotational barrier of 3-phenyl-1-propyne by molecular orbital calculations and the J method. Can. J. Chem. 65, in press (1987).

30. G. H. Penner, T. Schaefer, R. Sebastian and S. Wolfe. The benzylic anomeric effect. Internal rotational potentials of $ArCH_2X$

compounds (X = F, Cl, SH, SCH_3, $S(O)CH_3$, SO_2CH_3). Can. J. Chem. submitted.

31. T. Schaefer and G. H. Penner. The conformational properties of some phenyl esters. Molecular orbital and nuclear magnetic resonance studies. Can. J. Chem. 65, in press (1987).